

2012/1 vol.9



ACTA GEO TECHNICA SLOVENICA

2012/1

s. m. springman et al.

LESSONS LEARNT FROM FIELD TESTS IN SOME POTENTIALLY UNSTABLE SLOPES IN SWITZERLAND

m. f. amaral et al.

YIELDING IN THE ISOTROPIC COMPRESSION OF PORTO SILTY SAND

a. ristić et al.

SHALLOW-LANDSLIDE SPATIAL STRUCTURE INTERPRETATION USING A MULTI-GEOPHYSICAL APPROACH

m. laman et al.

NUMERICAL ANALYSIS OF CIRCULAR FOOTINGS ON NATURAL CLAY STABILIZED WITH A GRANULAR FILL

v. kalpakcı & m. y. özkan

A SIMPLIFIED APPROACH TO THE SETTLEMENT ESTIMATION OF PILED RAFTS

ISSN 1854-0171



ustanovitelji **founders**

Univerza v Mariboru, Fakulteta za gradbeništvo
University of Maribor, Faculty of Civil Engineering

Univerza v Ljubljani, Fakulteta za gradbeništvo in geodezijo
University of Ljubljana, Faculty of Civil and Geodetic Engineering

Univerza v Ljubljani, Naravoslovnotehniška fakulteta
University of Ljubljana, Faculty of Natural Sciences and Engineering

Slovensko geotehniško društvo
Slovenian Geotechnical Society

Društvo za podzemne in geotehniške konstrukcije
Society for Underground and Geotechnical Constructions

izdajatelj **publisher**

Univerza v Mariboru, Fakulteta za gradbeništvo
University of Maribor, Faculty of Civil Engineering

odgovorni urednik **editor-in-chief**

Ludvik Trauner University of Maribor

uredniki **co-editors**

Bojana Dolinar	University of Maribor
Borut Macuh	University of Maribor
Stanislav Škrabl	University of Maribor
Helena Vrecl Kojc	University of Maribor
Damijana Zlatolas	University of Maribor
Bojan Žlender	University of Maribor

posvetovalni uredniki **advisory editors**

Darinka Battelino	University of Trieste
Heinz Brandl	Vienna University of Technology
Chandrakant. S. Desai	University of Arizona
Pedro Seco e Pinto	National Laboratory of Civil Engineering

lektor **proof-reader**

Paul McGuinness

naklada **circulation**

300 izvodov - issues

cena **price**

25 EUR/izvod - 25 EUR/issue

tisk **print**

Tercia tisk d.o.o. Ptuj

Revija redno izhaja dvakrat letno. Članki v reviji so recenzirani s strani priznanih mednarodnih strokovnjakov. Baze podatkov v katerih je revija indeksirana: SCIE - Science Citation Index Expanded, JCR - Journal Citation Reports / Science Edition, ICONDA - The international Construction database, GeoRef. Izid publikacije je finančno podprla Javna agencija za knjigo Republike Slovenije iz naslova razpisa za sofinanciranje domačih periodičnih publikacij.

uredniški odbor **editorial board**

József Farkas	Budapest University of Technology and Economics
Theodoros Hatzigogos	Aristotle University of Thessaloniki
Rolf Katzenbach	Technical University Darmstadt
Nasser Khalili	The University of New South Wales, Sydney
Zlatko Langof	University of Sarajevo
Jakob Likar	University of Ljubljana
Janko Logar	University of Ljubljana
Bojan Majes	University of Ljubljana
Milan Maksimović	University of Belgrade
Borut Petkovšek	Slovenian National Building and Civil Engineering Institute
Mihael Ribičič	University of Ljubljana
César Sagaseta	University of Cantabria
Patrick Selvadurai	McGill University
Stephan Semprich	University of Technology Graz
Devendra Narain Singh	Indian Institute of Technology, Bombay
Abdul-Hamid Soubra	University of Nantes
Kiirchi Suzuki	Saitama University
Antun Szavits-Nossan	University of Zagreb
Ivan Vaniček	Czech Technical University in Prague
Jianhua Yin	The Hong Kong Polytechnic University

naslov uredništva **address**

ACTA GEOTECHNICA SLOVENICA
Univerza v Mariboru, Fakulteta za gradbeništvo
Smetanova ulica 17, 2000 Maribor, Slovenija
Telefon / Telephone: +386 (0)2 22 94 300
Faks / Fax: +386 (0)2 25 24 179
E-pošta / E-mail: ags@uni-mb.si

spletni naslov **web address**

<http://www.fg.uni-mb.si/journal-ags/>

The journal is published twice a year. Papers are peer reviewed by renowned international experts. Indexation data bases of the journal: SCIE - Science Citation Index Expanded, JCR - Journal Citation Reports / Science Edition, ICONDA - The international Construction database, GeoRef. The publication was financially supported by Slovenian Book Agency according to the Tender for co-financing of domestic periodicals.

VSEBINA

2	Ludvik Trauner UVODNIK
4	sarah M. Springman in drugi SPOZNANJA IZ TERENSKIH TESTOV NEKATERIH MOŽNOSTNIH NESTABILNIH POBOČIJ V ŠVICI
30	M. F. Amaral in drugi POPUŠČANJE V ENAKOSMERNEM STISKANJU PORTSKEGA MELJNEGA PESKA
46	Aleksandar Ristić in drugi RAZLAGA PROSTORSKE STRUKTURE PLIŤVEGA PLAZIŠČA Z UPORABO RAZLIČNIH GEOFIZIKALNIH METOD
60	Mustafa Laman in drugi NUMERIČNA ANALIZA OKROGLEGA TEMELJA NA NARAVNI GLINI, STABILIZIRANI Z ZANATIM POLNILOM
76	Volkan Kalpakcı and M.Y. Özkan POENOSTAVLJEN PARIŠTOP ZA OCENO POSEDANJA TEMELJNE PLOŠČE NA PILOTIH
86	NAVODILA AVTORJEM

CONTENTS

Ludvik Trauner EDITORIAL	3
sarah M. Springman et al. LESSONS LEARNT FROM FIELD TESTS IN SOME POTENTIALLY UNSTABLE SLOPES IN SWITZERLAND	5
M. F. Amaral et al. YIELDING IN THE ISOTROPIC COMPRESSION OF PORTO SILTY SAND	31
Aleksandar Ristić et al. SHALLOW-LANDSLIDE SPATIAL STRUCTURE INTERPRETATION USING A MULTI-GEOPHYSICAL APPROACH	47
Mustafa Laman et al. NUMERICAL ANALYSIS OF CIRCULAR FOOTINGS ON NATURAL CLAY STABILIZED WITH A GRANULAR FILL	61
Volkan Kalpakcı and M.Y. Özkan A SIMPLIFIED APPROACH TO THE SETTLEMENT ESTIMATION OF PILED RAFTS	77
INSTRUCTIONS FOR AUTHORS	87

UVODNIK

Pričujočo številko revije AGS smo prvič uredili z uporabo novega informacijskega sistema, ki je dostopen na spletni strani <http://www.fg.uni-mb.si/journal-ags/> ali direktno na <http://zalozba.uni-mb.si/index.php/ags/>. Zahvaljujemo se gospodu Boštjanu Kohnetu z Univerze v Mariboru, ki je sistem pripravil in ga redno vzdržuje, tako da ga sedaj lahko uspešno uporabljamo pri urejanju in recenziranju avtorskih prispevkov.

V tej številki objavljamo en pregledni članek in štiri znanstvene prispevke:

Profesorica Sarah M. Springman, predstojnica geotehnične raziskovalne skupine na Inštitutu za tehnologijo ETH v Zürichu, je imela v lanskem letu vabljen predavanje na 12. Šukljetovih dnevih (v Ajdovščini, 30. septembra 2011) z naslovom »Analiza stabilnosti enostavnega pobočja, glede na obnašanje/odziv nenasičenosti«. Predavanje, ki je bilo posvečeno pionirju geotehnike na slovenskem doajenu akademiku prof.dr. Lujju Šukljetu, je dopolnila skupaj s soavtorji: Amin Askarinejad, Francesca Casini, Sven Friedel, Peter Kienzler, Philipp Teyseire in Andrea Thielen, in ga tukaj objavljamo kot pregledni članek »Spoznanja iz terenskih testov nekaterih možnostnih nestabilnih pobočij v Švici«. Avtorji s svojim bogatim znanjem obravnavajo plazove, ki jih sprožajo padavine, predvsem v hribovitih območjih. Dr. S. M. Springman je prejela od Slovenskega geotehniškega društva najvišje priznanje za sodelovanje in odlično predstavitev na 12. Šukljetovih dnevih.

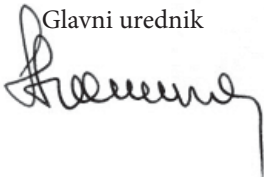
V drugem članku avtorji Miguel Ferreira Amaral, Sara Rios in António Viana da Fonseca prikazujejo analizo mesta popuščanja dobro zrnjavega meljnega peska s testi enakosmerne stiskanja in vrstičnim elektronskim mikroskopiranjem (SEM).

Avtorji, Aleksandar Ristić, Biljana Abolmasov, Miro Govedarica, Dušan Petrovački in Aleksandra Ristić, v tretjem članku predstavljajo metodologijo za natančnejšo in manj negotovo prostorsko strukturo razlago majhnih, plitkih plazišč. Ta metodologija vključuje uporabo metod georadarja (GPR), električne upornostne tomografije (ERT) in lasersko skeniranje površja (TLS) in so jo avtorji preverili na majhnem, plitvem plazišču.

Četrty članek avtorjev, Murat Ornek, Ahmet Demir, Korkut Ata, Mustafa Laman, Abdulazim Yildiz in Mustafa Laman, predstavlja numerične napovedi obsega učinka na okrogle temelje, podprtih z delno zamenjanimi in zgoščenimi plastmi na usedlinah naravne gline. Pojav obsega učinka je analiziran glede na velikost temelja. Določen je količnik nosilne kapacitete (BCR) za določitev izboljšane učinka ojačenega sistema z delno zamenjanih odloženih naravnih glin.

V petem članku avtorja, Volkan Kalpakçı in M. Yener Özkan, prikazujeta poenostavljen pristop za oceno posedanja temeljnih plošč na pilotih, ki ležijo na sedimentiranih prekonsolidiranih glinah. Za ta namen je bil izveden niz ravninsko deformacijskih in tridimenzionalnih analiz, njihovi rezultati pa so bili primerjani z razpoložljivimi podatki iz literature.

Ludvik Trauner
Glavni urednik



EDITORIAL

The current issue of the journal AGS was the first to be edited using the new information system that is now available on the website <http://www.fg.uni-mb.si/journal-ags/> or <http://zalozba.uni-mb.si/index.php/ags/>. Special thanks go to Mr. Boštjan Kohne from the University of Maribor, who has prepared and regularly maintained the system so that it can now be successfully used for editing and reviewing the authors' contributions.

In this issue we have published one review article and four scientific contributions:

Prof. Dr. Sarah M. Springman, principal of the Geotechnical Research Group at the Institute for Geotechnical Engineering ETH in Zürich, presented an invited lecture at the 12th Luj Šuklje Memorial Day (Ajdovščina, 30 September 2011) with the title "Simple slope stability analyses while considering unsaturated behaviour/response". Together with her co-authors, Amin Askarinejad, Francesca Casini, Sven Friedel, Peter Kienzler, Philipp Teyseire and Andrea Thielen, she complemented the lecture, which was dedicated to doyen academic prof. Luj Šuklje, and is here published as a review article "Lessons learnt from field tests in some potentially unstable slopes in Switzerland". With their rich knowledge, the authors treat the landslides caused by precipitations mostly in hilly regions. Dr. S. M. Springman received the highest acknowledgment for cooperation and gave a superb presentation at the 12th Šukljet's Days organised by the Slovenian Geotechnical Society.

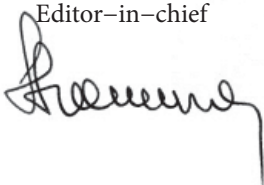
In the second article, the authors Miguel Ferreira Amaral, Sara Rios and António Viana da Fonseca have analysed the yielding locus of a well-graded silty sand by means of isotropic compression tests and scanning electron microscopy (SEM).

The authors Aleksandar Ristić, Biljana Abolmasov, Miro Govedarica, Dušan Petrovački and Aleksandra Ristić in the third article have presented the methodology for a more detailed and less ambiguous spatial structure interpretation of small, shallow landslides. This methodology involves the use of ground-penetrating radar (GPR), electrical resistivity tomography (ERT) and terrestrial laser scanning (TLS) techniques. The verification of the methodology was made on a small, shallow landslide.

The fourth article by Murat Ornek, Ahmet Demir, Korkut Ata, Mustafa Laman, Abdulazim Yildiz and Mustafa Laman presents numerical predictions of the scale effect for circular footings supported by partially replaced, compacted layers on natural clay deposits. The scale-effect phenomenon was analyzed according to the footing sizes. The Bearing Capacity Ratio (BCR) was defined to evaluate the improved performance of the reinforced system of the partially replaced, natural clay deposits.

In the fifth article, the authors Volkan Kalpakçı and M. Yener Özkan have presented a simplified approach to the settlement estimation of piled rafts resting on over-consolidated clay deposits. For this purpose, a series of plane-strain and three-dimensional analyses were performed and their results are compared with the available data in the literature.

Ludvik Trauner
Editor-in-chief



SPOZNAVANJA IZ TEREKSKIH TESTOV NEKATERIH MOŽNOSTNIH NESTABILNIH POBOČIJ V ŠVICI

SARAH M. SPRINGMAN, AMIN ASKARINEJAD, FRANCESCA CASINI, SVEN FRIEDEL,
PETER KIENZLER, PHILIPP TEYSSEIRE IN ANDREA THIELEN

o avtorjih

Sarah M. Springman
Institute for Geotechnical Engineering
ETH Zürich, Švica

Amin Askarinejad
Institute for Geotechnical Engineering
ETH Zürich, Švica

Francesca Casini
Institute for Geotechnical Engineering
ETH Zürich, Švica

Sven Friedel
Comsol Multiphysics GmbH
Zürich, Švica

Peter Kienzler
Institute for Geotechnical Engineering
ETH Zürich, Švica

Philipp Teysseire
Teyseire & Candolfi, Visp
Švica

Andrea Thielen
Friedlipartner AG,
Zürich, Švica

izvleček

Nestabilnost pobočij, ki jih povzroča dež, predstavlja pomembno ogroženost v Švici, Sloveniji in drugod po Evropi. Ta prispevek je bil še posebej pripravljen za 12. Šukljetove dneve in prikazuje takšne plaziščne pojave v hribovitih območjih, kot tudi v nižinskih predelih v času med in po izjemnimi nalivnimi pogoji. Inštitut (in profesorji) za geotehniško inženirstvo pri švicarskem Zveznem inštitutu za tehnologijo (ETH Zürich) je bil več let vključen v projekte, ki so se ukvarjali z opisom lastnosti, monitoringom in modeliranjem obnašanja pobočij, zlasti v poroznem zrnastem mediju na širokih predelih nadmorskih višin v Švici. V prispevku je povezano delo doajena Šukljetovega dne z obravnavo nestabilnosti pobočij, tej pa sledi predstavitev treh primerov plazov ter razlaga njihovega odziva na sezonsko deževje. V dveh izmed teh treh primerov je prišlo do sprožitve malega zdrsa, za katera so bili preiskani sprožilni dejavniki, ki so predstavljeni v prispevku. Le-ti so se zgodili zaradi načina drenažnega delovanja v pobočju tako, da so se tla nasičila in zaradi tega je nastala obsežna možnostna nestabilnost tal. Preprosta stabilnostna analiza z uporabo mejnega ravnovesja in z izboljšavo zemeljskih parametrov za nezasičene zemljine je bila najdena funkcija, ki je dobra za pobočja, predvsem z zrnastim medijem.

ključne besede

plazovi, povzročeni z dežjem, stabilnost pobočja, primeri iz prakse, monitoring, opis lastnosti, modeliranje

LESSONS LEARNT FROM FIELD TESTS IN SOME POTENTIALLY UNSTABLE SLOPES IN SWITZERLAND

SARAH M. SPRINGMAN, AMIN ASKARINEJAD, FRANCESCA CASINI, SVEN FRIEDEL, PETER KIENZLER, PHILIPP TEYSSEIRE AND ANDREA THIELEN

about the authors

Sarah M. Springman
Institute for Geotechnical Engineering
ETH Zurich, Suisse

Amin Askarinejad
Institute for Geotechnical Engineering
ETH Zurich, Suisse

Francesca Casini
Institute for Geotechnical Engineering
ETH Zurich, Suisse

Sven Friedel
Comsol Multiphysics GmbH
Zürich, Suisse

Peter Kienzler
Institute for Geotechnical Engineering
ETH Zurich, Suisse

Philipp Teyssere
Teyssere & Candolfi, Visp
Suisse

Andrea Thielen
Friedlipartner AG,
Zurich, Suisse

abstract

Rain-induced slope instability is a significant natural hazard in Switzerland, Slovenia and elsewhere in Europe. This contribution was prepared especially for the 12th Šuklje Symposium, and recognises that landslides occur both in mountain regions as well as in lowland regions during and following extreme-rainfall conditions. The Institute (and Professorship) for Geotechnical Engineering at the Swiss Federal Institute of Technology (ETH Zürich) has been engaged over several years in projects concerned with the characterisation, monitoring and modelling behaviour of slopes in mainly granular porous media across the full range of altitudes in Switzerland. A link is made to the doyen of the Šuklje day and then three case histories are presented and discussed to demonstrate the principal

reactions to seasonal rainfall. A small slip was released in two of these cases and the “triggering” factors have been investigated and are discussed in this contribution. It transpires that the mode of inslope drainage influences the way in which the ground saturates and hence the volume of the potentially unstable ground. Simple stability analyses using limit equilibrium and soil parameters that have been amended to account for unsaturated soil behaviour were found to function well for slopes in largely granular media.

keywords

rain-induced landslides, slope stability, case histories, monitoring, characterisation, modelling

1 PROF. DR. LUJO ŠUKLJE: ON LANDSLIDES AND HIS CONTRIBUTIONS

Academician Professor Dr Lujo Šuklje (Fig. 1; [1]) was the pioneer of Slovenian Soil Mechanics. He was appointed to a full Professorship at the University of Ljubljana in the year of the first author's birth and died in the year that she came to ETH Zurich at the same professorial grade. He was reputed to have been a strict, yet caring teacher, who left his mark on the development of conceptual soil mechanics, particularly on the rheological behaviour of soils [2], including creep, anisotropy,

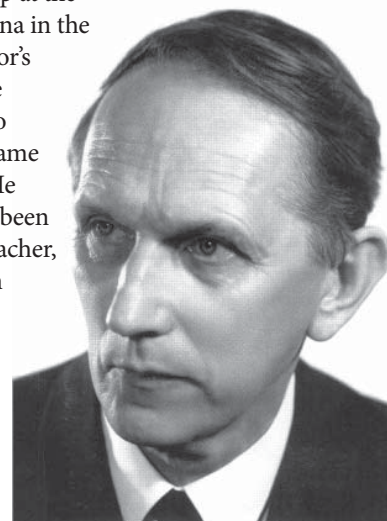


Figure 1. Academician Professor Dr. Lujo Šuklje [1].

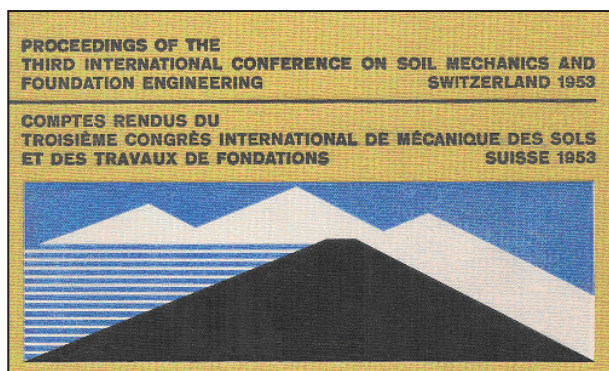


Figure 2. Proceedings of the third International Conference of Soil Mechanics and Foundation Engineering, Switzerland 1953 [3].

viscoplasticity and consolidation. Slope stability is treated too, in his highly regarded text book 'Rheological Aspects of Soil Mechanics' [2], with 4 chapters in Section 5. He insists that the laboratory testing of specimens should be conducted in the direct shear and the triaxial apparatuses following consolidation. This theme is taken up later in this paper, which is dedicated to celebrating 101 years after his birth in Jelsa, Hvar Island, in September 1910.

Interestingly, records of the discussion on Session 4 concerning 'the foundations of buildings and dams, bearing capacity, settlement observations, regional subsidences' held at the 3rd International Conference of Soil Mechanics and Foundation Engineering (Fig. 2; [4a]) that was held in Zürich in 1953, report written discussions from Mr L. Šuklje, which were presented in French. In the first, he took issue with a Mr S.J. Button concerning his treatment of foundation stability with a $\phi=0$ assumption, when shear resistance changes with depth. He mentioned that the position of the most unfavourable slip zones could also include thin bands of lower shear resistance and were also affected by the presence of rigid or flexible foundations. Interestingly, both themes were investigated in recent doctoral theses in the first author's group [5,6]. He also makes some fascinat-



ing comments on using either a grease or slimy mud to represent soft soils subjected to rigid foundation loads in physical models [7], initially at the Building and Public Works Laboratory in Paris and later at the Soil Mechanics Laboratory at the ETS of Ljubljana. These resulted in satisfactory analytical solutions by applying circular failure surfaces, again an area of interest to the authors.

The second written discussion [4a] presented tests demonstrating the effect of secondary settlement and a means for calculating the duration thereof, by using laws of similarity to apply test results to full-scale experiments. Professor Šuklje considered the micromechanics by explaining that the grains slid into more stable positions during this process and he either agreed or took issue with the General Reporter (Mr M. Buisson) and the ISSMFE-Harvard-MIT hierarchy (Prof. Terzaghi, Casagrande, Taylor).

The last discussion [4b] was an oral one in the session on 'stability and deformations of slopes and earth dams, research on pore-pressure measurements, groundwater problems'. He again referred to the adoption of a $\phi=0$ approach by a former doctoral researcher at ETH Zürich, who was then Director at the NGI in Norway, Dr Laurits Bjerrum. He was probably thinking of the Zalesina landslide, which is discussed below, and pointed out that this approach could not be used in Yugoslavia since most of the landslides occurred in heterogeneous clay soils and that effective stresses should be used at all times. It was also of great importance to include the influence of water pressures due to standing and flowing water. These last two are central tenets, which will form the backbone to this paper.

'En général, les expériences acquises montrent que l'eau souterraine peut en réalité réduire à rien la stabilité des talus, non seulement par la dissolution des forces de cohésion (adhésion), mais aussi par l'effet mécanique de la sous-pression ou de la pression du courant..... Le calcul montre une sécurité qui n'existe pas..... Il faudra, sous le même point de vue, reconsidérer également l'application de la méthode $\phi=0$.' [4b].

Fifth Technical Session: Influence of Ground-Water on Slope Stability

Friday morning, 24 September, 1954

Session 5/1

LANDSLIDE ZALESINA

by

ERVIN NONVEILLER and LUJO ŠUKLJE

Figure 3. Extract from the Fifth Technical Session of the Conference on Stability of Earth Slopes hosted in Stockholm, with photograph of the Zalesina landslide [8].

Professor Šuklje's contribution to the understanding of the cause of landslides, and his proposals for remediation, bear further mention and consideration in the context of this invited lecture. In conjunction with his former student Ervin Nonveiller (Fig. 3; [8]), he contributed to the Fifth Technical Session of the Conference

on Stability of Earth Slopes hosted in Stockholm. The paper was entitled 'Influence of Groundwater on Slope Stability' and concerned the Zalesina Landslide, then within Yugoslavia and now in the Republic of Croatia, due south of Obcima Kostel in southern Slovenia.

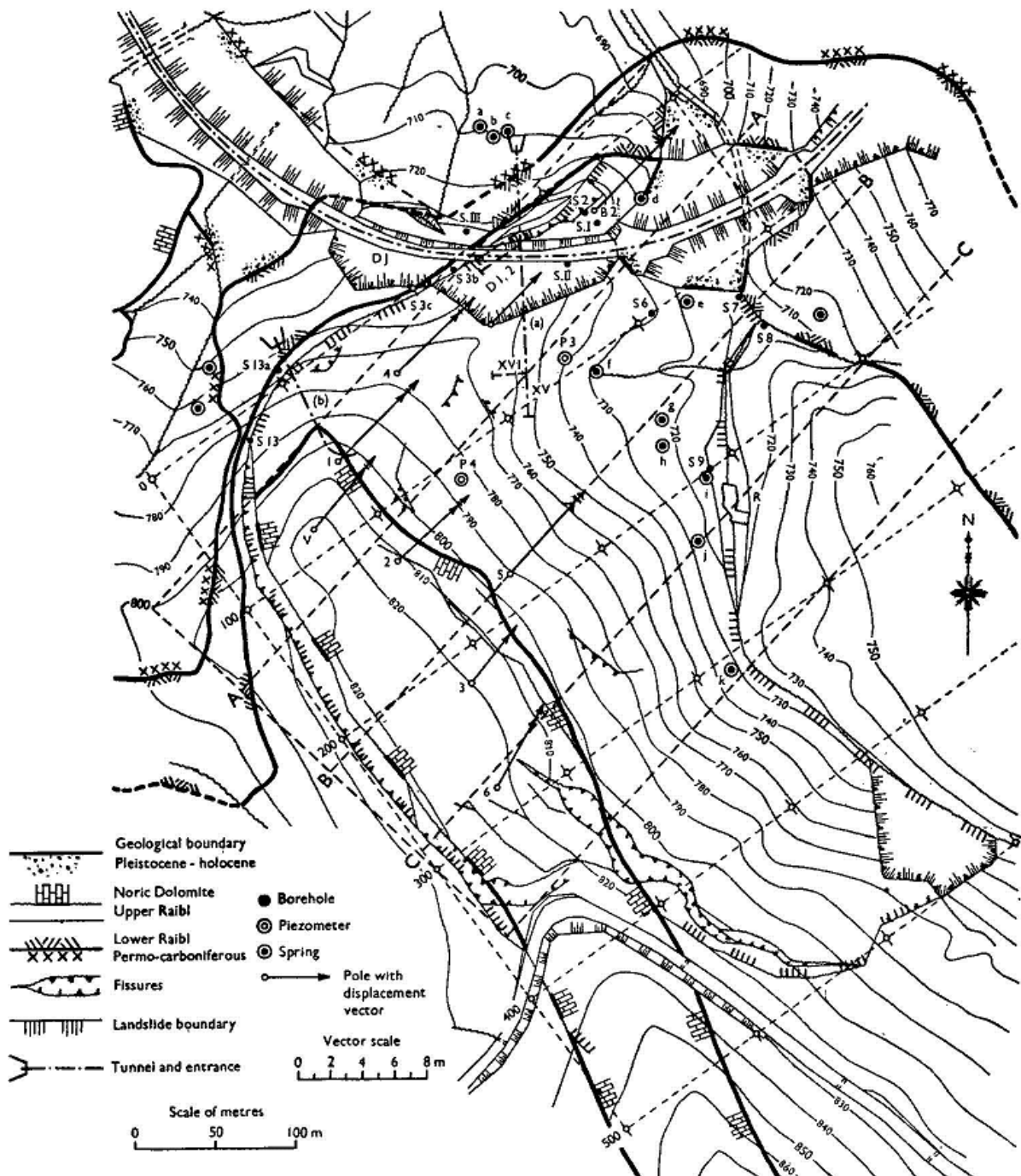


Figure 4. Mapping the Zalesina Landslide, Croatia, (Republika Hrvatska) [8].

A slope above a railway line demonstrated 'a spontaneous natural phenomenon' (Fig. 4; [8]), with a maximum length of the front being 500 m, and an average of 300 m. This was caused by a combination of 'tectonic processes (dinaric and transversal faults), long-term erosive creek action and internal erosion', while newly developed springs emerging from the slope played a major role as well, with one delivering 200 litres/min [8]. After a drought year in 1950, in which a continuous crack was observed running along a fault line over the railway line down to the creek, 2 m of net downslope movement was accompanied by an average of 6-mm/day rainfall over 6 months at the end of 1951 into early 1952. This comparison between the rainfall and the movement also showed that a cumulative total of more than 1000 mm of rain fell before the masses came to a more stable position [8].

Initiated at the contact between two strata between the Upper Raibl formation (siliceous or dolomitic sandstone with various forms of schisty shale, slate and limestone) and the overlying Noric Dolomite, cracks developed mainly perpendicular to the main direction of movement and played a crucial role in enhancing macro-permeability. A combination of large, deeper slides, older slides and secondary, comparatively shallow landslides in the weathered upper layers and steep slopes were probably caused by uplift and seepage pressures, through exfiltration from the bedrock, which could be treated effectively by remedial drainage. Some exploration tunnels were excavated to reveal the extent of the location of the shear zone.

The authors concluded a number of points that remain wholly relevant to today and were, at this time, still somewhat visionary.

1. An effective stress analysis must be conducted based on parameters derived from consolidated specimens in a ring-shear apparatus and from consolidated, undrained (quick and slow) triaxial tests.
2. Friction is more important than cohesion in tectonically disturbed beds, which govern the sliding conditions; a statement that would be "music to the ears" of one of the first author's mentors, Professor Andrew Schofield FRS FREng [9].
3. Uplift and seepage pressures play a major role in slopes during heavy rainfall and must be accounted for in the stability calculations.
4. The sliding may occur over a broad zone, here approximately 7 m, but the whole mass slides mainly as a solid body.
5. Monitoring of the groundwater level should be achieved using piezometers and geoelectrics, the latter being a method that is now finding considerable favour.

6. The method of potential slip surfaces can still be applied (assumed here to be limit equilibrium calculations), notwithstanding the approximations made, likewise an approach dwelt on briefly in this contribution.
7. Partial natural stabilisation was achieved, which could be improved by:
 - a. removal of mass from the top to the foot of the slide;
 - b. draining the sliding masses with a drainage system;
 - c. a combination of a) and b).

SURFICIAL RAINFALL INDUCED LANDSLIDES

Surficial rainfall-induced instabilities triggered in unsaturated slopes have been reported over many decades (e.g., [10-15]). Systematic studies of the most important triggering effects have been pursued as Pan-European multidisciplinary projects in recent years (e.g., MOUNTAIN RISK, TRAMM, SAFELAND).

Lateltin et al. [16] commented that periods of extreme rainfall, combined with a long humid winter and a cool late spring, as well as rising groundwater due to infiltration from snowmelt, have proved to be highly significant in causing landslides in Switzerland. This is supported by evidence from historical, Swiss meteorological data calibrated against landslide events derived from dendrochronology [17].

Colleagues in SE Asia report other leading studies (e.g., [18-22]), which have contributed data to earlier opinions on whether 2-3 weeks of steady rainfall is more dangerous [e.g., 11,12] than localised short, sharp, intense rainfall events [13,23]. Sometimes, there is a critical combination of antecedent rainfall over a specific duration followed by a shorter and more intense storm [24]. However, no one has been able to achieve a universal link between the intensity and duration of rainfall despite the best efforts of a generation of researchers from [25] through to [26] (see Fig. 5).

It is clear from Fig. 5 that rainfall-induced landslides present a significant natural hazard. Consequently, the field monitoring of slopes has been carried out by numerous researchers [e.g., 18-22, 31-39] and the statistics of rain-induced landslides have been presented for a series of storms in Switzerland in 2005 [40] and in neighbouring Austria [41] from 1950 to 2000. However, uniform conclusions have not emerged, largely due to the wide variety of sites, instrumentation as well as different levels of sophistication and investment in the characterisation,

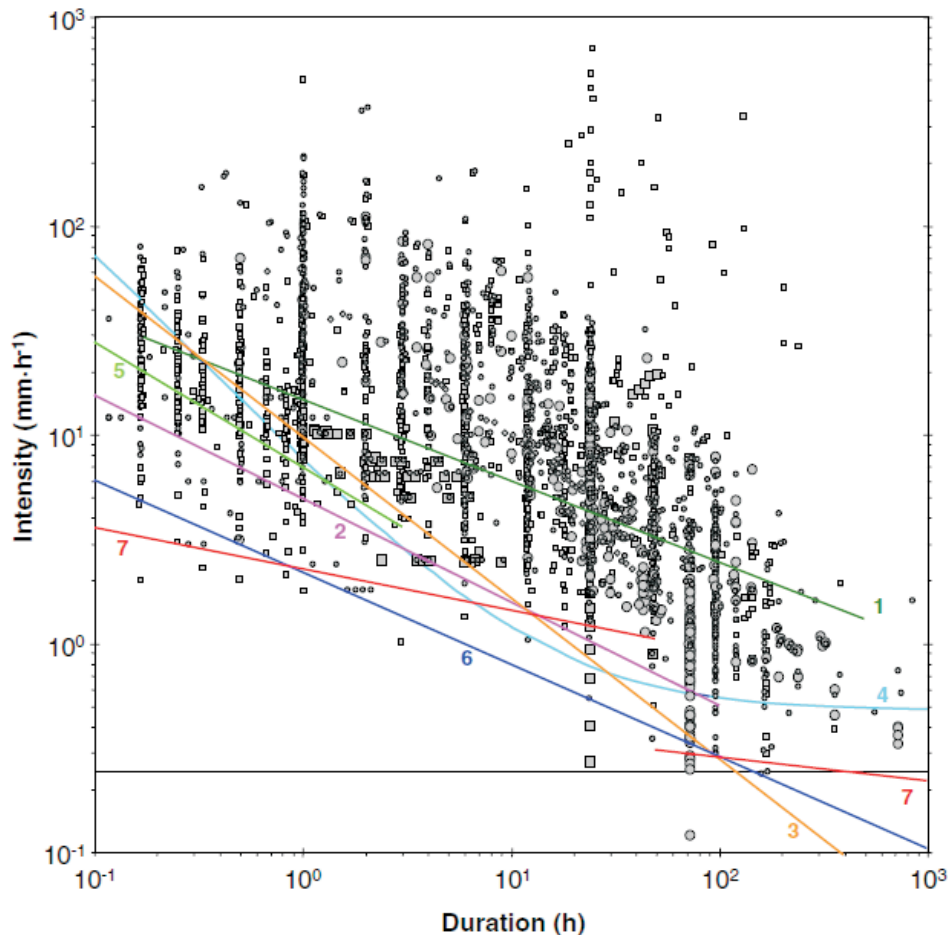


Figure 5. Global Intensity-Duration thresholds based on Guzzetti et al., [26] with published global (worldwide) Intensity-Duration rainfall thresholds proposed by: 1 [25]; 2 [27]; 3 [28]; 4 [29]; 5 [30]; 6 Inferred from this data; 7 thresholds inferred from the probability estimates of the rainfall conditions, for two different rainfall periods ($D < 48$ h, $D \geq 48$ h). The horizontal line shows a 0.25-mm/h rainfall intensity.

monitoring and modelling. This contribution attempts to add to the database obtained from past field tests and endeavours to provide a structure with which to accord a typology. It focuses on slopes that are predominantly in granular media and is accompanied by a very simple mode of analysis that would have common roots with Professor Šuklje's work.

Key factors affecting the likelihood of a mass movement being triggered are largely due to the location and origin of the slope (geological, geomorphological, anthropogenic factors), which are more or less constant with time in comparison with the more variable environmental effects, largely due to meteorology, hydrological, altitude and specifically precipitation [42] affecting infiltration [43] and water regimes, vegetation and temperature. Some impacts and outcomes that bear consideration are listed below, although they may not be the sole arbiters of whether a slope will remain stable or not:

1. topographical-soil engineering influences, particularly the slope angle related to the friction angle of the relevant strata derived from the original geology, in terms of deposition modes, anisotropy, macro-micro permeability with soil layering and underlying bedrock (in terms of the depth and the shape of bedrock surface);
2. precipitation-infiltration into the ground (soil) [44], groundwater flow processes, weathering at the soil-rock interface with attendant influence on permeability, exfiltration from the rock into the overlying soil layers and drainage into the underlying rock (e.g. [45-50]);
3. other factors affecting stability, such as the reinforcing effects of vegetation [51,52] and biological [51] or chemical [53] cementation;
4. triggering mode (extreme rainfall, changing groundwater and thermal regimes, seismicity and volcanic effects etc.; e.g. [54];

5. surface area, volume, aspect and mobility of failing debris, which have been found to be due largely to the initial void ratio as well as the availability of water to fill, or enlarge, the voids to form debris flows.

The locations of the three monitoring field sites (Table 1) discussed in this paper are given on a topographical map of Switzerland (based on [55]; Fig. 6;), showing the Alps (south) and Jura (north) mountains running approximately WSW to ENE, with the more highly populated areas (in pink) mainly located around the cities and in the 'Mittelland', between both mountain ranges. Also shown are cartoon pictures of the ground and a brief description of the main components. Some characteristics are extracted from each of the sites to enable subsequent analyses to be conducted and conclusions to be drawn.

Two main mechanisms were observed. These were a function of the inhomogeneity and permeability of the soil and rock layers as well as possible drainage channels in the soil and rock forming the slope. These will be described as top-down or bottom-up saturation, with the attendant influence on the volume of debris mobilised in

the failure mode and hence the risk entailed by failure. Infiltration into and exfiltration from the bedrock are found to be key factors as well.

The interaction between the air and the pore water in the soil pores played a major role as did the cyclical response of the slope to rainfall and groundwater flow, as it became saturated or drained. For example, Petkovšek et al. [69] have measured this for unbound base and sub-grade layers for several roads in Slovenia and the case histories discussed here rely on the instrumentation listed in Table 1.

Determining the soil state close to failure is dependent upon the stress path followed by the soil elements undergoing saturation. This is significant. Some laboratory stress path tests are presented and discussed for two of the sites to represent rainfall infiltration, together with data from a variety of direct shear box tests.

GRUBEN

The field data from the Gruben field test (Table 1) demonstrate that the fine-grained component of the matrix was significant at $15.9\% < 63\mu\text{m}$, and with $< 2\%$ at $< 2\mu\text{m}$ (from two representative surface samples

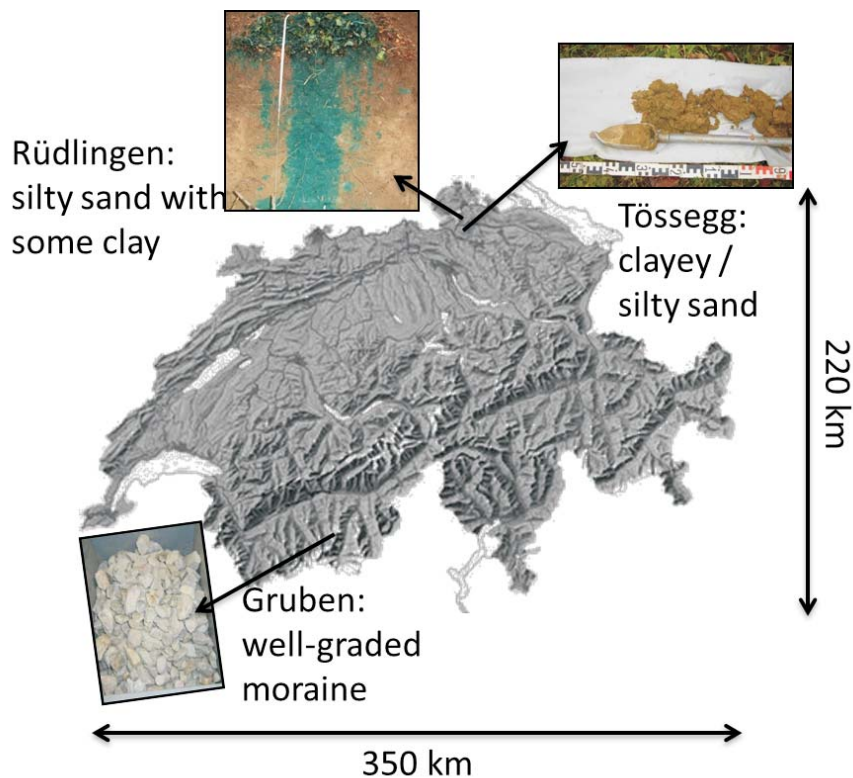


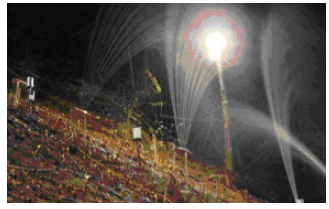


Figure 6. Location of three field-monitoring and test sites on a topographical map of Switzerland [55], which are described more fully in Table 1.

Table 1. Summary of field test sites in Switzerland.

Test field & Canton	Gruben Valais	Tössegg Zurich	Rüdlingen Schaffhausen
Dates	1998-2000	2004-2007	2008-2009
Picture			
Geology	scree slope, glacial debris / moraine, (Fletschhorn crystalline; Pretriassic Bernhard Plate of muscovite-rich gneiss / slate with some albite, chlorite, biotite)	quaternary outwash gravels mixed with finer grained deposits overlying horizontally layered sandstone (upper salt-water marls) above the lower freshwater marls	landslide debris (e.g. blocks & fine-grained soils) covering horizontally layered marls and sandstones in steep wooded areas
Soil layers	well graded angular granular soil particles with 10% fines < 60 µm	grassy surface with clayey sand overlying silty sand until rock at 1-2 m depth	roots in loose layer silty sand with %clay increasing with depth
Preferential infiltration & drainage systems	dense soil, voids $e \sim 0.3$, vertical & probably slope parallel flow with surficial run-off	channels from roots & animals in clayey sand, sometimes slope-parallel flow in silty sand, with little run-off and some infiltration into bedrock	primarily vertical drainage in pores ($e=0.9$) & along roots, infiltration into & exfiltration from bedrock
Test area & masl§	12 m (B) x 8 m (L)=100 m ² and 5.2 m (B) x 10.5 m (L)=55m ² 2750 masl	15 m (B) x 13 m (L)=195 m ² 367 masl	8 m (B) x 35 m (L)=280 m ² 385 masl
Slope α	31° (did not fail) & 42° (failed)	27° lower slope to 17° upper slope (did not fail)	38-42° (2008: did not fail; Mar. 2009 failed)
Instrumentation*	MS, TDR, MP, JFT, FO	MS, TDR, MP, JFT, ST, UV, G-ERT	MS, TDR, MP, JFT, EDZ, P, SG, INC, PG, ST, AS, G-ERT (UNIL)
Friction angle φ	39° (triaxial) & 41° (direct shear)	31° & 39° clayey & silty sand respectively in direct shear	30-32° (triaxial and direct shear)
Sponsors	Canton Wallis; BAFU	HazNETH, CCES / TRAMM	CCES / TRAMM
Dissertations	[56,57#]	[58,59#]	[60,61#]

§ masl metres above sea level, B breadth, L length

* MS Meteorological data such as air temperature, rainfall, humidity etc., plus UV Ultraviolet radiation, Measurement of volumetric water content: TDR Time Domain Reflectometry, MP Moisture Point, Suction: JFT Jetfill Tensiometer, pore-water pressure: P Piezometer, Earth pressure: EDZ earth pressure cell with P, ST soil temperature, Deformations: FO fibre optic cables, SG strain gauges, INC inclinometer, PG photogrammetry (plus AS Acoustic Sensors (STEP/ETHZ), G – Geophysical monitoring through ERT – Electrical Resistance Tomography); UNIL – University of Lausanne, BAFU - Federal Office for Environment; HazNETH – Natural Hazards Network ETHZ, CCES - Competence Centre for Environmental Sustainability / TRAMM – Triggering of Rapid Mass Movements.

These are doctoral dissertations. Additional semester or Masters' dissertations conducted on the Rüdlingen landslide include [62-68].

at up to 1 m depth, which were taken adjacent to Field 1; [70-72]. These fine grains and interstitial capillary space controlled the permeability and some aspects of the shear strength, in particular relating to the development of suctions. Furthermore, full saturation was not achieved and hence suctions were not dissipated

completely, even after almost one week of intense rainfall in 1999 with a minimum baseline (after the first 2 days) of 10 mm/h.

In total, 1.9 m of rainfall was applied artificially (averaging 13 mm/h over the week in 1999, Fig. 7). The Mois-

ture Point readings (Fig. 7, [70]), which averaged the volumetric water content over a given length, indicated that ‘full’ saturation was being approached only over the top 15 cm, following a gradual increase in the second half of the week. Even then, Sr was only 92% at the end of the experiment in 1999. Interestingly, there was a strong response to the raised rainfall intensity to > 20 mm/h on the morning of the 12th of July, in which little change was observed in the top 15 cm, but there seems to have been a consistent ‘breakthrough’ suddenly within a couple of hours to all sensors monitoring 15-30 cm, 30-60 cm, 60-90 cm and 0.9-1.2 m. Recovery to lower degrees of saturation occurred somewhat variably as the rainfall intensity dropped to 10 mm/h for the ensuing 16 hours.

Both test fields (2000/1 & 2000/2: slopes of 31° and 42° respectively) were subjected to a lower rainfall intensity in 2000, (8-22 mm/h: 0.76 m and 0.7 m of cumulative artificial rainfall on Fields 1 and 2 respectively). Fig. 8 shows the calibration of saturation data from 1999 to 2000 from using the same Field 1 (but with slightly less instrumentation), although this is only for ~2 days of rainfall, when there was a surficial failure in the steeper Field 2 (42°) and the tests were stopped. After failing to measure suctions in any instrument in 1999 due to the challenging environment [40], this was achieved in 2000 on Field 1 and the results were consistent with the measurement of water content, showing the initial and latest responses in terms of loss of suction at the shallowest and the deepest tensiometers, respectively. A summary of the net loss is shown in Fig. 8 [71].

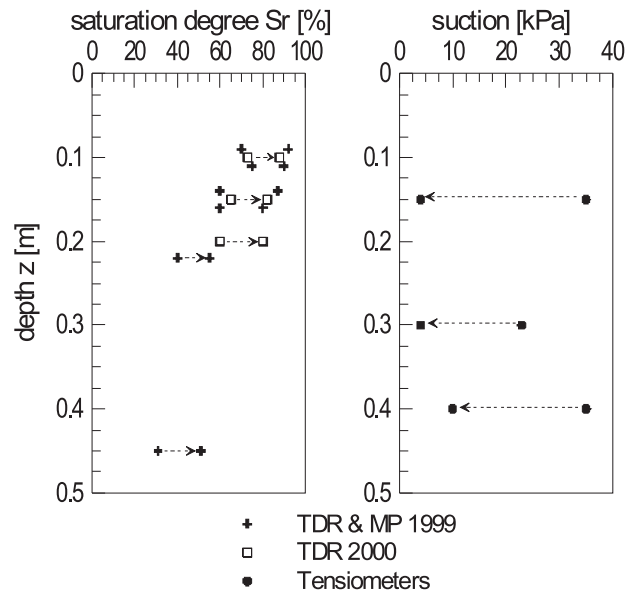


Figure 8. Gruben: summary of immediate pre- and post-rainfall event data showing increase in saturation combined with loss of suction as infiltration progresses (a) saturation degree determined from TDR and MP probes: Fields 1/1999 & 1/2000 (31° slope), (b) Suctions determined from tensiometers: Field 1/2000 (31° slope), Gruben [71].

TÖSSEGG

The Tössegg site is located in Canton Zurich on the banks of the river Rhine. It was selected due to a series of extreme events in May 2001 in which 42 surficial landslides occurred nearby following 10cm of rainfall in

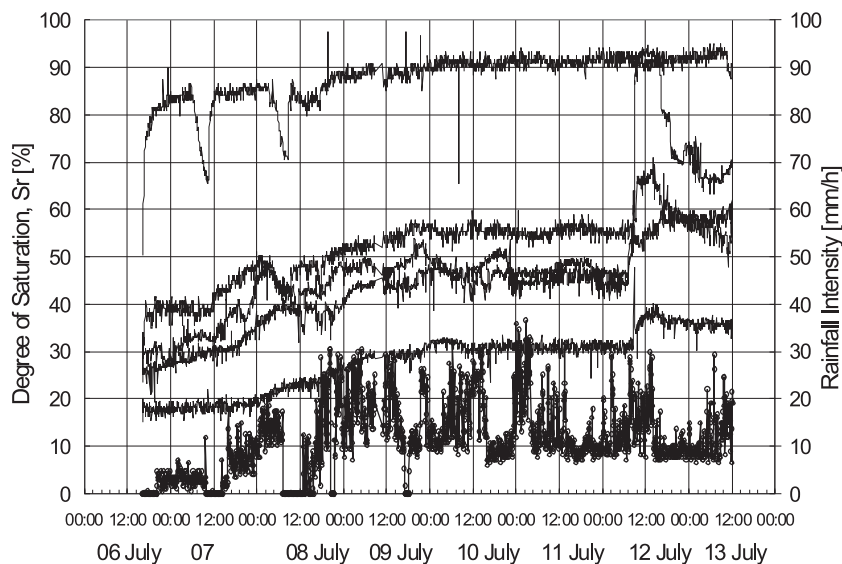


Figure 7. Gruben: Rainfall intensity and Moisture Point (MP) measurements in terms of saturation degree with time: Field 1/1999 (31° slope) [70].

40 minutes [73]. The slope was investigated and characterised using geophysical, geological and geotechnical methods [58,74-76]. A clayey sand was revealed below the grassy humus layer, with a silty sand overlying sandstone-marl bedrock at between just less than 1 m to nearly 2 m depth.

The electrical resistivity tomograms shown in Fig. 9 were developed for measurements made over the extent of the grassy slope in 8/2003 and 7/2004 [75], whereby resistivity depends on porosity, degree of saturation and mineral content. The rainfall differed significantly in the summer 2003 and summer 2004, in which 2003 was a very dry summer, reflected in the higher surface resistivities determined in Fig. 9. Variations in resistivity can be explained by changes in saturation, since other parameters remain more or less constant. The saturation of the layer below the topsoil, and up to about 1 m depth, on top of the underlying bedrock is greater in July 2004 in the lower part of the slope, where the instrumentation was ultimately installed for the monitoring experiment [74].

Table 2. Tösslegg test field: layers at location of upper / lower / right / left instrument clusters (after [58]).

Layer thicknesses (cm)	Upper left	Bottom left	Upper right	Bottom right
Topsoil	25	20	30	25
Clayey sand	60	135	0	100
Silty sand	10	45	150	45
Depth to bedrock (cm)	95	200	180	170

The reactions to summer (mid-August 2005) and winter (April 2005) rainfall events in terms of volumetric water content θ are shown with depth before, during and after the rainfall event for instruments installed at the four corners of the test field in Fig. 10, with soil conditions recorded in Table 2. The highest saturation was reached in winter (Fig. 10a) over the top 60 cm, mainly in the clayey sand, after 24 hours of rainfall with a greatest change in volumetric water content up to 0.075. There was some saturation of the underlying silty sand layer at about 1.2 m depth, on the right-hand side of the field, indicating percolation and a short-term increase in saturation in the more permeable layer. The saturation degree reverts to the original state four days after the rainfall event.

The maximum saturation for the summer event (Fig. 10b) was increased over the top 45 cm only, from a relatively dry state by increments of θ up to 0.15. The volumetric water content was generally lower prior to the

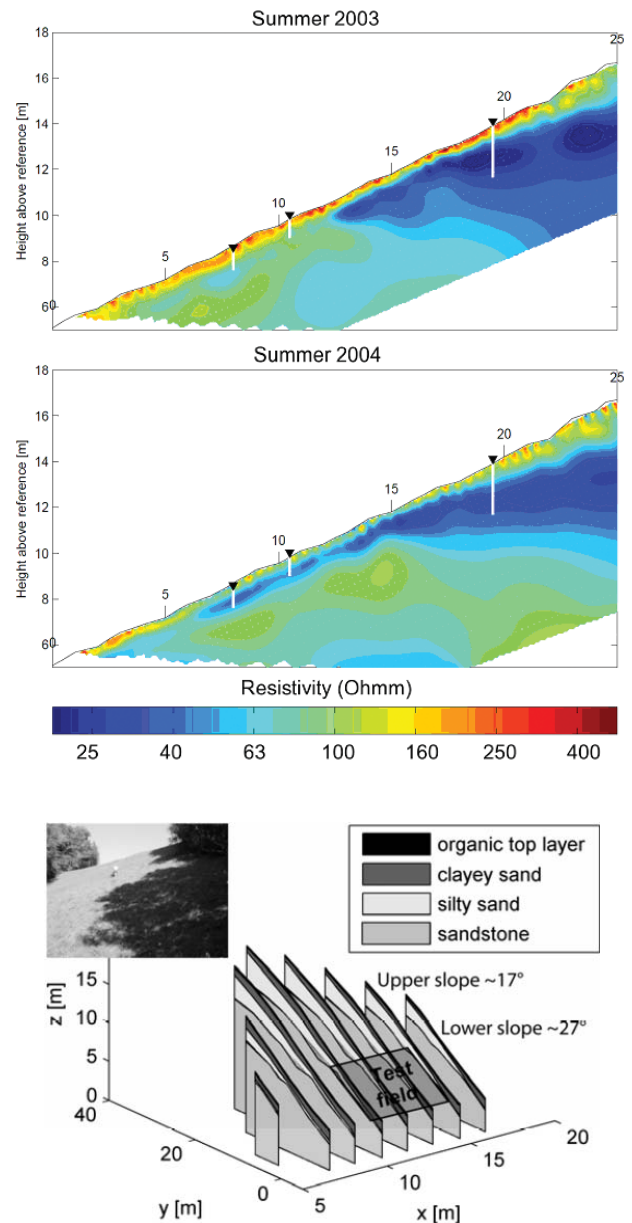


Figure 9. Tösslegg: Comparison of electrical resistivity tomograms taken in August 2003 and in July 2004 [75] combined with ground model and location of the test site [74].

summer event, than when fully saturated in winter [58]. Most of the rainwater had infiltrated with low runoff and there was little reduction in saturation over 48 hours after the rainfall stopped because both the temperatures and the evapotranspiration rate were low for this season during the days after the rainfall event.

Small-scale sprinkling experiments, covering a circular area of 1 m², were used after the monitoring period to

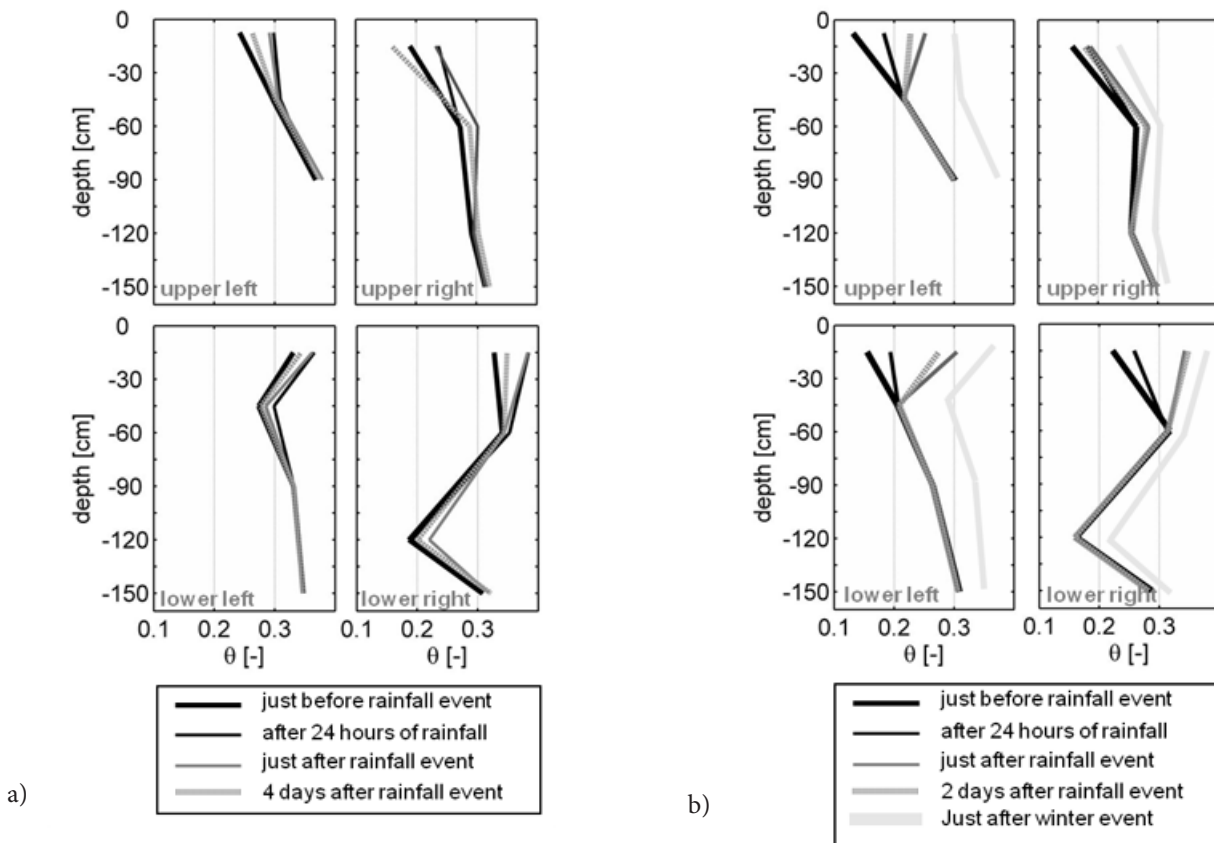


Figure 10. Volumetric water content with depth for rainfall events in

(a) winter (April 2005) (b) summer (mid-August 2005) for locations upper / lower / right / left referring to instrument clusters [76].

investigate the infiltration characteristics [77]. Brilliant blue FCF food dye [78] was added as a tracer (4 g/l) to water to visualise the flow paths and sprinkled at an intensity of 60 mm/h over a period of 2 hours. Runoff was collected from the bottom of the ring and measured with a tipping bucket. Vertical soil sections were excavated to a depth of 1 m on the day after sprinkling to reveal a high infiltration capacity with the topsoil stained homogeneously to a depth of about 30 cm, and with no overland flow (Fig. 11a). Preferential flow occurred below, with little matrix interaction showing clearly the small-scale variability of the infiltration flow paths. Lateral flow was detected at the transition to weathered bedrock (silty sand) and deeper percolation into the weathered sandstone was revealed by several stained flow paths and fractures below (Fig. 11b). Thus, perched saturation might be expected at the transition between the topsoil and the subsoil, as well as at the transition to bedrock. Such a formation of perched water tables can be assumed to support instability. Finally, the excavations revealed a fissure in the bedrock that was extremely effective in preventing groundwater-table rise at this location (Fig. 11c).

RÜDLINGEN

The forested Rüdlingen experimental site with dimensions of 35 m upslope x 8 m width (Table 1) is located about 2 km upriver from Tössegg on the west bank of the Rhine [79]. The slope gradient was 38-42°. Extensive characterisations of the soil [62,63,79,80] and root distributions (Figs. 12a-c; [52]) were conducted in test pits (and on specimens extracted in the laboratory) for a determination of the strata and the key soil properties prior to failure. Colluvium (silty sand with some clay) overlay sandstone and marlstone, which were located at a depth of between 0.5 m to more than 5 m. Figures 12a-c and Colombo [62] show that the macro-permeability between the pedes was significantly greater than the micro-permeability within them, aided by the presence of roots that promoted drainage of the coloured water down to the bedrock (Fig. 12a). A high infiltration capacity, with homogeneous matrix flow, was revealed in combined sprinkling and dye-tracer tests. No overland flow was observed during 60 mm/hr sprinkling for 5 hours over an area of 1 m² [76]. Some sections remained unsaturated though, as can be seen in Figures 12b-c.

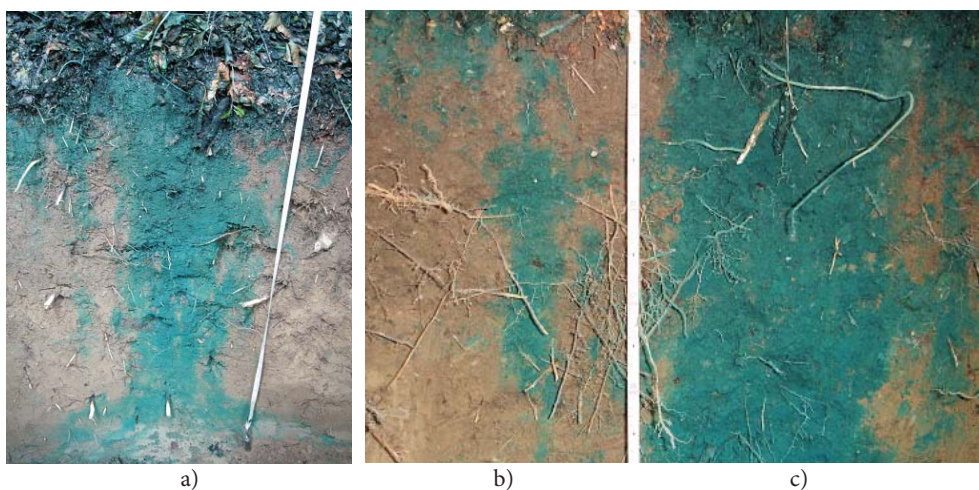
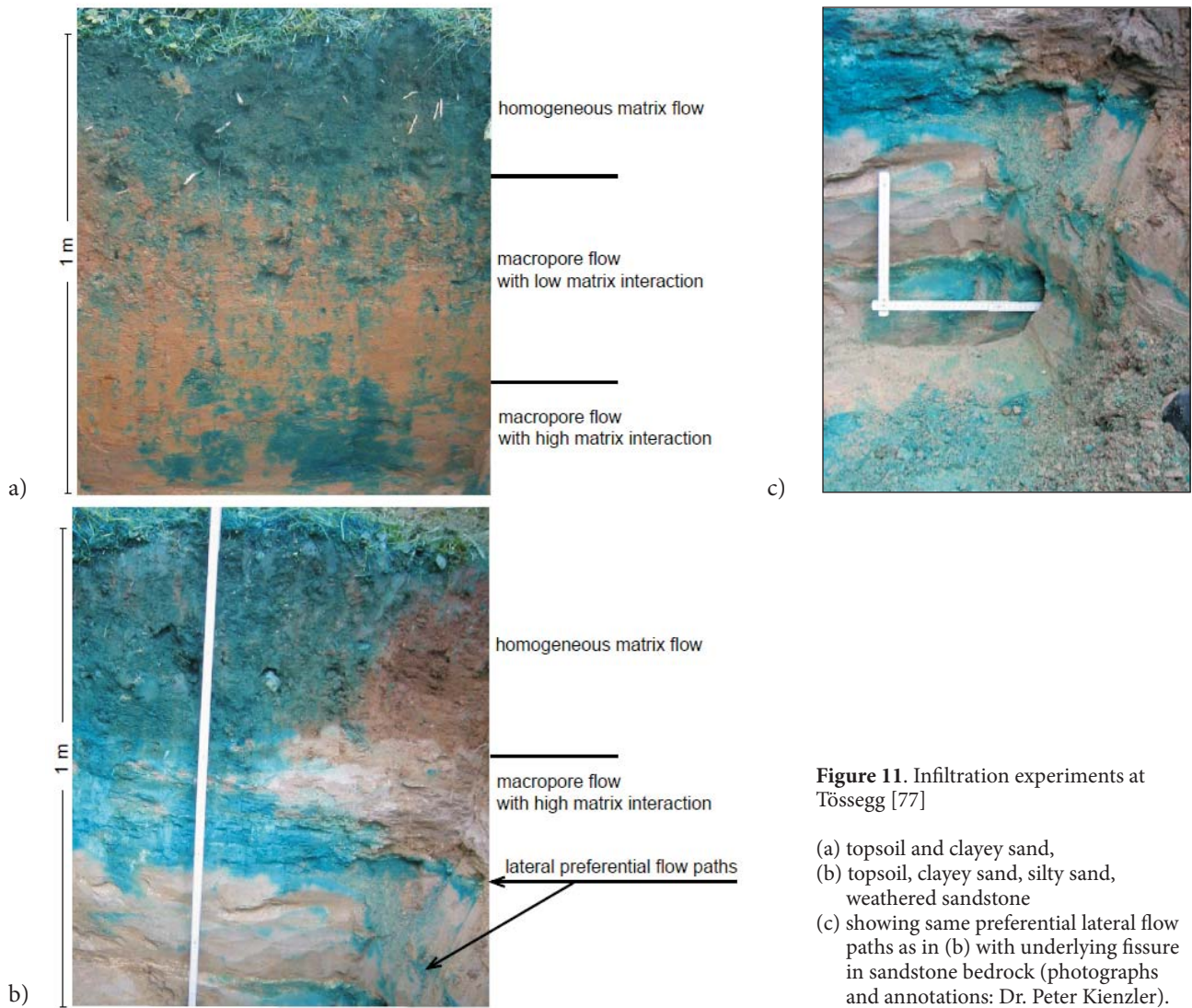


Figure 12. Rüdlingen: excavation of pits following infiltration tests (a) primarily vertical flow with lateral spreading above rock [79], (b) indications of partially saturated flow (c) root matrix (photographs: Dr. Peter Kienzler).

Beck [64,65] and Askarinejad et al., [81] also reported intermediate-scale laboratory infiltration tests to examine the influence of the soil structure on the saturation and hydraulic conductivity.

Lateral flow and perched saturation are observed above the bedrock (Fig. 12a). These results hinted strongly at the vulnerability of the slope to failure with the possibility for a water table to build up above the rock and with expectations of a failure above the transition to bedrock rather than a more surficial failure that is typical for many rainfall-induced landslides [71]. However, some stained fractures below the subsoil also implied that substantial percolation into the bedrock might occur, which could prevent complete saturation and failure of the instrumented slope (Fig. 13; [79]). This was indeed noted by Brönnimann et al., [70] in permeability tests in the lower part of the slope just prior to the first of two sprinkling experiments that were conducted to represent an extreme rainfall event, in October 2008 and March 2009. She observed that 100 litres were poured into the borehole over a few minutes, which drained immediately without

developing a groundwater table. The ERT geophysical characterisation [82] also indicated the presence of saturated fissures in the bedrock in the lower half of the slope.

Over 1.3 m of rain (370 m^3) was applied in the first event over almost 5 days in October, largely directed towards the lower half of the slope. The increase in water table was minimal with a maximum value measured as an almost negligible excess pore pressure of 2 kPa. Movement was measured by photogrammetric methods in the upper-right part of the slope [83], but no failure developed.

Much less rainfall (232 mm; 65 m^3) was applied in the second (March) experiment, focused mainly at the top of the slope. 130 m³ of debris were mobilised 15 hours after the rainfall started. Movements on the centimetre scale were noted about 2 hours before failure occurred, initially near the surface and subsequently at 1.3 m depth [84]. Strains accelerated about 30 minutes before failure, as observed by three inclinometers that had been developed in house [85].



a)



b)

Figure 13. Rüdlingen: picture of the instrumented test field a) prior to and b) post failure (Photographs: Amin Askarinejad).

Suctions reduced (Fig. 14; [77]) following the start of sprinkling and positive pore pressures developed almost immediately at a depth of 60 cm in the top cluster (3). Saturation was slightly slower in the middle (2) and bottom (1) clusters until pore pressures reached 5-10 kPa at a depth of 1.5 m at the moment of failure. The data show a higher water table at the top of the slope, which is also supported by piezometer measurements. Water flow out of the back scarp of the failure scar immediately following failure contributed additional pore pressures, in the form mentioned by Professor Šuklje in relation to the Zalesina landslide. These were assumed to have triggered the destabilisation from the top, which took about 48 seconds from observation of the formation of a tension crack at the top of the slope to reach the protection net at the base of the slope. A scar was formed of dimensions 17 m downslope, approximately 7.5 m wide and approximately 1.3 m deep, on the left side, and 0.5 m deep, on the right.

SATURATION AND DESATURATION MECHANISMS

Several mechanisms are presented to describe the saturation of slopes. Infiltration is dominant in the first case and the saturation develops from the surface downwards, 'top down' (Fig. 15a, and in the summer regime for Fig. 15b). The wetting front increases the saturation

in the upper layer, decreasing the suctions, and hence resistance induced by partial saturation. Unsaturated soil mechanics must be included in the analysis of slope stability. Slopes with an inclination α steeper than a critical friction angle φ'_{cv} , as for example in Gruben (Table 1a), will most probably slip surficially (see next section).

An overlying layer (1) was mainly fully saturated in the second case, for example for the winter regime in Tössegg (Fig. 15b). The underlying, and more permeable, layer (2) was saturated from the 'bottom up' from groundwater flow along the bedrock in Tössegg (Fig. 15b) and at the top of the slope in Rüdlingen (Fig. 15c). The shear surface would be at a depth of more than 1 m, causing more debris material to be released in an unstable situation. In this case, the evaluation of slope stability should follow methods based on 'saturated' soil mechanics. Analyses for both cases are presented in the next sections.

SHEAR PARAMETER DETERMINATION THROUGH TRIAXIAL STRESS PATH TESTS

Infiltration processes cause an increase in the pore-water pressure, which decreases the mean effective stress leading to failure of the slope. It is essential to model the effective stress paths followed in the field in the laboratory when determining shear parameters (e.g., [4,87]), which can be done mainly in two ways:

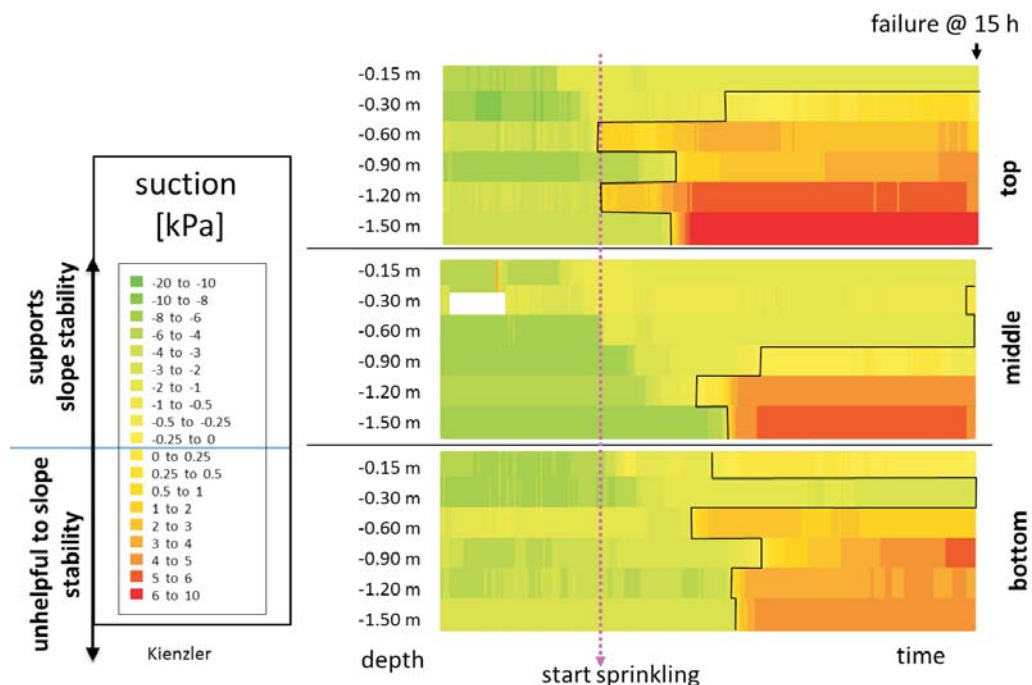


Figure 14. Rüdlingen: suctions and pore pressures measured at each of the 3 clusters from the top to the bottom of the slope, for the 15-hour duration of the sprinkling experiment in March 2009 (after [44, 77]).

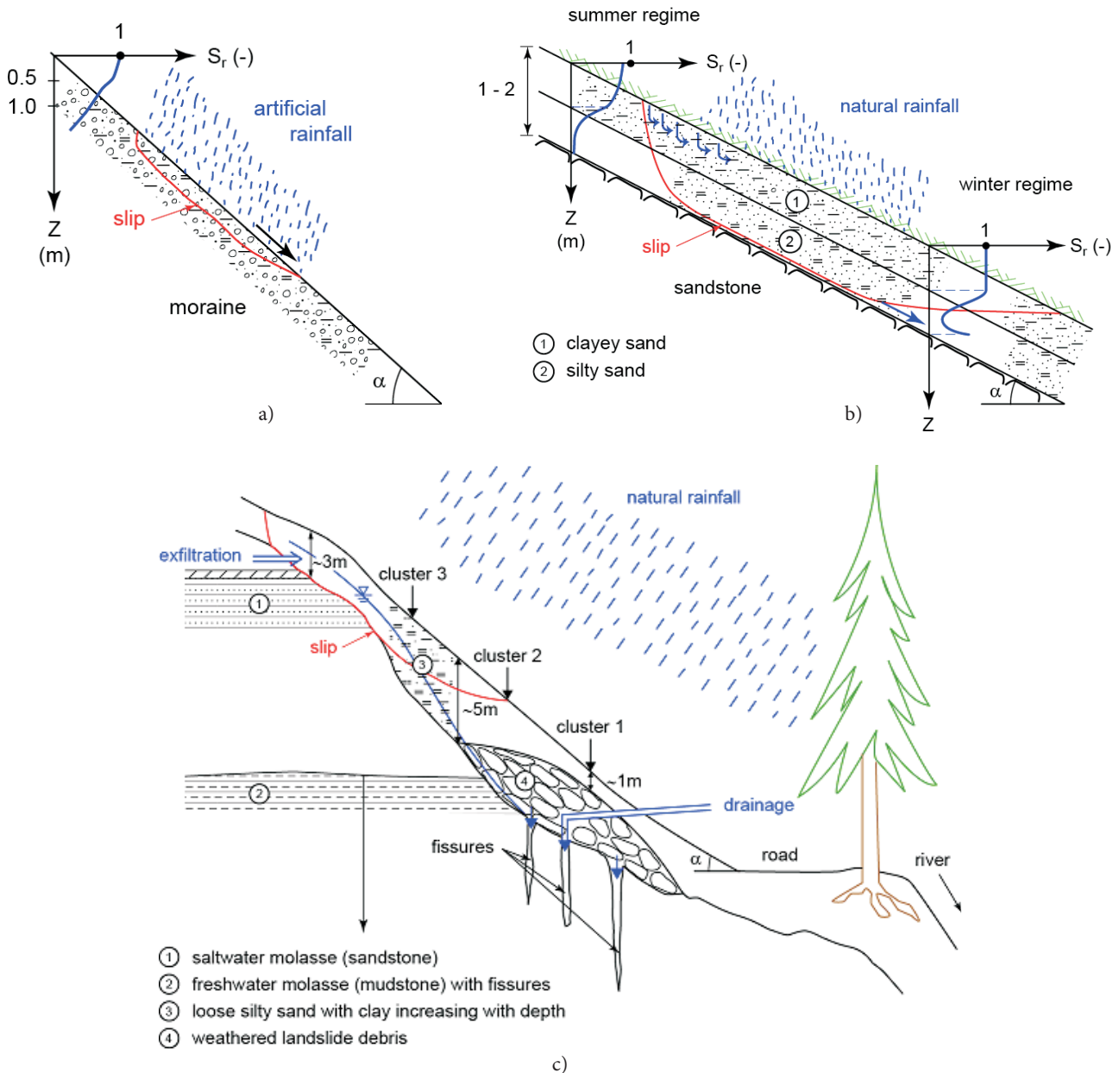


Figure 15. Saturation mechanisms after Springman [86] with a) ,top down' saturation through infiltration, typically moraine as in Gruben [57,71]; b) in summer regime ,top down', in winter regime additional ,bottom up' through run-off above bedrock, as for Tössegg [76]; c) exfiltration from and infiltration into underlying rock at Rüdlingen (sketch interpreted from [60]).

- 1) maintaining a constant pore-water pressure and decreasing the total stress accordingly (e.g., [71] after [35,88,89]);
- 2) maintaining a constant total stress and increasing the pore-water pressure (e.g., [80]).

The first was adopted for the Gruben site (Fig. 16) as principal effective stresses σ'_1 and σ'_3 (where σ'_1 and σ'_3 are the axial and radial effective stresses), were reduced at the same rate (0.5 kPa/h) until reaching failure, as

Constant Shear (deviator) stress Drained (CSD) paths in a large triaxial device [71]. Details of the sample preparation and consolidation paths for three CSD tests on 250-mm diameter, reconstituted, medium dense, moraine specimens, with a height of 500 mm and a maximum particle size up to 45 mm are described fully in [57] and [71]. Volumetric dilation and a slight hardening develop towards failure, with the gradient of the critical state line drawn as 1.59 in q - p' space ($q = \sigma'_1 - \sigma'_3$; $p' = (\sigma'_1 + 2\sigma'_3)/3$ for this stress path), through the fail-

ure state of the three tests, and leading to a value of $\phi' = 39^\circ$ at failure (Fig. 16). This is slightly lower than that deduced from the shear box data (41°) that are presented in the next section.

Another approach was adopted by Casini et al. [80] for the Rüdlingen silty sand (Fig. 17) to model the expected

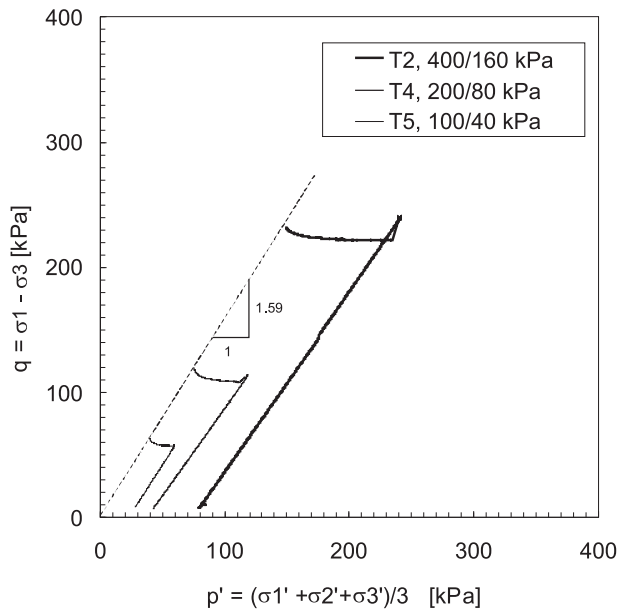


Figure 16. Constant Shear Drained (CSD) triaxial stress path tests on reconstituted Gruben moraine: stress path data shown in q - p' space with consolidation to σ_1'/σ_3' as shown in the legend, prior to shear (after [71]).

loss of p' due to a net increase in pore pressure without a change in the total stresses. Specimens were reconstituted and consolidated anisotropically before being subjected to drained shear under constant axial load (CADCAL). The mean effective stress was decreased by increasing pore-water pressure at a rate of 1 kPa/h for all drained stages, with the top and bottom drainage lines connected to a pore-pressure controller. The applied vertical load and radial stress were held constant throughout the tests [80].

Both specimens reached an ultimate failure stress ratio lying above a critical state line interpreted at an inclination of 1.3, representing $\phi' = 32.5^\circ$, and reaching values of $q/p' = \eta = 1.4$. Both specimens also demonstrated dilatant modes of failure; however, there had been concern that this soil might exhibit instability through shear strain acceleration towards failure, increase in plastic volume, accompanied by a significant loss in deviator and mean effective stress [80]. The behaviour of the soil was not

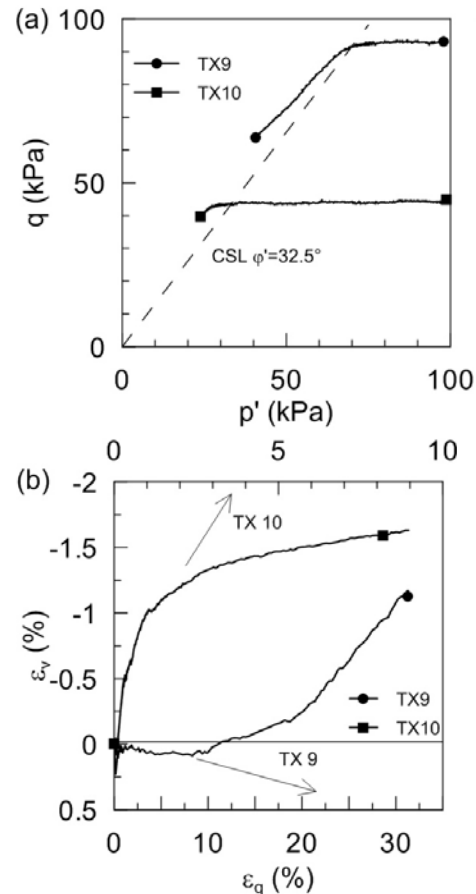


Figure 17. Anisotropic consolidation drained shear under constant axial load (CADCAL) triaxial stress path tests on reconstituted Rüdlingen silty sand: (a) stress path data shown in q - p' space; (b) ϵ_q - ϵ_v space, with strain axes at the top of TX10 and bottom for TX9 [80].

properly unstable in the stress paths analysed (e.g., [90]), but temporary instability, denoted by strain acceleration at constant external loading rate, triggered the soil failure in any case [80]. Unsaturated conditions and these transitional characteristics of the soil behaviour should be modelled, including the typical volumetric behaviour of fine-grained soils, strain-induced anisotropy, and time dependence. Possibly, the migration of the fines content during shear led to time-dependent, high compressibility while limiting the potential unstable mechanisms as the matrix developed a more stable orientation, much as proposed by Professor Šuklje in 1953 for one-dimensional secondary creep. The dilatant mode of failure observed in these CADCAL tests might be a possible explanation of drops of measured piezometric levels about 1 hour before the failure in the second Rüdlingen test [91]. The time of occurrence of these drops is comparable with the time at which the acceleration of the bending strains is measured by inclinometers, which can support this hypothesis.

SHEAR PARAMETER DETERMINATION THROUGH DIRECT SHEAR TESTS

A simple slope stability analysis is based on the assumption of an infinite slope and a suitable constitutive model, such as the Mohr Coulomb criterion, with some flexibility over the choice of appropriate parameters, including a cohesion c' as well as an internal friction angle ϕ' . For saturated soils with a shear strength τ_f along a shear plane:

$$\tau_f = c' + (\sigma_n - u_w) \tan \phi' \quad (1)$$

(where σ_n is the normal stress, u_w is the pore water pressure). The shear strength at failure along a base failure plane parallel to the slope surface (Eqns. 2 & 3) is enhanced by an apparent cohesion (here as c^*) for unsaturated conditions, which can also be related to the suction s by Gens [92]:

$$\tau_f = c'_{total} + (\sigma_n - u_a) \tan \phi',$$

where $c'_{total} = c' + s / (\cot \phi' + (\frac{s}{c}))$ (2a)

or as a function of the saturation degree S_r (e.g. [93]) from a Water Retention Curve (WRC) (e.g., [94,95]):

$$\tau_f = (\sigma_n - u_a) \tan \phi' + (u_a - u_w) S_r \tan \phi' \quad (2b)$$

Equation 2b can be written, as follows, with S_r and suction ($u_a - u_w$), which were determined from in-situ measurements (Fig. 18; [71]):

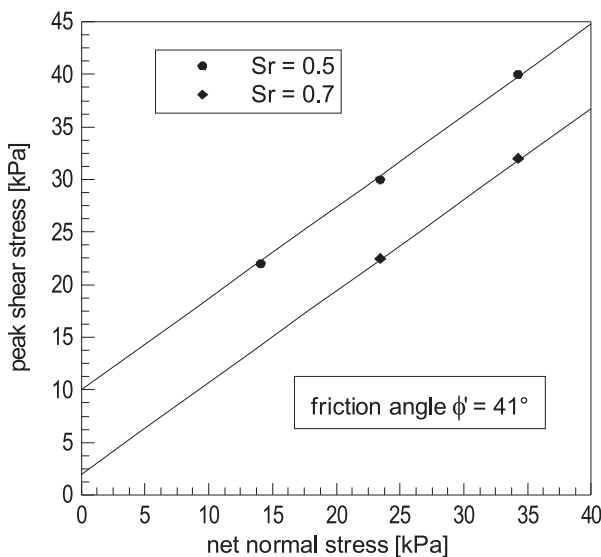


Figure 18. Gruben: shear-strength envelopes mobilised as a function of saturation degree: Peak shear stress v. net normal stress [71].

$$\tau_f = c^* + \sigma_n \tan \phi' \quad (3)$$

whereby for $u_a = 0$, with $c^* = (-u_w) S_r \tan \phi'$, the apparent cohesion c^* can be presented as a function of saturation degree, as in Fig. 19, for carrying out simple stability analyses. The intercept from Fig. 18 can be taken from the test series at different values of S_r , and plotted in Fig. 19 as a guide to selecting a suitable value of c^* for Equation 3. This data was derived from in-situ field direct shear tests [57,71], after the method developed by Fannin and Wilkinson [96]. This response is consistent with preceding experimental data (e.g., [97-98]).

The natural soil samples tested with in-situ direct shear tests exhibited marked dilatancy at failure for the applied stress levels [71]. Moreover, the TDRs installed in the vicinity of the eventual failure surface showed decreases in the degree of saturation at approximately 6 and 1.5 hours before the slip in the sprinkling experiment in 2000. This observation can be attributed to the dilative behaviour of the soil, which was measured in these series

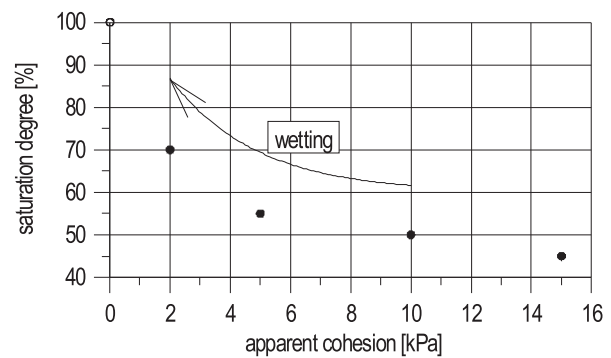


Figure 19. Relationship between saturation degree and apparent cohesion for alpine moraine in direct shear tests in the field [71].

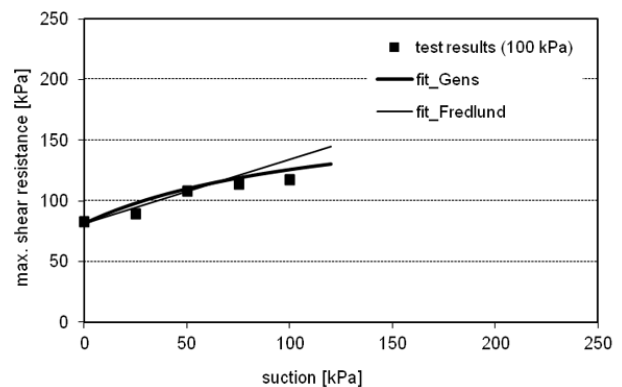


Figure 20. Tössegg: Shear strength envelopes for suction-controlled direct shear tests on silty sand with peak shear stress mobilised as a function of suction [after 58].

of in-situ direct shear box tests, or to the piping of fine-grained soil particles [91].

Thielen [58] used Gens' [92] simple criterion to represent the data for shear box tests conducted at the University of Catalunya on both the silty and the clayey sand in an apparatus designed to impose specific values of suction (Fig. 20). She reported values of ϕ' of 31° and 39° for clayey and silty sand, with c^* of 300 kPa at $\sigma_n = 40$ kPa and 1000 kPa at $\sigma_n = 100$ kPa for clayey sand and c^* of 100 kPa at $\sigma_n = 100$ kPa for silty sand. Also fitted against Thielen's [58] data was Fredlund et al.'s [99] criterion, although this is not pursued further in this paper.

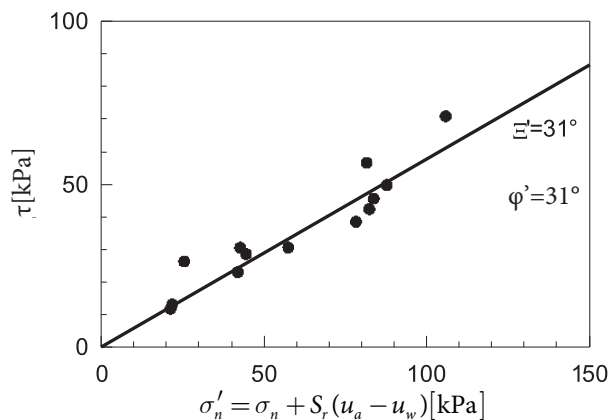


Figure 21. Rüdlingen: Interpretation of direct shear tests at constant water content to predict the critical state angle of friction for the reconstituted silty sand [100].

Shear data derived from direct shear tests conducted on unsaturated reconstituted Rüdlinger silty sand soil at constant water content [63], with a known value of water in the voids e_w compared to the total voids e , with the degree of saturation $S_r = e_w/e$ [100]. The results (Fig. 21) were interpreted from Equation 2b by allowing for the effects of suction derived from the WRC (e.g., [71,93,101,102]), which led to a lower bound of $\phi' = 31^\circ$ for these reconstituted specimens.

LIMIT EQUILIBRIUM CALCULATIONS

infinite slope conditions

Unsaturated conditions on the base shear plane

A global factor of safety SF against failure can be guaranteed to be considerably over 1.0 for many slopes in their natural states through the enhancement to shear resistance caused by suction. Stability calculations may be simplified to infinite-slope conditions in some

cases, whereby the shear zone at depth z is shallow relative to the width of the slope, which is assumed to be infinitely long. Balancing the force acting on each slice, assuming that the phreatic surface lies below the section concerned (e.g., after [71,103]), the following equation can be deduced for the factor of safety SF:

$$SF = \frac{\{(c^* / \cos^2 \alpha) + \gamma z \tan \phi'\}}{\gamma z \tan \alpha} \quad (4)$$

where γ is the unit weight of the soil (kN/m^3) and α the slope inclination. The necessary value of c^* for SF = 1.0 can be determined through Equation 5.

$$c^* = \gamma z \cos^2 \alpha \{ \tan \alpha - \tan \phi' \} \quad (5)$$

Saturated conditions on the base shear plane

A more traditional approach with a positive pore-water pressure was placed in Equation 6 based on an infinite saturated slope, with the groundwater level at a depth of z_1 and a shear surface at a depth of $z_1 + z_2$, in cases where the saturation developed from 'bottom up' (after Figs. 15b & c, although the failure surface is rather deep compared to the length), given by:

$$SF = \frac{c' + (\gamma z_1 + \gamma' z_2) \cos^2 \alpha \tan \phi'}{(\gamma z_1 + \gamma_{sat} z_2) \sin \alpha \cos \alpha} \quad (6)$$

where γ_{sat} is the unit weight of the soil in saturated conditions and $\gamma' = \gamma_{sat} - \gamma_w$.

two and simplified three dimensional approaches

Approximations can be made to adopt an inclined channel, with α as the slope angle, for cases in which the depth of the shear zone, z , is significant in comparison with the width, d , of a failure mechanism. The shear strength can be determined to include unsaturated conditions for homogeneous ground along the sides and base of the channel, if the shear surfaces are above the groundwater level [e.g. 63,100] and root reinforcement in the form of an additional cohesion c_r (e.g., [104]) also along the sides and base as may be required. An estimation of the relevant earth-pressure coefficient K was necessary to determine the effective stresses acting horizontally over the sides with depth. Amending c_r to account for changes with depth is indicated in Equation 7, in which a combined apparent cohesion can be input to the requisite equation to calculate the factor of safety for a channel of a specific width with a base shear plane at depth z :

$$c^* = S_r(u_a - u_w)\tan\varphi' + c_r(z) \quad (7)$$

Askarinejad et al., (2012b) present some two and three dimensional limit equilibrium solutions for these cases.

Application to Gruben

Why slopes become unstable during or shortly after intensive rainfall can be explained for a case history from a 42° steep moraine slope in Gruben (2000/2) with insitu unit weight $\gamma = 20.2 \text{ kN/m}^3$ and $\varphi' = 39^\circ$. Although saturation only reached 95% at a depth of $z < 0.5 \text{ m}$, a surficial failure occurred at this depth. Infinite slope conditions were assumed since the extent of the zone (Area $> 50 \text{ m}^2$) was large relative to the depth of failure ($< 0.5 \text{ m}$).

The minimum factor of safety (Eqn. 4) was calculated to be smaller than 1.0 without a contribution from an apparent cohesion. Although the failure in Gruben was only surficial, the value of $c^* < 1 \text{ kPa}$ was deduced at depths $z < 0.5 \text{ m}$, which agreed well with the results from the direct shear tests in the field ($40\% < S_r < 100\%$), (Figs.18 & 19), $0.2 < c^* < 0.5 \text{ kPa}$ for $0.9 < S_r < 0.95$ ($z \sim 0.2 \text{ m}$). Although some of these assumptions cannot represent the failure mechanism exactly, at least they help to explain why a failure surface at a depth of $< 0.5 \text{ m}$ is possible for a 42° slope, when $S_r = 0.95$.

Application to Tössegg

Although the shape of the critical failure surface is transitional towards a slip circular form at Tössegg [58], the outcomes are briefly described here. Thielen [58] used coupled thermo-hydraulic (TH) finite-element analyses within the Geostudio code VADOSE/W [105] both to model the slope response during the monitoring period at Tössegg, using data from one year to calibrate

the model and then to insert the parameters obtained in the second year of data to complete a validation. This was quite successful and then the relevant parameters and state in the ground were input to the parallel two-dimensional limit equilibrium SLOPE/W model [106] to find the critical failure mechanism. This was selected by the programme itself from the most critical case according to the approaches proposed by Morgenstern and Price [107], Spencer [108], Bishop and Morgenstern [109] or Janbu [110].

Calculations were carried out at monthly intervals for 2005 (Fig. 22). The lowest (2D) factor of safety was 1.74 on 1.2.2005, reflecting the saturated state of the clayey sand in the winter months and partial saturation in the underlying silty sand layer (see Figs. 11a&b; 15b). This is also conservative because side friction is ignored. It is unlikely that the factor of safety will approach unity given a lowest angle of friction of 31° and a steepest slope angle of 27° unless significant artesian pressures develop in the silty sand.

Application to Rüdlingen

Fig. 23 summarises a simplified stability analysis using a channel of infinite length and the dimensions shown as a slope inclination $\alpha = 40^\circ$, width of $d = 8 \text{ m}$ (Figs. 23a-d). A void ratio $e = 0.9$, a lateral earth pressure of $\sigma'_h = K(\sigma_v + S_r(u_a - u_w))$ and $K = 1 - \sin\varphi'$, with the water table at depths of $z = 0.8 \text{ m}$, 1.2 m , 4 m , and $\varphi' = 31^\circ$ were chosen as representative values for the field conditions in Rüdlingen.

The contribution from c_r was varied with depth (Eqn. 7) showing, as was deduced from the first experiment in October 2008, that the presence of roots and a deep water table was essential for stability (Fig. 23d). This is entirely consistent with the position described due to bottom

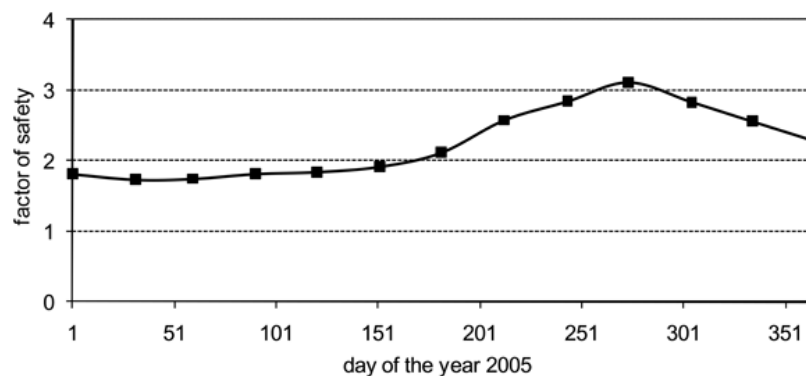


Figure 22. Tössegg: seasonal variation of factor of safety in 2005 against slope failure calculated using SLOPE/W after coupling with suctions and pore pressures obtained from TH Modelling with VADOSE/W (after [58]).

up saturation to build a water table above the bedrock (e.g. Fig. 15c) as the SF drops and with the critical shear surface at the boundary with bedrock as the water table rises from 4 m (Fig. 15d) to 1.2 m (Fig. 15c) to 0.8 m (Fig. 15b). The failure body (Fig. 13b) bottomed out on rock even though it has not followed a channel form with the base shear surface parallel to the surface and vertical sides.

A constant value of $c_r = 5\text{ kPa}$ along the sides and the base contributes to the stability in comparison with the case in which there is no contribution from the roots, or merely a local effect close to the surface (two other models with c_r constant at 5 kPa over the top 0.2 m of soil or with c_r reducing from 3 kPa over the top 0.2 m, decreasing by 1 kPa each additional 0.2 m).

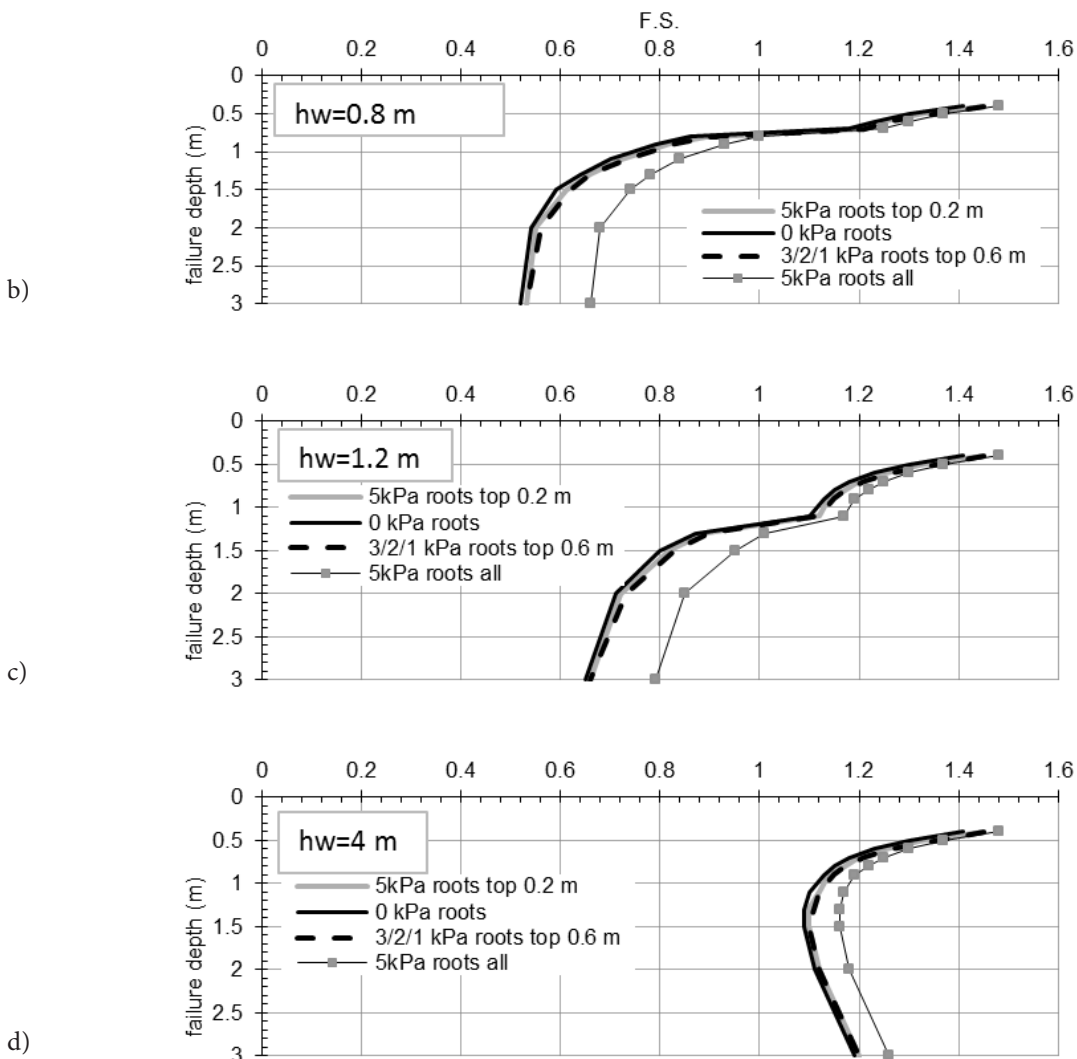
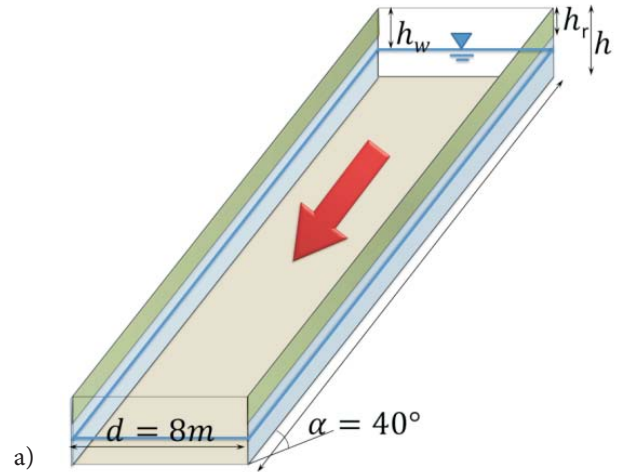


Figure 23. Two-dimensional limit equilibrium stability calculations for a channel geometry, including suctions (when above the water table) and root reinforcement on the sides and base: (a) channel dimensions with parameters appropriate for Rüdlingen; results for various values of c_r and water tables at (b) $z = 0.8\text{ m}$ (c) $z = 1.2\text{ m}$ (d) $z = 4\text{ m}$.

Fig. 23d shows the effect of suction combined with roots, in which the critical depth for such a failure mechanism with the lowest SF occurs between 1.2 to 1.4 m, depending upon the degree of root reinforcement. This was not too dissimilar from the values obtained, notwithstanding the differences between the geometry assumed in Fig. 23a and that observed in Fig. 13b.

Subsequently, Bischof [66], Malecki [67] and Askarinejad et al. [111] have investigated the development of failure mechanisms using more advanced coupled finite-element analyses, and further work is underway.

A PRACTICAL APPLICATION: CONDITION INDICATORS

'Condition Indicators' were adopted for the use of the observational method (Peck, 1969) to determine safe access to the test site in Rüdlingen (after Fig. 24) during the artificial rainfall experiments. The critical combination of S_r and suction $s (= u_a - u_w)$ in an infinite slope stability analysis, as described in Equations 4 above with $c^* = S_r(u_a - u_w)\tan\phi'$, was applied to the Ruedlingen slope. These provided the basis for an alarm system and were supported by observational markers: green ($s > 20$ kPa) – no restrictions on access or behaviour; orange (20 kPa $> s > 7$ kPa) – warning, within the uncertainty envelope for failure, restrictions to access on, below or within 10 m to the sides and above the slope; red ($s < 7$ kPa) - danger - whereas several activities could be permitted or limited, to reduce any risk to the participants and public.

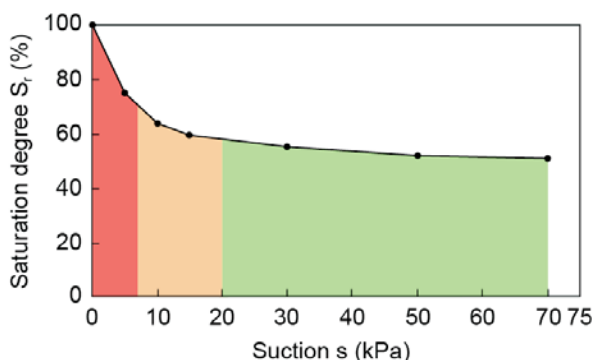


Figure 24. Relationship between saturation degree and suction of Rüdlingen silty sand in the laboratory based on the wetting branch of the Water Retention Curve [80] superimposed with alarm levels [86].

SUMMARY

Leroueil [113] observed that 'the failure of natural slopes constitutes an important geotechnical problem that involves a variety of geomaterials in a variety of geologi-

cal and climatic contexts, and which has a major socio-economic impact in many countries.' This paper reviews the state of knowledge for rainfall-induced landslides in primarily granular materials, examining the influence of partial saturation, infiltration and saturation regimes on slope failure.

The infiltration of rainfall has led to surface instability in slopes steeper than the internal angle of friction, just prior to full saturation being reached in three field sites in Switzerland that have been well characterised and instrumented. Each slope has contributed significant learnings and a generic approach to categorising the saturation of slopes has been proposed. This has been accompanied by several calculation methods that have been presented in this short contribution for adoption in making a preliminary judgement of slope stability.

Triaxial, field and laboratory shear box data have been used to determine the shear parameters for the mobilised shear strength at failure using a simple Mohr-Coulomb analysis and assuming the effect of suction is modelled by an apparent cohesion, which depends on the saturation degree. Alternatively, suction may be estimated from the saturation degree at various depths and included in a shear-strength envelope, which is dependent on suction and saturation degree. Prediction of this 'apparent cohesion' term has been made, by adopting a factor of safety equal to unity under simple limit equilibrium, infinite-slope stability analysis with an extension to a simplified three-dimensional case where necessary.

An apparent cohesion, depending upon saturation degree, offers a simple option for modelling the significantly more complex unsaturated behaviour in a slope, whereas the modelling benefits greatly from understanding of the slope hydrology and the way in which the cyclical saturation and drainage processes develop with time. Despite the simplicity of the analyses and extreme heterogeneity of the moraine, it was found for the moraine slope in both cases that the factor of safety reduced almost to unity at depths of ≤ 0.5 m for the 42° slope, as had been observed from the field test.

Despite modern computational capacity and highly advanced, multi-parameter, constitutive models, a case is made that the use of simple models is still as valid today as they were in Professor Šuklje's time. The presence of water in slopes, as discussed by Professor Šuklje, will always challenge the calculation of stability. However, understanding the mechanisms and applying simple and robust models and good engineering judgement can often lead to the ability to make challenging decisions about slope safety.

ACKNOWLEDGEMENTS

While the 2011 Šuklje lecturer and first author was never privileged enough to have met Professor Šuklje herself, she acknowledges his signal contribution to soil mechanics with gratitude, remembering, with great pleasure, the most excellent Balkan Conference in Ljubljana in 2006, organised so well by his students and mentees [114].

The authors would like to thank Ernst Bleiker, Marco Sperl, Dr. Cornelia Brönnimann, Prof. Cristina Jommi, Dr. Massi Schwarz, Dr. Barbara Suski, Francesca Gambazzi, Gernot Michlmayr, Werner Attinger, Karl Steiner, Dr. Christian Rickli, Dr. Manfred Stähli, Dr. Andreas Schmid, Dr. Peter Lehmann, Prof. Dani Or, Dr. Mathieu Nuth, René Rohr for their various contributions to the fieldwork presented here. We would also like to express our warm gratitude to Ms Mengia Amberg and Mrs Gabriela Laios for their help with graphics and text, also to Dr.-Ing. Jan Laue, Dipl. Ing. ETH Ralf Herzog, Dipl. Ing. Pierre Mayor, Adrian Zweidler, Heinz Buschor, Fredy Ehrbar, Anita Meyer for their help and advice in the workshops and laboratory. Constructive discussions with Prof. Paolo Burlando, Dr. Peter Molnar, Dr. Les Davison, and Dr. Muni Budhu are also recognised.

The authors extend grateful thanks to various funding bodies including the Department for Construction, Environment and Traffic of the Canton of Valais and the Federal Office for Water and Geology, HazNETH, Mr and Mrs Fritschi, Mrs Hildebrand and Mr Gehring, the Gemeinde Rüdlingen and the Canton of Schaffhausen, the Competence Centre for Environmental Sustainability at ETH Zurich (project Triggering Rapid Mass Movements) and the project SAFELAND funded by the EU 7th Framework Programme for their technical and financial support for these projects.

REFERENCES

- [1] Majes, B. (2010). At the occasion of the 100th anniversary of academician Prof. Dr. Lujo Šuklje. *Proc. Zbornik Referatov, 11. Sukljetovi dnevi*, September 17, 2010, Brdopri Kranju.
- [2] Šuklje, L. (1969). *Rheological Aspects of Soil Mechanics*. Wiley-Interscience, John Wiley & Sons Ltd, London, New York, Sydney, Toronto.
- [3] ICOSOMEF, (1953). *Proc. of the Third Int. Conference on Soil Mechanics and Foundation Engineering*.
- [4] Šuklje, L. (1953). General reports, (a) Session 4, Foundation of Buildings and Dams, Bearing Capacity, Settlement Observations, Regional Subsidence, p. 167/168. (b) Session 8, Stability and Deformations of Slopes and Earth Dams, Research on Pore-Pressure Measurements, Groundwater Problems, p. 211. *Proc. of the Third Int. Conference on Soil Mechanics and Foundation Engineering*, August 16-27, 1953, Zurich, Switzerland, Vol. III.
- [5] Nater, P. (2005). Belastungs- und Verformungsverhalten von geschichteten Bodensystemen unter starren Kreisfundationen; (Load and deformation response of stiff foundations on layered soil) ETH-Diss. Nr. 16319.
- [6] Arnold, A. (2011). Tragverhalten von nicht starren Flachfundationen unter Berücksichtigung der lokalen Steifigkeitsverhältnisse; ETH-Diss. Nr. 19516.
- [7] Springman, S.M. (2002). Constitutive and Centrifuge Modelling: Two Extremes. Balkema, Rotterdam.
- [8] Nonveiller, E. and Šuklje L. (1954). "Landslide Zalesina". *Proc. of the European Conference on Stability of Earth Slopes*, September 20-25, 1954, Stockholm, Sweden, Vol. 1. also repeated as Nonveiller, E. and Suklje L. (1955). "Landslide Zalesina". *Géotechnique*, Volume V, London, Great Britain.
- [9] Schofield, A.N. (2005). *Disturbed Soil Properties and Geotechnical Design*. Publisher: Thomas Telford Ltd., London.
- [10] Henkel, D.J. and Skempton, A.W. (1955). A Landslide at Jackfield, Shropshire, in a Heavily Over-Consolidated Clay. *Géotechnique*, Vol. 5, No. 2, pp. 131-137.
- [11] Peck, R.B. (1967). Stability of natural slopes. *Journal of Geotech. Eng. Div. ASCE*, Vol. 93, No. 4, pp. 403-418.
- [12] Lumb, P.B. (1975). Slope failures in Hong Kong. *Quarterly Journal of Eng. Geology*, Vol. 8, pp. 31-65.
- [13] Brand, E.W., Premchitt, J. and Phillipson, H.B. (1984). Relationship between rainfall and landslides in Hong Kong. *Proc. 4th Int. Symp. on Landslides I*, pp. 377-384.
- [14] Alonso, E., Gens A. and Lloret, A. (1995). Effect of rain infiltration on the stability of slopes. *Unsaturated Soils*, pp. 241 - 249.
- [15] FAN-Agenda. (2008). Special issue of TRAMM including 9 short articles. *Fachleute Naturgefahren Schweiz*.
- [16] Lateltin, O., Bollinger, D., Hegg, C. and Keusen, H-R. (2001). The analysis of the 1999 landslides in Switzerland. *Proc Int. Conf. on Landslides*, Davos, pp. 159-167.
- [17] Dapples, F., Oswald, D. and Raetzo, H. (2001). Landslides in the Western Swiss Alps: Causes,

- Triggers and dynamic aspects from former to present times. *Proc Int. Conf. on Landslides*, Davos, pp. 3-11.
- [18] Lim, T.T., Rahardjo, H., Chang, M.F. and Fredlund, D.G. (1996). Effect of rainfall on matric suctions in a residual soil slope, *Can. Geotech. J.*, Vol. 33, pp. 618-628.
- [19] Low, T.H., Faisal, H.A. and Saravanan, M. (2000). Suction and infiltration measurements on cut slope in highly heterogeneous residual soil. *Unsaturated Soils for Asia*.
- [20] Ng, C.W.W, Zhan, L.T., Bao, C.G., Fredlund, D.G. and Gong, B.W. (2003). Performance of an unsaturated expansive soil slope subjected to artificial rainfall infiltration. *Géotechnique* Vol. 53, No. 2, pp. 143-157.
- [21] Ng, C.W.W., Springman, S.M. and Alonso, E.E. (2009). Monitoring the Performance of Unsaturated Soil Slopes. *Geotechnical and Geological Engineering*, Vol. 26, No. 6, pp. 799-816, Special Issue on Laboratory and Field Testing of Unsaturated Soils. <http://dx.doi.org/10.1007/s10706-008-9203-6> and Book Chapter in Laboratory and Field Testing of Unsaturated Soils.(eds. A. Tarantino,E. Romero, Y.-J. Cui), Springer Verlag, 187-204.
- [22] Rahardjo, H., Hua, C.J., Leong, C. and Santoso, V.A. (2010). Performance of an Instrumented Slope under a Capillary Barrier System, *5th International Conference on Unsaturated Soils*, Barcelona.
- [23] Premchitt, J., Brand, E.W. and Phillipson, H.B. (1986). Landslides caused by rapid groundwater changes. *Groundwater in Engineering Geology*. Geological Soc., London, Eng. Geol. Spec. Pub 3: pp. 87-94.
- [24] Ng, C.W.W. and Shi, Q. (1998). Influence of rainfall intensity and duration on slope stability in unsaturated soils. *Quarterly J. of Eng. Geology*, Vol. 31, pp. 105-113.
- [25] Caine, N. (1980). The rainfall intensity-duration control of shallow landslides and debris flows. *Geografiske Annaler*. Vol. 62A, pp. 23-27.
- [26] Guzzetti, F., Peruccacci, S., Rossi, M. and Stark, C.P. (2008). The rainfall intensity-duration control of shallow landslides and debris flows: an update. *Landslides* Vol. 5, pp. 3-17. DOI 10.1007/s10346-007-0112-1 Springer-Verlag.
- [27] Innes, J.L. (1983). Debris flows. *Prog. Phys. Geogr.*, Vol. 7, pp. 469-501.
- [28] Clarizia, M., Gullà, G. and Sorbino, G. (1996). Sui meccanismi di innesco dei soil slip. International conference. *Prevention of hydrogeological hazards: the role of scientific research*. 1, pp. 585-597, (in Italian).
- [29] Crosta, G.B. and Frattini, P. (2001). Rainfall thresholds for triggering soil slips and debris flow. Mediterranean storms. *Proceedings of the 2nd EGS Plinius Conference on Mediterranean Storms*. Siena, Italy, pp. 463-487.
- [30] Cannon, S.H. and Gartner, J.E. (2005). Wildfire-related debris flow from a hazards perspective. *Debris flow hazards and related phenomena*. Springer, Berlin, pp. 363-385.
- [31] Chipp, P.N., Henkel, D.J., Clare, D.G. and Pope, R.G. (1982). Field measurements of suction in colluvium covered slopes in Hong Kong. *Proceedings, 7th Southeast Asian Geotechnical Conference*, Hong Kong, Vol. 1, pp. 49-61.
- [32] Sweeney, D.J. (1982). Some in situ soil suction measurements in Hong Kong's residual soil slopes. *Proceedings, 7th Southeast Asian Geotechnical Conference*, Hong Kong, Vol. 1, pp. 91-106.
- [33] Krahn, J., Fredlund, D.G. and Klassen, M.J. (1989). Effect of soil suction on slope stability at Notch Hill. *Canadian Geotechnical J.*, Vol. 26, pp. 269-278.
- [34] Affendi, A.A. and Faisal, A. (1994). Field measurement of soil suction. *13th Int. Conf. on Soil Mechanics and Foundation Engineering*, New Delhi, India, pp. 1013-1016.
- [35] Zhu, J.-H. and Anderson, S.A. (1998). Determination of shear strength of Hawaiian residual soil subjected to rainfall-induced landslides, *Géotechnique*, Vol. 48, No. 1, pp. 73-82.
- [36] Zhang, J., Jiao, J.J. and Yang, J. (2000). In situ rainfall infiltration studies at a hillside in Hubei Province, China. *Engineering Geology*, Vol. 57, pp. 31-38.
- [37] Ridley, A.M., Dineen, K., Burland, J.B. and Vaughan, P.R. (2003). Soil matrix suction: some examples of its measurement and application in geotechnical engineering, *Géotechnique*, Vol. 53, No. 2, pp. 241-252.
- [38] Rahardjo, H., Lee, T.T., Leong, E.C. and Rezaur, R.B. (2005). Response of a residual soil slope to rainfall. *Canadian Geotechnical J.*, Vol. 42, pp. 340-351.
- [39] Smethurst, J.A., Clarke, D. and Powrie, W. (2006). Seasonal changes in pore water pressure in a grass-covered cut slope in London Clay. *Géotechnique*, Vol. 56, No. 8, pp. 523-537.
- [40] Raetzo, H. and Rickli, C. (2007). Rutschungen. Ereignisanalyse Hochwasser 2005. BAFU Bern & WSL Birmensdorf. pp. 195-209.
- [41] Brandl, H. (2010). Rock engineering for structures in unstable slopes. *Keynote paper of the ISRM Regional Symposium EUROCK 2009 Rock Engineering in Difficult Ground Conditions - Soft Rocks*

- and Karst. Dubrovnik, Croatia. pp. 37-48.
- [42] Sandersen, F., Bakkehoi, S. and Lied, K. (1996). The influence of meteorological factors on the initiation of debris flows, rockfalls, rockslides and rock-mass stability. *Landslides, Glissement de terrain*, Vol. 1, pp. 97-114.
- [43] Spiereburg, S.E.J., van Esch, J.M. and Koehorst, B.A.N. (1995). Slope stability during infiltration. *Unsaturated Soils*, pp. 309-314.
- [44] Kienzler, P., Brönnimann, C., Thielen, A., Lehmann, P., Kauer, S. and Springman, S.M. (2010). Water flow and saturation of hillslopes prone to shallow landslides. *CCES Latsis Symposium*, Zürich, Switzerland.
- [45] Flint, A.L. and Flint, L.E. (2005). Infiltration and percolation processes in shallow soils underlain by fractured bedrock. *Abstract in Salt Lake City Annual Meeting*, Salt Lake City, Utah.
- [46] Wilson, J.L. and Guan, H. (2005). Water percolation across the soil-bedrock interface in mountainous terrain. *Abstract in Salt Lake City Annual Meeting*, Salt Lake City, Utah.
- [47] Brönnimann, C. and Tacher, L. (2009). Water related triggering mechanisms of shallow landslides: Numerical modelling of hydraulic flows in slopes verified with field experiments. *European Geosciences Union General Assembly*, Vienna, Austria.
- [48] Brönnimann, C., Tacher, L., Askarinejad, A., Kienzler, P. and Springman, S. (2009). Porewater pressure modelling in a rainfall triggered shallow landslide: the sprinkling experiment in Ruedlingen, Canton of Schaffhausen. *7th Swiss Geoscience Meeting*, Neuchâtel, Switzerland.
- [49] Tacher, L., Springman, S.M., Askarinejad, A., Kienzler, P., Holliger, K. and Or, D. (2010). The slope failure of the Rüdlingen triggering experiment with regard to the geological setting and hydrogeological processes. *TRAMM International conference, Triggering the Rapid Mass Movements in Steep Terrains - Mechanisms and Risk, Monte Verità, Switzerland, Poster*.
- [50] Brönnimann, C., Tacher, L., Jaboyedoff, M., Jongmans, L., Springman, S.M. and Askarinejad, A. (2010). The effect of bedrock originated groundwater on the triggering mechanism of different landslides in Switzerland. *European Geosciences Union, General Assembly 2010, Vienna, Austria, Poster*.
- [51] Frei, M. (2009). Validation of a new approach to determine vegetation effects on superficial soil movements. ETH-Diss. Nr. 18455.
- [52] Schwarz, M. (2010). Hydro-mechanical characterization of rooted hillslope failure: from field investigations to fiber bundle modeling. ETH-Diss. Nr. 19124. DOI: 10.3929/ethz-a-006371197.
- [53] Müller, C.J. (2005). Pozzolan activity of Natural Clay Minerals with Respect to Environmental Geotechnics. ETH-Diss. Nr. 16299.
- [54] Friedel, S., Byrdina, S., Jacobs, F. and Zimmer, M. (2004). Self-potential and ground temperature at Merapi volcano prior to its crisis in the rainy season of 2000 – 2001. *J. of Volc. and Geothermal Res.*, Vol. 134, No. 3, pp. 149-168, DOI: 10.1016/j.jvolgeores.2004.01.
- [55] Atlas der Schweiz. (2002). www.atlasderschweiz.ch/.
- [56] Cortona, L. (2001). Laboratory and field investigations on morainic soils: Diplomarbeit SS 1999, jointly for IGT-ETH Zurich and Politecnico di Torino.
- [57] Teyssie, P. (2005). Geotechnische Eigenschaften von Moränen (Geotechnical properties of (alpine) moraine), ETH-Diss. Nr. 16322: <http://e-collection.ethbib.ethz.ch/view/eth:28575>
- [58] Thielen, A. (2007). Einfluss der Bodensättigung auf die Stabilität von Hängen (Influence of soil saturation on the stability of slopes), ETH-Diss. Nr. 17303: <http://e-collection.ethbib.ethz.ch/view/eth:29862>.
- [59] Gilgen, M. (2008). Hydrological Simulation of a Hillslope Prone to Shallow Landslides. Diploma thesis. Dept. Environmental Sci., ETH Zürich, DOI: 10.3929/ethz-a-005676916.
- [60] Brönnimann, C. (2011). Effect of Groundwater on Landslide Triggering. EPFL Dissertation.
- [61] Askarinejad, A. (2012). Failure mechanisms in unsaturated silty sand slopes triggered by rainfall. Dissertation Dr.sc. ETH.
- [62] Colombo, L. (2009). Large shear box for analysing strength mobilisation in unsaturated conditions. Politecnico di Milano Master thesis.
- [63] Minder, P. (2010). Shear resistance of silty sand from the Rüdlingen monitoring and triggering test site. Semester Project. Institute for Geotechnical Engineering, ETH Zurich.
- [64] Beck, A. (2011a). Measurement of unsaturated hydraulic conductivity with the instantaneous profile method. Semester Project. Institute for Geotechnical Engineering, ETH Zurich.
- [65] Beck, A. (2011b). Measurement of Unsaturated Hydraulic Conductivity with the Instantaneous Profile Method. Masters Dissertation. Institute for Geotechnical Engineering, ETH Zurich.
- [66] Bischof, P. (2011). Modelling the interaction of the bedrock and slope in terms of drainage and exfiltration. Semester Project. Institute for Geotechnical Engineering, ETH Zurich.
- [67] Malecki, C. (2011). Finite element parametric study of landslide induced by rainfall. Masters

- Dissertation. Institute for Geotechnical Engineering, ETH Zurich.
- [68] Hilber Schob, I. (2011). Impact of root growth on soil microstructure, Rüdlingen, SH. Masters Dissertation. Master of Advanced Studies. ETH Zurich.
- [69] Petkovšek, A., Pavsic, P., Kokot, D. and Leben, B. (2006). Using dielectric measurements to predict seasonal water movement in unbound road base and sub-grade layers. *Proc. of the XIIIth Danube-European Conference on Geotechnical Engineering, Ljubljana, Slovenia*, Vol. 2.
- [70] Springman, S.M. and Teyssiere, P. (2001). Artificially induced rainfall instabilities on moraine slopes. *Proc Int. Conf. on Landslides, Davos*, pp. 209-223.
- [71] Springman, S.M., Jommi, C. and Teyssiere, P. (2003). Instabilities on moraine slopes induced by loss of suction: a case history. *Géotechnique*, Vol. 53, No. 1, pp. 3-10.
- [72] Teyssiere, P., Cortona, L. and Springman, S.M. (2000). Water retention in a steep moraine slope during periods of heavy rain. *Proc. Unsaturated Soils for Asia, Singapore*, pp. 831-836.
- [73] Fischer, C., López, J. and Springman, S.M. (2003). Remediation of an eroded steep slope in weathered sandstone after a major rainstorm. *International Conference on Slope Engineering, Hong Kong*.
- [74] Thielen, A. and Springman, S.M. (2005). First results of a monitoring experiment for the analysis of rainfall induced landslides. *EXPERUS 2005 Advanced Experimental Unsaturated Soil Mechanics, Trento, Italy*, pp. 549-554.
- [75] Friedel, S., Thielen, A. and Springman, S.M. (2006). Investigation of a slope endangered by rainfall-induced landslides using 3D resistivity tomography and geotechnical testing. *J. of Applied Geophysics*, Vol. 60, No. 2, pp. 100-114.
- [76] Thielen, A., Springman, S.M., Kienzler, P. and Friedel, S. (2012). A long term field study for the investigation of rainfall induced landslides. *Géotechnique*. In review.
- [77] Kienzler, P., Naef, F. and Springman, S.M. (2008). Hillslope hydrology and landslide triggering. *International Workshop on Unsaturated Soils IWUS, Trento*.
- [78] Flury, M., Flühler, H., Jury, W.A. and Leuenberger, J. (1994). Susceptibility of soils to preferential flow of water: a field study. *Water Resources Res.*, Vol. 30, No. 7, pp. 1945-1954.
- [79] Springman, S.M., Kienzler, P., Casini, F. and Askarinejad, A. (2009). Landslide triggering experiment in a steep forested slope in Switzerland. *17th Int. Conf. of Soil Mech. & Geot. Eng. Alexandria, Egypt*, pp. 1698-1701.
- [80] Casini, F., Jommi, C. and Springman, S.M. (2010). A laboratory investigation on an undisturbed silty sand from a slope prone to landsliding. *Granular Matter*, Vol. 12, No. 3, pp. 303-316. DOI: 10.1007/s10035-010-0182-y.
- [81] Askarinejad, A., Beck, A., Casini, F. and Springman, S.M. (2012). Unsaturated hydraulic conductivity of a silty sand with the instantaneous profile method. *II European Conference on Unsaturated Soils (E-UNSAT2012)*, Naples, Italy.
- [82] Lehmann, P., Gambazzi, F., Suski, B., Baron, L., Askarinejad, A., Springman, S.M., Holliger, K. and Or, D. (2012). Evolution of wetting patterns preceding hydro-mechanically induced landslide inferred from electrical resistivity tomography. *Water Resources Res.* Submitted.
- [83] Akca, D., Gruen, A., Askarinejad, A. and Springman, S.M. (2011). Photogrammetric monitoring of an artificially generated land slide. *International Conference on Geo-information for Disaster Management (Gi4DM)*, Antalya, Turkey, Published on CD-ROM only.
- [84] Askarinejad, A., Casini, F., Bischof, P., Beck, A. and Springman, S.M. (2012). Rainfall induced instabilities in a silty sand slope: a case history in northern Switzerland. *Rivista Italiana di Geotecnica*. Submitted.
- [85] Askarinejad, A. (2009). A method to locate the slip surface and measuring subsurface deformations in slopes. *4th International Young Geotechnical Engineers' Conference, Alexandria, Egypt*, pp. 171-174.
- [86] Springman, S.M. (2008). Einfache Hangstabilitätsanalyse mit Berücksichtigung ungesättigter Verhältnisse - Analyse simple de la stabilité des pentes sous considération de conditions non saturées. *TRAMM, FAN Fachleute Naturgefahren Schweiz Agenda*, pp. 7-11.
- [87] Mayne, P.W., Coop, M.R., Springman, S.M., Huang, A.B. and Zornberg, G.R. (2009). Geomaterial behavior and testing. *17th International Conference on Soil Mechanics & Geotechnical Engineering ICSMGE, Alexandria, Egypt*, Vol. 4, pp. 2777-2872.
- [88] Anderson, S.A. and Sitar, N. (1994). Procedures for analysis of the mobilization of debris flow. *Proceedings of 13th International Conference on Soil Mechanics and Foundation Engineering, New Delhi, India*, pp. 255-258.
- [89] Ng, C.W.W., Fung, W.T., Cheul, C.Y. and Zhang, L. (2004). Influence of stress ratio and stress path on behavior of loose decomposed granite. *J. Geotech. Eng. ASCE*, Vol. 130, No. 1, pp. 36-44.
- [90] Chu, J., Leroueil, S. and Leong, W.K. (2003). Unstable behaviour of sand and its implication for slope instability. *Canadian Geotechnical J.*, Vol. 40, pp. 873-885.

- [91] Askarinejad, A. Casini, F. Kienzler, P., Teyssere, P. and Springman, S.M. (2010). Mountain risks: two case histories of landslides induced by artificial rainfall on steep slopes. *International Conference 'Mountain Risks: Bringing Science to Society'*, Florence, Italy, pp. 201-206.
- [92] Gens, A. (1993). Shear strength. Proceedings of the Unsaturated Soils: Recent developments and applications. *Civil Engineering European Course*, Barcelona, pp. 1-13.
- [93] Öberg, A. and Sällfors, G. (1997). Determination of shear strength parameters of unsaturated silts and sands based on the water retention curve. *Geotechnical Testing J.*, Vol. 20, No. 1, pp. 40-48.
- [94] Van Genuchten, M.T. (1980). A closed-form for predicting the hydraulic conductivity of unsaturated soils, *Soil Sci. Soc. Am. J.*, Vol. 44, pp. 892-898.
- [95] Fredlund, D.G. and Xing, A. (1994). Equations for the soil water characteristic curve, *Canadian Geotechnical J.*, Vol. 31, pp. 521-532.
- [96] Fannin, R.J. and Wilkinson, J.M.T. (1995). An analysis of the Jamieson Creek landslide. *Proc. 48th Canadian Geotech. Conf.*, Vancouver, pp. 635-642.
- [97] Nicotera, M.V. (2000). Interpretation of shear response upon wetting of natural unsaturated pyroclastic soils. *Experimental Evidence and Theoretical Approaches in Unsaturated Soils*, pp. 77-192.
- [98] Evangelista, A. and Scotto di Santolo, A. (2001). Mechanical behaviour of unsaturated pyroclastic soils. *Proc. Int. Conf. on Landslides*, Davos, pp. 35-44.
- [99] Fredlund, D.G., Morgenstern, N.R. and Widger, R.A. (1978). The shear strength of unsaturated soils. *Canadian Geotechnical J.*, 15(3): 313-321.
- [100] Casini, F., Minder, P. and Springman, S. (2010). Shear strength of an unsaturated silty sand. *5th International Conference on Unsaturated Soils*, Barcelona, Spain, pp. 211-216.
- [101] Miao, L., Yin, Z., and Liu, S. (2001). Empirical function representing the shear strength of unsaturated soils. *Geotechnical Testing J.*, Vol. 24, pp. 220-223.
- [102] Vaunat, J., Romero, E., Marchi, C. and Jommi, C. (2002). Modeling the shear strength of unsaturated soils. *3rd Int. Conf. on Unsaturated Soils*, Vol. 2, pp. 245-251.
- [103] Lambe, T.W. and Whitman, R.V. (1979). *Soil Mechanics*. SI Version. John Wiley & Sons, New York.
- [104] Wu, T.H. (1995). *Slope stabilization. Slope Stabilization and Erosion Control: A Bioengineering Approach*. E&FN Spon, Chapman & Hall, London.
- [105] Krahn, J. (2004a). *Vadose Zone Modeling with VADOSE/W. An engineering methodology, Manual, GeoStudio software.*
- [106] Krahn, J. (2004b). *Stability Modeling with SLOPE/W. An engineering methodology, Manual, GeoStudio software.*
- [107] Morgenstern, N.R. and Price, V.E. (1965). The Analysis of the Stability of General Slip Surfaces. *Géotechnique*, Vol. 15, No. 1, pp. 79-93.
- [108] Spencer, E. (1967). A Method of Analysis of Embankments and Slopes. *Géotechnique*, Vol. 17, No. 1, pp. 11-26.
- [109] Bishop, A.W. and Morgenstern, N.R. (1960). Stability coefficients for earth slopes. *Géotechnique*, Vol. 10, No. 4, pp. 164-169.
- [110] Janbu, N. (1954). Applications of Composite Slip Surfaces for Stability Analysis. *Proceedings of the European Conference on the Stability of Earth Slopes*, Stockholm, pp. 39-43.
- [111] Askarinejad, A., Bischof, P., Casini, F. and Springman, S.M. (2012). The effects of hydraulic properties of bedrock on the stability of slopes. *II European Conference on Unsaturated Soils (E-UNSAT2012)*, Naples, Italy.
- [112] Peck, R.B. (1969). Advantages and limitations of the observational method in applied soil mechanics. *Géotechnique*, Vol. 19, No. 2, pp. 171-187.
- [113] Leroueil, S. (2001). Natural slopes and cuts: Movement and failure mechanisms, *Géotechnique*, Vol. 51, No. 3, pp. 197-243.
- [114] Logar, J., Gaberc, A. and Majes, B. eds. (2006). "Active Geotechnical Design in Infrastructure Development". *Proc. of the XIIIth Danube-European Conference on Geotechnical Engineering*, Ljubljana, Slovenia, Vol. 2: Papers.

POPUŠČANJE V ENAKOSMERNEM STISKANJU PORTSKEGA MELJNEGA PESKA

MIGUEL FERREIRA AMARAL, SARA RIOS ĀN ANTÓNIO VIANA DA FONSECA

o avtorjih

Miguel Ferreira Amaral
University of Porto,
Portugalska
E-pošta: mfamaral@fe.up.pt

Sara Rios
University of Porto,
Portugalska
E-pošta: dec06004@fe.up.pt

António Viana da Fonseca
University of Porto,
Portugalska
E-pošta: viana@fe.up.pt

izvleček

Analizirano je mesto popuščanja dobro zrnjavega meljnega peska s testi enakosmernega stiskanja in vrstičnim elektronskim mikroskopiranjem (SEM). Testi so izvedeni z natančnimi instrumenti, za notranje in zunanje meritve deformacij, in meritve hitrosti strižnega valovanja s pomočjo upogibnih elementov. Z namenom, da bi določili natančno napetostno tečenje, so bile nazadnje uporabljene štiri različne metode - dve sta dokaj dobro znani in ostali dve sta novosti - kar je pripeljalo do zanimivih zaključkov.

ključne besede

meljni pesek, točka popuščanja, enakosmerno stiskanje, visok pritisk, potresni valovi

YIELDING IN THE ISOTROPIC COMPRESSION OF PORTO SILTY SAND

MIGUEL FERREIRA AMARAL, SARA RIOS and ANTÓNIO VIANA DA FONSECA

about the authors

Miguel Ferreira Amaral
University of Porto,
Portugal
E-mail: mfamaral@fe.up.pt

Sara Rios
University of Porto,
Portugal
E-mail: dec06004@fe.up.pt

António Viana da Fonseca
University of Porto,
Portugal
E-mail: viana@fe.up.pt

abstract

The yielding locus of a well-graded silty sand was analysed by means of isotropic compression tests and scanning electron microscopy (SEM). The tests were performed with precise instrumentation, for internal and external strain measurements, and shear-wave velocity measurements by means of bender elements. Finally, aiming at an accurate evaluation of the yield stress, four different methods were applied – two quite well know and the other two being innovative – leading to interesting conclusions.

keywords

silty sand, yield point, isotropic compression, high pressure, seismic waves

1 INTRODUCTION

Modelling the behaviour of a soil, rock or concrete due any stress path, necessarily requires a yield-locus assumption [1] – a point on a curve if that is the object of the analysis – that separates the elastic from the elasto-plastic region. This point indicates the instant at which any stress increment causes irreversible strains that may arise in granular soils from particle crushing

or other processes associated with the increase in the compressibility [2,3,4]. However, the beginning of particle crushing is usually gradual; therefore, it is usually difficult to define a clear elastic limit due to an initial load [5]. During reloading and unloading, the soil shows a stiffer behaviour as the particles remain broken [5].

Since the very early years of soil mechanics, researchers created criteria and formulated models in order to explain the concept of yielding in materials [3,6,7]. This paper focuses on the yielding phenomena of a well-graded silty sand subjected to isotropic compression, leading to a definition of practical criteria to evaluate the yield point of a soil submitted to a specific compression test and makes a comparison between them. The isotropic yield pressure can be obtained in the laboratory through the Normal Compression Line (NCL) and Swelling Line (SL) [8], obtained by triaxial isotropic compression tests. Among the most used methods for a yield-point evaluation are [9], [10], [11] and [12]. Other methods were identified based on the plastic work [3]. Later, [13] estimated this parameter using bender-elements testing, having a reference in the constitutive model proposed by [14].

2 EXPERIMENTAL PROGRAM

The experimental program comprised two, isotropic, high-pressure, compression tests over samples moulded with two different void ratios. In these tests a very complete instrumentation was used, including shear-wave velocity (V_S) measurements. Scanning electron microscope (SEM) analyses were also performed for the tested samples.

2.1 SOIL DESCRIPTION

In this study, a unique soil was used: a silty sand resulting from the residual soil generated in the weathering of Porto granite [15,16], recoiled in the University of Porto Experimental Site. These soils are found extensively in the north and central regions of Portugal and are usually

classified as a SM (silty sand) in the Unified Classification System, being very well graded with about 30% of fines. The grain size distribution (Fig. 1) reflects an effective diameter (D_{50}) of 0.25mm, and the uniformity and curvature coefficients are 113 and 2.7, respectively. For the laboratory tests presented here the soil was used in remoulded conditions.

This soil, with values of the liquid limit equal to 34% and a plastic limit of 31%, is considered non-plastic. The maximum dry unit weight obtained in the modified Proctor test is 18.55kN/m³ and the optimum water content is 13.1%(Fig. 2). The particle-specific density (G) is 2.72 and a mineralogical analysis demonstrated that larger grains are essentially quartz, while the smaller are predominantly kaolinitic, with small portions of mica (as will be seen below in Fig. 4).

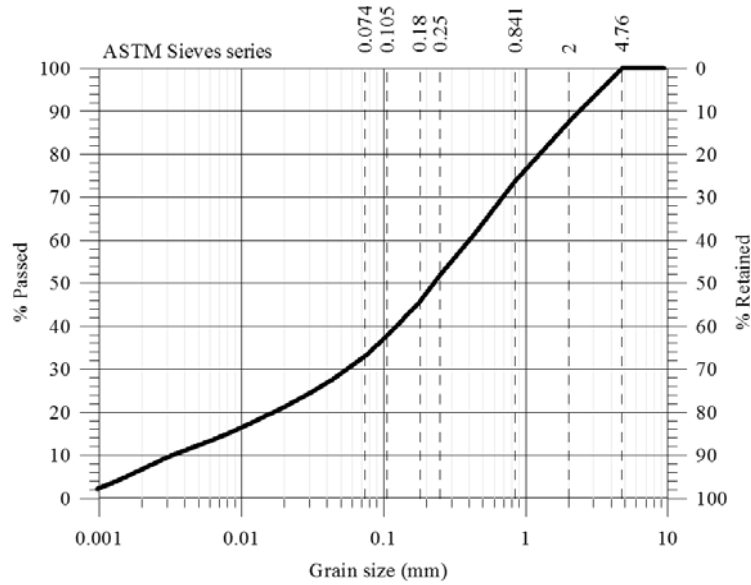


Figure 1. Porto silty sand grain-size distribution.

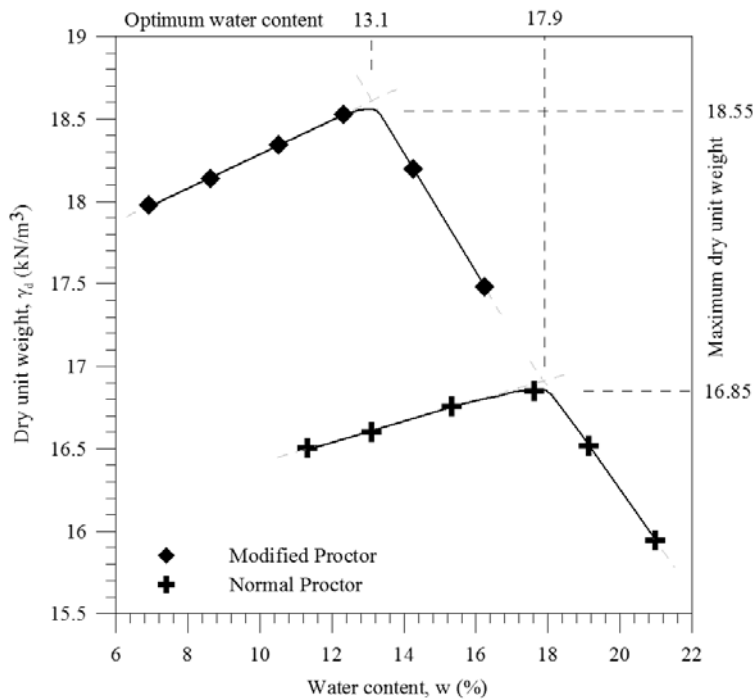


Figure 2. Normal and Modified Proctor test of the Porto silty sand.

2.2 SAMPLE PREPARATION

The moulding procedure consisted of a mixture of the right quantities of dry soil and water in order to obtain the desired void ratio and water content. Specimens were statically compacted in a cylindrical mould with a 50mm diameter and around 100mm in length, in two different void ratios ($e_i=0.60$ and $e_i=0.76$). After determining the hygroscopic water content of the air dried soil, it was possible to identify the necessary amount of water (distilled water was used) to add to the mixture in order to reach the reference water content of 12%.

The total volume of the mixture was divided into three equal portions and the compaction was made in three layers on a lubricated compacter. After the compaction of one layer, its surface was slightly scarified for better interpenetration with the subsequent layer. At the end of the compaction, the specimens were removed from the mould, measured, weighed, and quickly placed in the tri-axial cell in order to avoid any loss of water. The mass, diameter and length were measured with accuracies of 0.01g and 0.02mm, respectively. The water content was calculated from two small samples of the remaining mixture before compaction.

The samples suitability for testing was defined by the following tolerances:

- Dry Unit Weight (γ_{di}) within $\pm 1\%$ of target value,
- Water Content (w_i) within $\pm 1\%$ of the target value,
- Diameter (ϕ_i) within $\pm 0.5\text{mm}$,
- Height (H_i) within $\pm 1\text{mm}$.

3 METHODS

3.1 EQUIPMENT

The tests were performed in a Hoek-type, high-pressure, tri-axial cell in a room with temperature and humidity control, which were kept in around $20\pm 1^\circ\text{C}$ and $99\pm 1\%$, respectively. A hollow piston connects the cell fluid between the top and the radial confinement, allowing isotropic compression tests with $\sigma_1 = \sigma_3$.

High-precision instrumentation was used: 2 high-pressure LVDT's to monitor the internal axial strains, 1 high-pressure shear gauge to measure the internal radial deformation, 1 external axial LVDT, 2 GDS[®] water pressure/volume controllers connected to the specimen's top and bottom – allowing two draining borders – for back-pressure application, pore-pressure measurement and volume-change control, and 1 GDS[®] silicone oil

pressure/volume controller for the cell pressure. At the top and bottom of the sample porous discs were placed, from which a pair of University-of-Bristol-type connection bender elements protruded [17]. These transducers were used to measure the shear-wave velocity (V_s) during the isotropic compression tests.

Finally, a Field-Emission Scanning Electron Microscope was used to obtain micrographs of the tested samples, i.e., before and after being submitted to very high isotropic pressures.

3.2 TEST PROCEDURES

Immediately after being removed from the mould the sample was accurately measured and then, small holes for the bender elements' insertion and coupling had to be introduced at the top and bottom ends of the sample. This procedure did not take more than 10 minutes and therefore considerable moisture losses were not expected. The specimen was then weighed again ($m_{i,2}$), and so the dry mass of soil lost on the bender elements' holes ($m_{d,L}$) is given by equation (1), relating the difference between the sample mass before and after the holes with the compaction water content (w_i).

$$m_{d,L} = \frac{m_{i,1} - m_{i,2}}{1 + w_i} \quad (1)$$

The acquisition system was connected just after the conclusion of specimens' installation in the tri-axial cell. A valve connected to the cell was opened, beginning the flow of silicone oil into the cell. At the end of this transference the high-pressure tri-axial cell was sealed.

Small pressures were then applied to the sample to ensure the desired water percolation: 10kPa of cell pressure (CP) and 10kPa of back pressure at the bottom end (BP), with the top of the sample connected by an opened valve to atmospheric pressure.

After the percolation of the total volume of water (200ml) the saturation stage begins, keeping a mean effective stress (p') equal to 10kPa.

$$p' = \frac{\sigma'_1 + 2\sigma'_3}{3} \quad (2)$$

The saturation is automatically controlled by the three pressure/volume controllers programmed to increment their pressures at a rate of 0.1kPa/s, starting simultaneously. The increase of the pressure finished when CP and BP reached values of 1010kPa and 1000kPa, respectively; after which the pressures were kept constant until the cell

and pore volumes, as well as all the acquired deformations, presented a variation lower than the random noise.

Once the saturation stage ended, the isotropic consolidation stage could be initialised, applying constant-rate $\partial p' = 0.5 \text{ kPa/s}$ cell-pressure increments, while the back pressure remained equal to 1000 kPa. The consolidation was performed in stages, stopping the pressure increment at specific consolidation pressures, which allowed strain stabilization and very accurate seismic-wave measurements. During each consolidation step the Skempton parameter (B) was measured (see table 2):

$$B = \frac{\partial u}{\partial p'} \quad (3)$$

The necessary increase in the pore pressure, for that purpose, was achieved, so preventing for a short period the water transfer into the BP GDSs (avoiding water-volumes changes, the BP naturally increased). The consolidation went up to 19 MPa of effective confining pressure. At the end of each test, the specimens were again measured: final mass ($m_{f,2}$), final dimensions (H_f and ϕ_f) and, final water content (w_f) computed after drying the specimens. For the real final medium's density calculation (ρ_f) it is necessary to correct $m_{f,2}$ from the $m_{d,L}$ deduced from the soil mass lost on the bender elements' coupling holes. The corrected mass ($m_{f,1}$) is given by,

$$m_{f,1} = m_{f,2} + m_{d,L} \times (1 + w_f) \quad (4)$$

Then ρ_f is given by,

$$\rho_f = \frac{4 \times m_{f,1}}{\phi_f^2 \times \pi \times H_f} \quad (5)$$

The test results were considered suitable if the ratio between the final and initial dry masses was within certain values, as follows,

$$0.975 < \frac{m_{f,1}}{1 + w_f} \times \frac{1 + w_i}{m_{i,1}} < 1.025 \quad (6)$$

3.3 TEST CORRECTIONS

Table 1 presents the main measurements reported above at the beginning and at the end of the high-pressure isotropic tests, from which the geotechnical parameters presented in this paper were derived. The initial and final volumes (V_i and V_f , respectively) were computed using H_i , ϕ_i , H_f and ϕ_f . The specimens' nomenclature arises from the soil origin and their initial void ratios.

RSS means Residual Soil Soft ($e_i = 0.76$) and RSD means Residual Soil Dense ($e_i = 0.60$).

Table 1. Main parameters measured for the initial and final test conditions.

Specimen	w_i (%)	w_f (%)	$m_{i,1}$ (g)	$m_{f,1}$ (g)	V_i (cm^3)	V_f (cm^3)
RSS	12.21	19.23	353.78	356.16	204.06	166.53
RSD	12.36	17.93	390.68	411.16	204.64	170.21

It is not a novelty that the specimens submitted to a p' increase, suffer a volume reduction. Factors that could cause any strains (such as temperature, relative humidity or BP) were kept constant. Hence it can be assumed that this volume reduction only depends on the p' increase.

In this study, particularly in the bender elements' analysis, it was strictly necessary to estimate the tip-to-tip length between the bender elements ($H_{p'}$) and an average specimen medium's density ($\rho_{p'}$) for each step of the consolidation stage. These quantities also depend on the updated values of the water content ($w_{p'}$), mass ($m_{p'}$), external/internal axial strain ($\varepsilon_{a,p'}$) and volumetric strain ($\varepsilon_{v,p'}$), which is given by $\varepsilon_{a,p'}$ and the internal radial strain ($\varepsilon_{r,p'}$) according to equation (7). The volumetric deformation was either calculated with the external axial strain for seismic-wave measurements or with an internal axial deformation for the void-ratio calculation, in order to account for external effects like bedding errors,

$$\varepsilon_{v,p'} = 2 \times \varepsilon_{r,p'} + \varepsilon_{a,p'} \quad (7)$$

It is well known that volume adjustments caused by the membrane and the tri-axial cell sealing efforts are smaller for more compacted specimens ([15] and [18]). Therefore, $H_{p'}$ and $\rho_{p'}$ were predicted, taking into account final measurements such as H_f , V_f and w_f , as they represent values for more compacted conditions.

The bender elements had a 4.0 mm length, which means $H_{p'}$ can be expressed by equation (8). External instrumentation was used for the axial strain because it refers to the real distance between the bender elements.

$$H_{p'} = \frac{H_f}{1 - \varepsilon_{a,f}} \times (1 - \varepsilon_{a,p'}) - 2 \times 4.0 (\text{mm}) \quad (8)$$

where $\varepsilon_{a,f}$ is the final external axial strain.

For the updated medium's density determining,

$$\rho_{p'} = \frac{m_{p'}}{V_{p'}} \quad (9)$$

it is necessary to calculate the updated volume ($V_{p'}$),

$$V_{p'} = \frac{V_f}{1 - \varepsilon_{V,f}} \times (1 - \varepsilon_{V,p'}) \quad (10)$$

where $\varepsilon_{V,f}$ is the final volumetric strain given by the acquisition system.

In saturated conditions the updated mass ($m_{p'}$) is directly related with $w_{p'}$ and it may be estimated by,

$$m_{p'} = \frac{m_{f,1}}{1 + w_f} \times (1 + w_{p'}) \quad (11)$$

where $w_{p'}$ is calculated as follows,

$$w_{p'} = \left[w_f \times \frac{m_{f,1}}{1 + w_f} + \Delta m_{BP} \right] \times \frac{1 + w_f}{m_{f,1}} \quad (12)$$

where Δm_{BP} is the mass of the transferred water between each consolidation step.

Finally, the updated specimen medium's density is,

$$\rho_{p'} = \frac{\frac{m_{f,1}}{1 + w_f} \times \left[1 + \left(w_f \times \frac{m_{f,1}}{1 + w_f} + \Delta m_{BP} \right) \times \frac{1 + w_f}{m_{f,1}} \right]}{\frac{V_f}{1 - \varepsilon_{V,f}} \times (1 - \varepsilon_{V,p'})} \quad (13)$$

$\varepsilon_{a,f}$ is referred to as final external/internal axial strain because of its implications. When the seismic waves are analysed, the mean of the propagation is the specimens' total length. Thus, the external axial strains should be used. When the purpose is solely to investigate the void-ratio variation, the strains should be taken into account without external effects such as the bedding errors. Thus, the internal axial deformation is used.

4 ISOTROPIC COMPRESSION CURVES

The void-ratio variation is a very sensitive parameter, especially when analysing tri-axial test results. In isotropic tests, good reliability of the initial void ratio is of crucial importance as the relative position of some isotropic curves with respect to the others is controlled by this initial void ratio. On the other hand, being a parameter that can be obtained from different test measurements, it can be treated as a control variable.

During the tests, the specimen's updated void ratio ($e_{p'}$) was calculated by three independent methods given by equations (14) to (16). For this physical parameter estimation only the internal deformations were taken into account.

$$S \times e_{p'} = G \times w_{p'} \Leftrightarrow e_{p'} = \frac{G \times w_{p'}}{S} \quad (14)$$

where $S \approx 1$ is the saturation degree

$$-\varepsilon_{V,p'} = \frac{e_i - e_{p'}}{1 + e_i} \Leftrightarrow e_{p'} = e_i + \varepsilon_{V,p'} (1 + e_i) \quad (15)$$

where e_i is the initial void ratio

$$\rho_{p'} = \rho_s \times \frac{1 + w_{p'}}{1 + e_{p'}} \Leftrightarrow e_{p'} = \rho_s \times \frac{1 + w_{p'}}{\rho_{p'}} - 1 \quad (16)$$

where $\rho_s = 2720 \text{ kg/m}^3$ is the particle density of the soil grains.

Fig. 3 (on next page) shows the results of the high-pressure isotropic compression tests for both specimens. The plotted $e_{p'}$ values were computed by averaging all $e_{p'}$ given by equations (14) to (16).

A logarithmic regression was applied to the two line segments of each curve in order to obtain the compression and recompression indexes (C_c and C_r). The obtained values are presented in Fig. 3. It is clear from these results that both curves tend to converge to a unique normal compression line, typical behaviour of a "non-transitional" material [19] expressed in equation (17).

$$e = -0.103 \ln(p') + 1.25 \quad (17)$$

Even though the soil involved in these tests can be situated between clean sands and clays, non-significant transitional behaviour [20] was observed in the isotropic compression results and a single NCL was clearly defined. Since it is expected that only gap graded soils can exhibit transitional behaviour, as reported by [19], the very wide grain size distribution curve of this soil might be the reason for not exhibiting such a transitional behaviour.

5 MICROSCOPY

SEM micrographs were taken on a part of the specimens after being tested under high-pressure isotropic compression, and air dried. In Fig. 4 one of those micrographs is shown as an example. The SEM analysis also included the mineralogical composition of some points for particle identification. Being a very well graded soil with around 30% of particles less than 0.075 mm (ASTM sieve No. 200), the bigger particles are all involved by the fine matrix, i.e., with kaolinite giving rise to the texture observed in Fig. 4. However, this very thin layer of clay covering the grains prevents the correct identification of some particles.

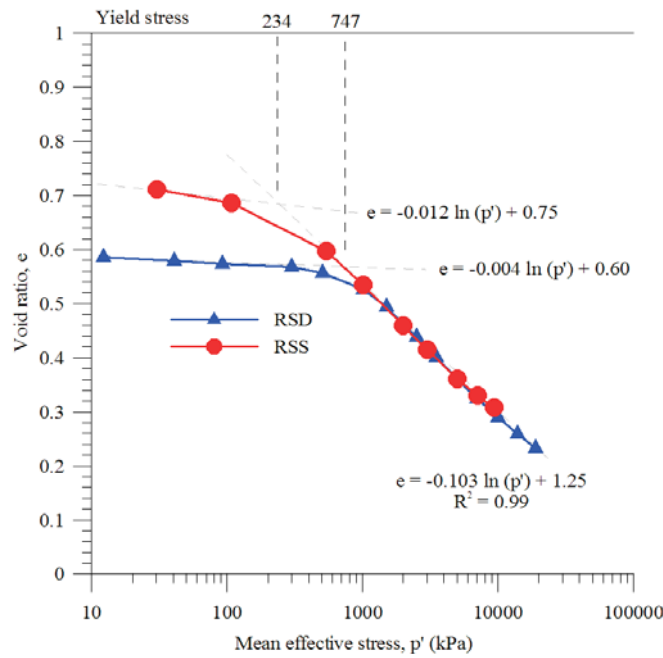


Figure 3. Normal and Modified Proctor test of the Porto silty sand.

In general, the yielding in granular materials is related to particle breakage or associated processes, as stated by several authors [5,21]. However, the amount of breakage is related to the type of grains and the stress level. Sometimes only the weaker grains break, while the strong grains like quartz remain intact [22].

The authors believe that, in this case, the yielding is not related to significant particle breakage (at least of strong quartz grains), but mostly due to the degradation in quartz connections through the kaolinite particles or the bending of micas. Some clear fractures are observed, like the one exhibited in Fig. 4, but they should result from a particle rearrangement with some fissures in the fine matrix of the soil.

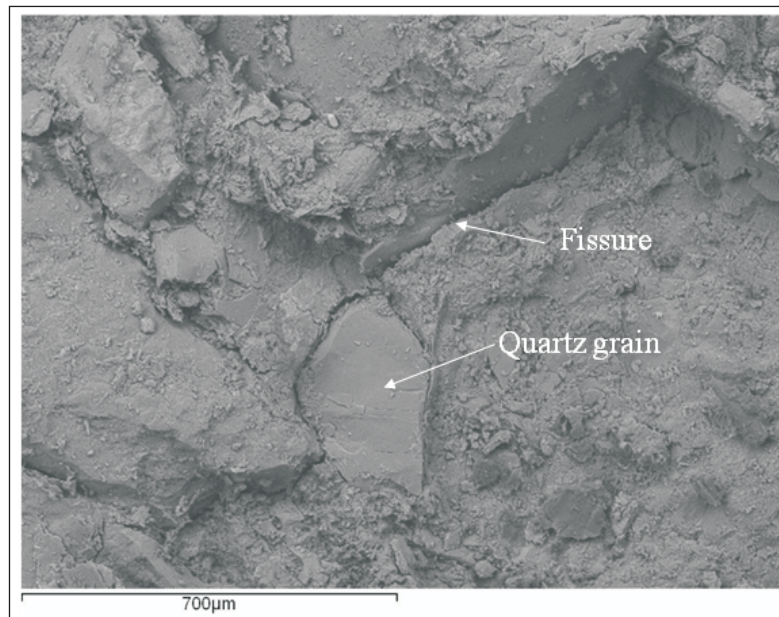


Figure 4. SEM photo of Porto silty sand after a saturated isotropic compression.

As relative movements between the quartz fragments were observed, the yield point and the void-ratio reduction may possibly be a sum of the particle breakage and a pure, non-particle-destructive rearrangement (converging to some qualitative indications referred to by [21]).

6 SEISMIC-WAVE MEASUREMENTS

6.1 INTRODUCTION

Bender elements – introduced in soil mechanics by [23] – are familiar in advanced geotechnical laboratory practices and growing in popularity all over the world. However, nowadays – although changing of the interpretation methods – bender elements are often used in laboratories in order to determine the simple dynamic properties of geomaterials [24,25,26,27,28], in particular the shear-wave velocity (V_s).

According to [29] V_s is related to the dynamic shear modulus (G_0) with the following expression,

$$V_s = \sqrt{\frac{G_0}{\rho_p'}} \quad (18)$$

where ρ_p' is the updated medium's density during the process described in equation 12.

6.2 TEST PROCEDURES

The seismic-wave measurements presented herein were only performed with S-waves transmitted vertically and horizontally polarized (V_{Svh}). As both specimens were tested under isotropic stress conditions, it is reasonable to assume that the results provided by a single axis are representative of the three principal directions of inertia. Nevertheless, the sensitivity for the object of this study, i.e., the identification of reliable criteria for yielding identification, is fairly independent of the directions of this transmission/polarization.

Before the tests the bender elements were placed in contact, leading to an approximately $2.0\mu s$ delay following the calibration standard procedures [16,30,31]. Fig. 5 illustrates the used connections scheme.

The shear-wave velocities were computed by dividing the tip-to-tip distance between the bender elements (H_p'), calculated using equation (8) from the external axial measurements, and the shear-wave propagation time (t_s). For the dynamic shear modulus calculation (G_0) the medium's density (ρ_p') was derived from equation (13), which was based on external measurements in order to have a global average value of the medium's density for the specimen. Due to border effects, the top and bottom of the sample is often less rigid than the central part, this is why the internal instrumentation is usually placed in

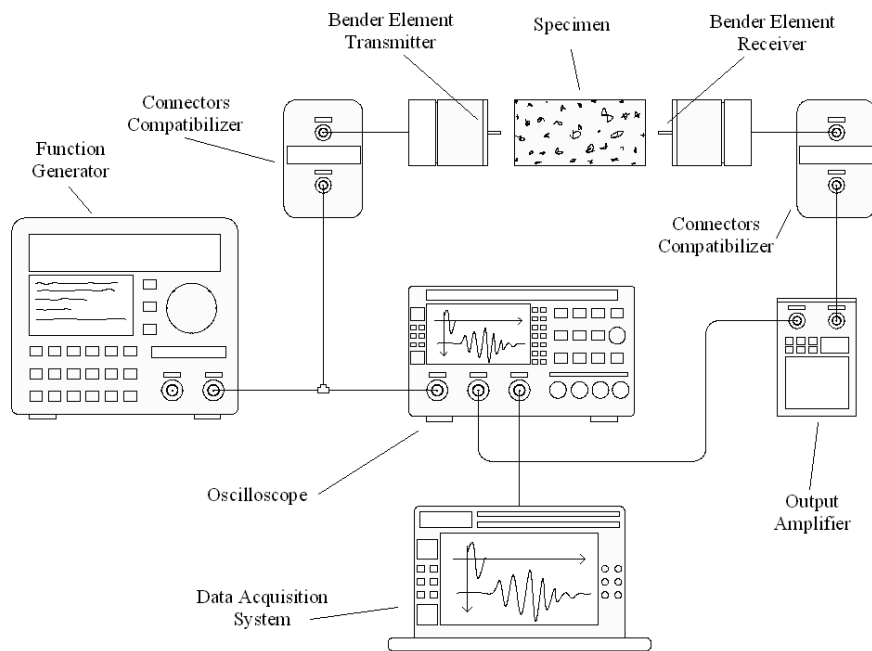


Figure 5. Schematic seismic-wave measurement connections.

that zone. As the wave propagates through the entire height of the sample, an average value of the medium's density was needed, and therefore, the use of external axial deformation and radial deformation for the $\varepsilon_{V,p'}$ computation was considered more appropriate. A simple analysis of the first arrival of the waves was performed based on the time-domain interpretation. As the saturated conditions usually promote fewer amplified signals, to improve the quality of the first arrival a square pulse was used instead of the commonly used sinusoidal pulse [30].

In all the specimens it was observed that the square wave showed more amplified first-arrival results than the sinusoidal ones (e.g., Fig. 6). For some sinusoidal frequencies (Sin. 50 kHz) the S-wave could only be identified further after the square wave's arrival, leading to a significant underestimation of V_S and, consequently, G_0 . These observations are in agreement with the numerical simulations of [30]. Based on this assumption, the square pulse was elected as the one that gave the more appropriate results.

6.3 SEISMIC-WAVE RESULTS

The seismic-wave measurements were performed in the consolidation stages after the stabilisation of the internal and external measurements. The following stress stages were considered for each sample: in soft sample (RSS) 8 stages were used at mean effective stresses of 100, 500, 1000, 2000, 3000, 5000, 7000 and 9300 (kPa); in the denser sample (RSD) waves were measured at 100,

300, 500, 1000, 1500, 2500, 3500, 5000, 7000, 10000 and 14000 (kPa) of p' totalising 11 stages.

Figs. 7 and 8 show, for both samples, the shear wave's first arrival in each stress stage.

The results show that the shear wave first arrivals not only tend to be quicker, but they also seem to be more energized with an increase in the effective isotropic stresses, p' . As table 2 testifies, the observed reduction in propagation time also means an increase in the shear-wave velocity, in spite of the progressive decrease in the tip-to-tip distance with the applied load. The results of the Skempton B parameter varying with p' are also presented in table 2, showing an increase in the saturation degree with the stress level, as was expected.

Table 2. V_S and B values as a function of p' .

p' (kPa)	RSD		RSS		
	V_S (m/s)	B (%)	p' (kPa)	V_S (m/s)	B (%)
100	495	76	100	488	82
300	496	77	500	483	83
500	496	79	1000	487	84
1000	497	79	2000	491	84
1500	500	80	3000	495	85
2500	504	82	5000	495	87
3500	505	84	7000	497	89
5000	509	85	9300	498	89
7000	509	87			
10000	508	89			
14000	507	91			

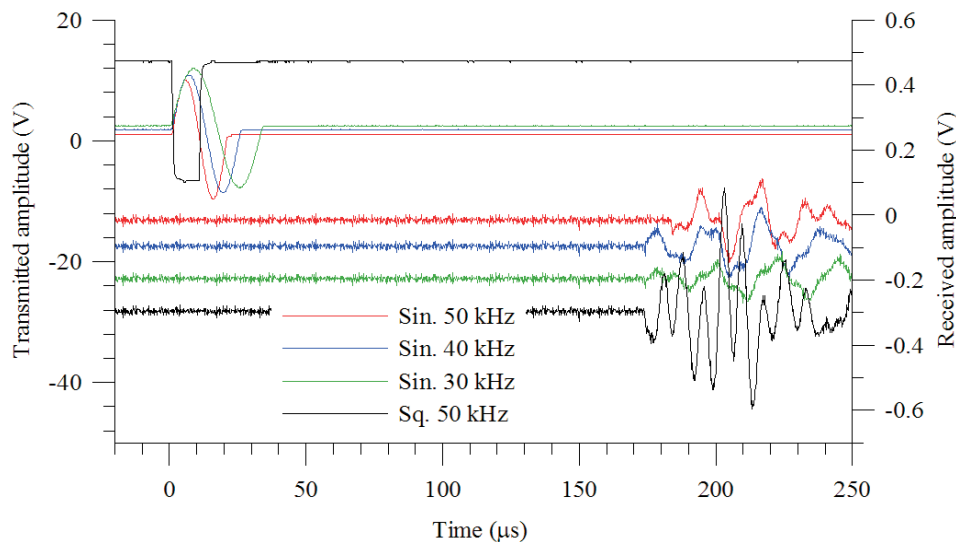


Figure 6. Sinusoidal and square-wave impulses: this last one has a higher amplified first-arrival sign.

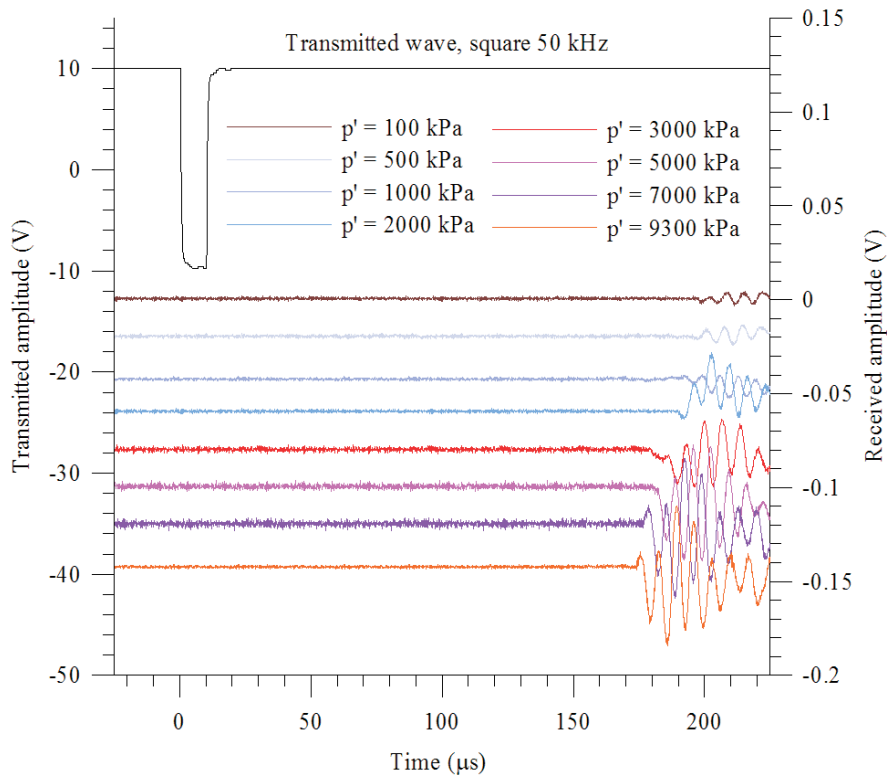


Figure 7. RSS first arrivals for each stress stage.

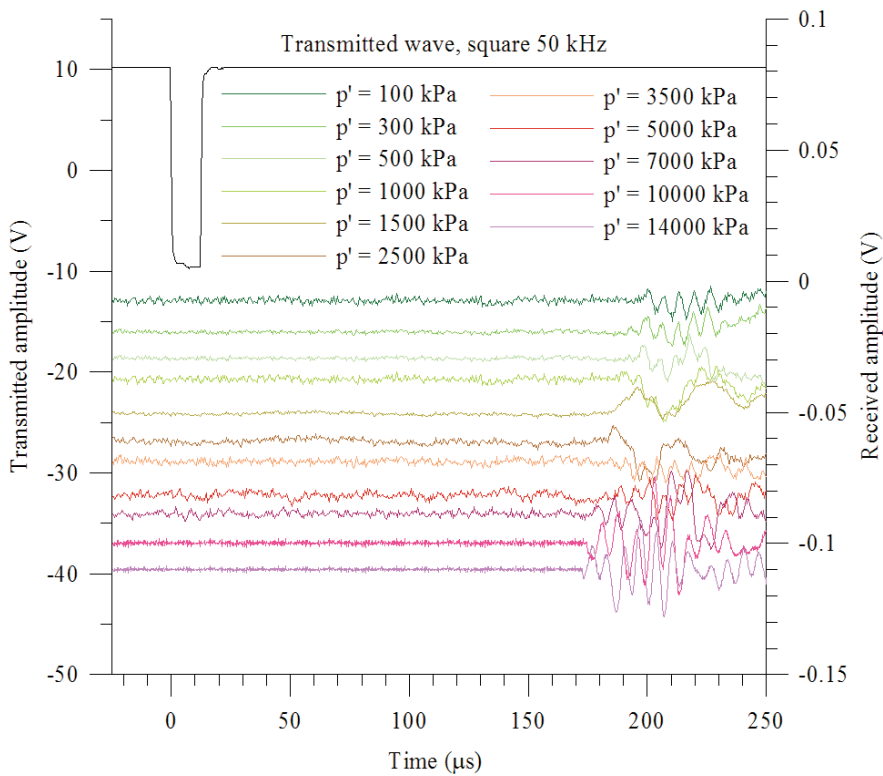


Figure 8. RSD first arrivals for each stress stage.

7 YIELD STRESS EVALUATION

7.1 INTRODUCTION

One of the aims of this research work was to study and evaluate the yield point of a specific type of geomaterial. Four distinct criteria were applied in order to have an accurate evaluation of this locus. Two of them are some of the most used criteria in soil mechanics; the other two represent an innovative variation of other known criteria.

In this paper – aiming at consistency among criteria – the considered yield point was the p' value of the interception point of two line segments. The first criterion takes into account the elastic and elasto-plastic work ($W_{p'}$) made by the specimens, in the sense that more plastic work means more plastic deformation, which characterises yielding.

The second criterion (G_0 criterion) is based on the maximum shear modulus. According to [13], yielding corresponds to a maximum of the dynamic shear modulus during the loading process, associated with the inflexion of its increase due to the evolution of the pressure towards a consistent drop due to plastic work, allowing the identification of the yield stress.

The third criterion is the most usual, relying on the void-ratio evolution. Finally, the fourth criterion expresses almost the same, as it uses the water-content evolution, which is the outflow of the voids' water. In fact, in saturated conditions the void ratio can be expressed through the water content once there is no air inside the specimen.

For all the criteria it was considered that there were two distinct regions of behaviour: the first one is defined by the predominance of elastic strains (ES), and the second is characterized mostly by its elasto-plastic strains (EPS). Also, for all the criteria, these two regions were defined by straight or logarithmic lines represented by their equations, which involve their slopes and a constant.

7.2 WORK CRITERIA

According to [3], the plastic work (W) in isotropic compression is calculated according to equation (19).

$$W = \int \sigma_3 \cdot d\varepsilon_v \quad (19)$$

where,

ε_v represents the plastic volumetric strains during isotropic loading.

Normalising that work with respect to volume, the following equation can be used,

$$W_{p'} = p' \times \varepsilon_{v,p'} \quad (20)$$

where,

$W_{p'}$ is the normalized work (J/m^3);

$\varepsilon_{v,p'}$ is the plastic volumetric strains that change with the stress level.

In Fig. 9, the total work per volume defined as the product of the total volumetric strains (derived from equation (7)) by the mean effective stress is plotted against this last, i.e., p' . The elastic strains are taken into account, defining a tangent line at the beginning of the curve corresponding to the elastic part. Another line, representing a linear regression of the last aligned points intersects the first, giving rise to the yield point.

As it is not plotted on a logarithmic scale, a correct ES definition demands a zoom of the graph to provide details of the elastic part being considered.

The interceptions between ES and EPS lead to mean effective stress yield points of 833kPa and 315kPa for the specimens RSD and RSS, respectively.

7.3 G_0 CRITERIA

This criterion consists of plotting the results from the maximum shear modulus G_0 against p' using a logarithmic scale, as expressed in Fig. 10. According to [14] there are three different yield points distinguishing the zones with different behaviour. These three yield locus concepts should be separated by the coefficients proposed by [14], being Y1 and Y2 applied by [13] for the present study. However, the results in Fig. 10 demonstrate that the Y1 and Y2 location is impossible. The authors believe that those coefficients have values that are too close, enough not to be distinguished by a high-pressure test on this soil.

As was performed in Section 7.2, for Fig. 9, a regression of the two line segments was applied. Once again, computing the ES and EPS interception it is possible to conclude the yielding of 753kPa and 333kPa for the specimens RSD and RSS, respectively.

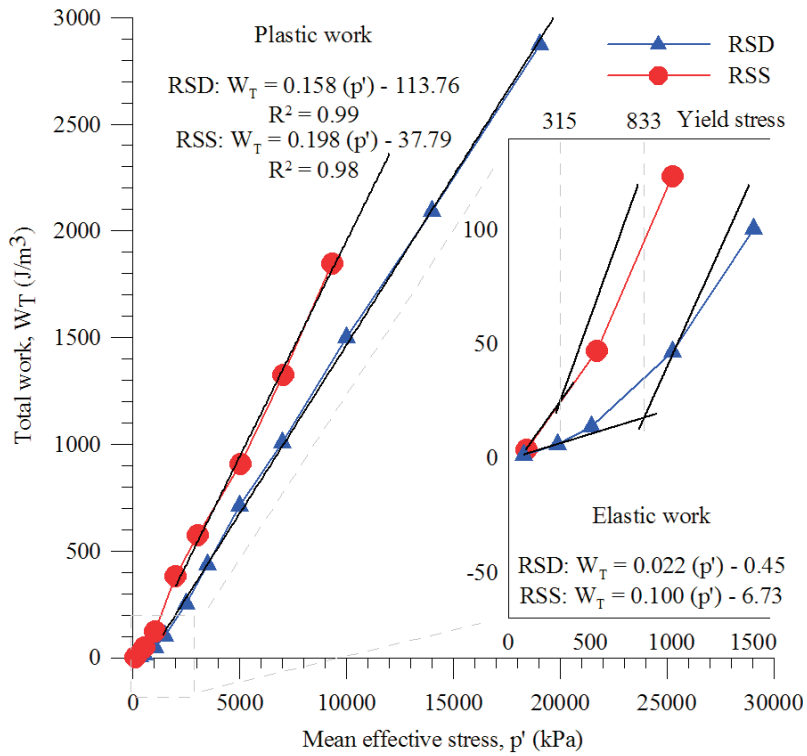


Figure 9. Total work criteria.

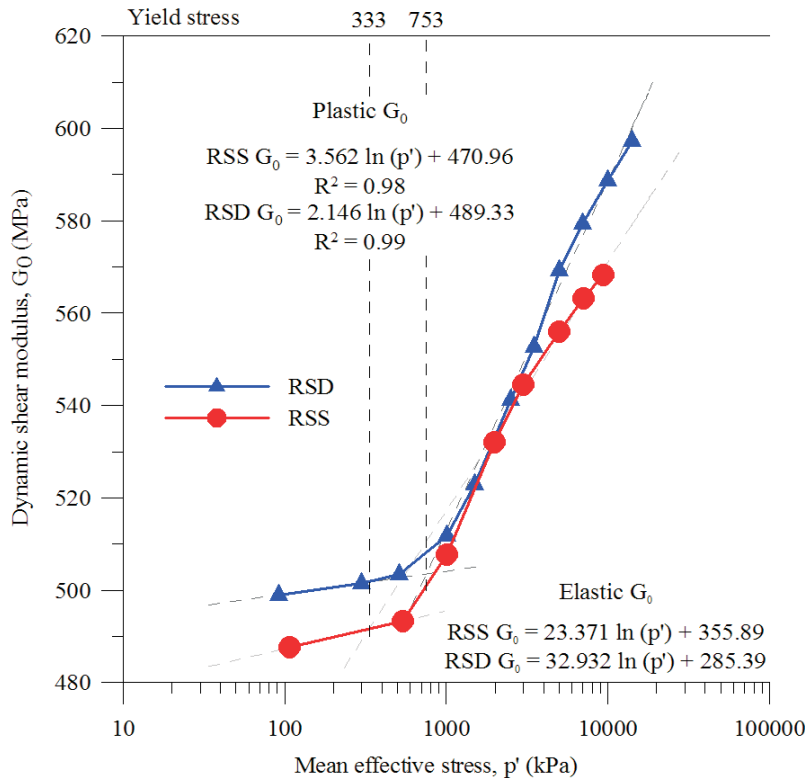


Figure 10. Dynamic shear modulus criterion.

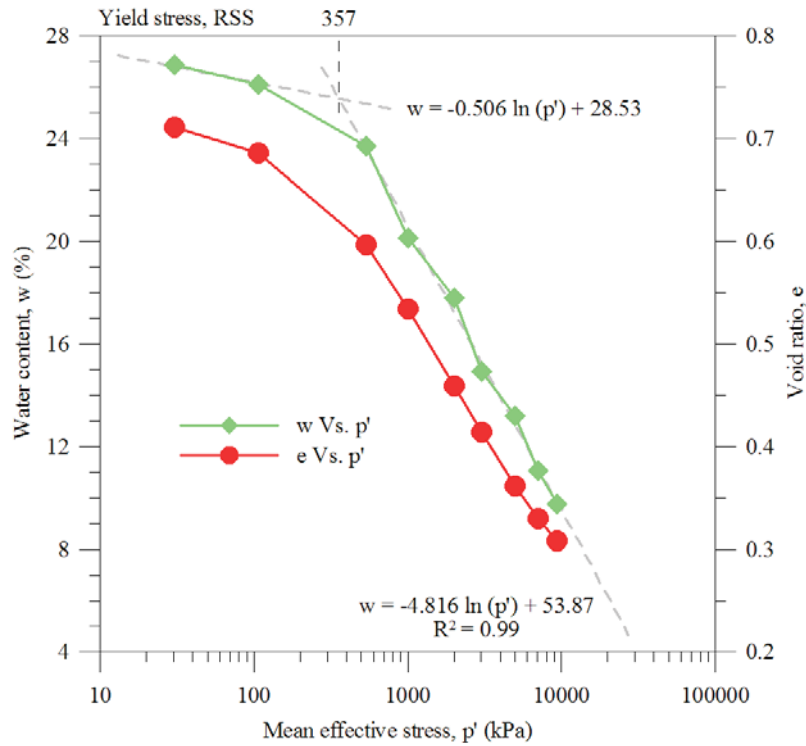


Figure 11. w_p and e_p consolidation variation in the RSD specimen.

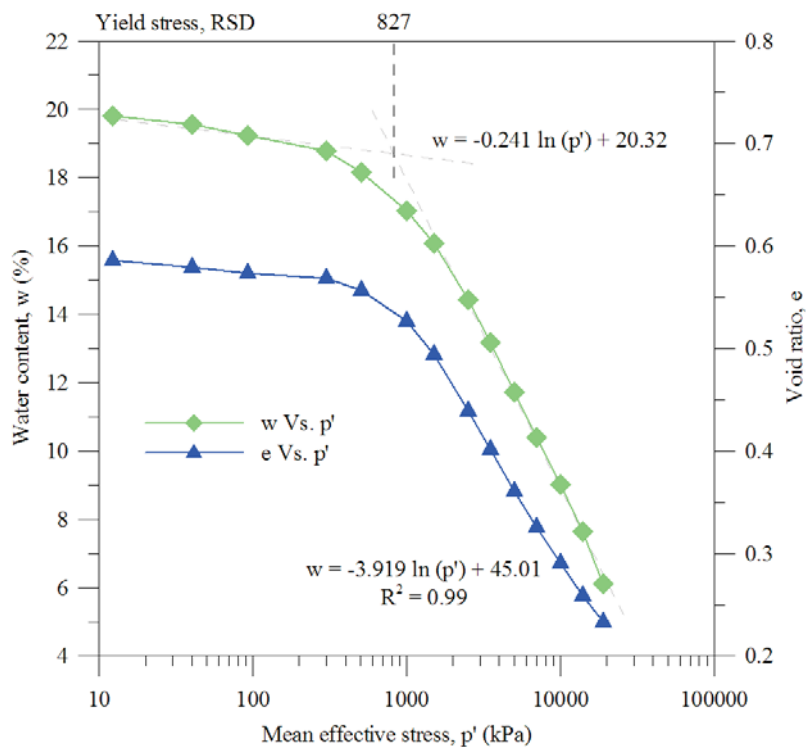


Figure 12. w_p and e_p consolidation variation in the RSS specimen.

7.4 VOID-RATIO AND WATER-CONTENT CRITERIA

As reported above, the third and fourth criteria are similar and thus, plotting e_p against p' should lead to very similar yield-point values than w_p against p' plotting, both on a logarithmic scale.

The isotropic compression curves are presented in Fig. 3, allowing a definition of the two line segments ES and EPS, the interception of which provided the following yielding points: 747kPa and 234kPa, for RSD and RSS, respectively.

According to [32], there is an exact relationship between the specimen's void water volume (w_p) and the consolidation pressure. Thus, w_p plotting – in saturated cases – against p' , should provide very similar results to e_p vs. p' . In Figs. 11 and 12 the curves of w_p and e_p against p' are plotted together, indicating similar yield points.

The interception of EP and EPS for the water-content curves gave rise to yield-point values of 827kPa and 357kPa for RSD and RSS, respectively. Not only are these values very similar to the void-ratio procedure, but also the graphical trend seems to be very consistent.

7.5 YIELD-STRESS VALUE COMPARISON

The four presented criteria proved to be appropriate in the yield-point evaluation (table 3). Although all the criteria show similar results, the ordinary e_p vs. p' plot showed better consistency in the ES and EPS characterization. However, this paper proved that for simple saturated specimens it is possible to define a yield point using a less rigorous method relating only to the mean effective stress and the water content. This fact allows models, in which the yield-stress definition is a primary concern, not to allow the possibility of simulating it very accurately; these are time-consuming and expensive tests. It was not possible to apply the [14] model, but the results of G_0 proved to be in agreement with the other criteria, defining a very consistent yield point.

Table 3. Results provided by the four yield-point computing criteria (kPa).

Specimen	w_p	e_p	W_p	G_0
RSD	827	742	833	753
RSS	357	218	315	333

CONCLUSIONS

The results provided by this paper lead the authors to the conclusion that yielding is a very sensitive parameter. For a good estimation of yield it is also necessary to use very-high-resolution equipment and very precise instrumentation.

Isotropic compression tests performed at very high pressures over samples moulded at two different void ratios showed that a unique normal compression line could be obtained. These tests were conducted together with seismic-wave measurements and SEM micrographs. The results show that yielding of the well-graded silty sand is not related to a significant particle breakage, but mainly due to fractures in the fine matrix and the bending of micas. Four methods were developed for the yield-stress evaluation, which proved to be quite consistent, giving rise to similar results in spite of the high sensitivity of this parameter.

ACKNOWLEDGMENTS

The authors would like to acknowledge the Universitat Politècnica de Catalunya and Imperial College of London for support of the test facilities and Prof. Marcos Arroyo, Prof. Enrique Romero, in UPC, and Prof. Mathew Coop, formerly at IC, for their interest in this work. This research was developed under the activities of FCT (Portuguese Foundation for Science and Technology) research unit CEC, in FEUP [PTDC/ECM/099475/2008], and financed by the European Community (QREN/UE/FEDER), Operational Program for Competitive Factors "COMPETE". The second author had the financial support of the PhD grant SFRH/ BD / 29346 / 2006.

REFERENCES

- [1] Mortara, G. (2008). A new yield and failure criterion for geomaterials. *Géotechnique*, Vol. 58, No. 2, pp. 125-132.
- [2] Vesic, A.S., Clough, G.W. (1968). Behavior of granular materials under high stresses. *J. of Soil Mech. & Found. Div.*, Vol. 94, No. SM 3, pp. 661-688.
- [3] Lade, P. V. (1977). Elasto-plastic stress-strain theory for cohesionless soil with curved yield surfaces. *Int. J. for Solids Struct.*, Vol. 13, No. 11, pp. 1019-1035.

- [4] Konrad, J.M. (1998). Sand state from cone penetrometer tests: a framework considering grain crushing stress. *Géotechnique*, Vol. 48, No. 2, pp. 201-215.
- [5] Coop, M.R. (1990). The mechanics of uncemented carbonate sands. *Géotechnique*, Vol. 40, No. 4, pp. 607-626.
- [6] Matsuoka, H., Nakai, T. (1974). Stress-deformation and strength characteristics of soil under three different principal stresses. *Proc. Jpn. Soc. of Civ. Eng.*, Vol. 232, pp. 59-70.
- [7] van Eekelen, H.A.M. (1980). Isotropic yield surface in three dimensions for use in soil mechanics. *Int. J. Numer. Anal. Methods Geomech.*, Vol 4, No. 1, pp. 89-101.
- [8] Taylor, D.W. (1948). *Fundamentals of soil mechanics*. New York, John Wiley & Sons.
- [9] Casagrande, A. (1936). The determination of the pre-consolidation load and its partial significance. *Proc. 1st Int. Conf. On Soil Mech. & Found. Engin.*, Cambridge, Vol. 3, pp. 60-64.
- [10] Burmister, D. (1951). The application of controlled test methods in consolidation testing. *Proc. 54th Annu. Meet. of the ASTM, Symp. on Consol. Test. of Soils*, pp. 83-98. (Spec. Tech. Pub., 126).
- [11] Schmertmann, J.H. (1955). The undisturbed consolidation behaviour of clay. *Trans. Soc. Civ. Eng.*, Vol. 120, pp. 1201-1233.
- [12] Culley, J.L.B., Larson, W.E. (1987). Susceptibility to compression of a clay loam Haplaquoll. *Soil Sci. Soc. Am. J.*, Vol. 51, pp. 562-567.
- [13] Alvarado, G. and Coop, M.R. (2011). On the performance of bender elements in triaxial tests. *Géotechnique*, Vol. 62, No. 1, pp. 1-17.
- [14] Jardine, R.J., Fourie, A., Maswoswe, J. and Burland, J.B. (1985). Field and laboratory measurement of soils stiffness. *Proc. 11th Int. Conf. in Soil Mech. and Found. Engin.*, San Francisco, Vol. 2, pp. 511-514.
- [15] Viana da Fonseca, A., Matos Fernandes, M., Silva Cardoso, A. (1997). Interpretation of a footing load test in a saprolitic soil from granite. *Géotechnique*. Vol. 47, No. 3, pp. 633-651.
- [16] Viana da Fonseca, A., Carvalho, J., Ferreira, C., Santos, J. A., Almeida, F., Pereira, E., Feliciano, J., Grade, J., Oliveira, A. (2006). Characterization of a profile of residual soil from granite combining geological, geophysical, and mechanical testing techniques. *Geotech. & Geolog. Engin.*, Vol. 24, pp. 1307-1348.
- [17] Lings, M.L. and Greening, P.D. (2001). A novel bender/extender element for soil testing. *Géotechnique*, Vol. 51, No. 8, pp. 713-717.
- [18] Germaine, J.T., Ladd, C.C. (1988). Triaxial testing of saturated cohesive soils. *ASTM Spec. Tech. Pub.*, No. 977, pp. 421-459.
- [19] Nocilla, A.M.R.; Coop, M., Colleselli, F. (2006). The mechanics of an Italian silt; an example of "transitional" behaviour. *Géotechnique*, Vol. 56. No. 4, pp. 261-271.
- [20] Martins, F.B., Bressani, L.A., Coop, M.R., & Bica, A. (2001). Some aspects of the compressibility behaviour of a clayey sand. *Can. Geotech. J.*, Vol. 38, pp. 1177-1186.
- [21] Carrera, A., Coop, M.R., Lancellota, R. (2011). Influence of grading on the mechanical behaviour of Stava tailings. *Géotechnique*, Vol. 61, No. 11, pp. 935-946.
- [22] Yamamuro, J.A., Lade, P.V. (1996). Drained sand behavior in axisymmetric tests at high pressures. *J. of Geotech. Engin.*, Vol. 122, No. 2, pp. 109-119.
- [23] Shirley, D.J. and Hampton, L.D. (1978). Shear-wave measurements in laboratory sediments. *J. Acoust. Soc. Am.*, Vol. 63, No. 2, pp. 607-613.
- [24] Arroyo, M., Muir Wood, D., Greening, P.D., Medina, L., Rio, J. (2006). Effects of sample size on bender-based axial G0 measurements. *Géotechnique*, Vol. 56, No. 1, pp. 39-52.
- [25] Vilhar, G., Jovičić, V. (2009). Measurement and interpretation of the small strain stiffness of boštanj silty sand. *Acta Geotechnica Slovenica*, Vol. 6, No. 2, pp. 57-75.
- [26] Viana da Fonseca, A., Ferreira, C., Fahey, M. (2009). A framework interpreting bender element tests, combining time-domain and frequency-domain methods. *Geotech. Test. J.*, Vol. 32, No. 2, pp. 1-17.
- [27] Amaral, M.F., Viana da Fonseca, A., Arroyo, M., Cascante, G., Carvalho, J., 2011. Compression and shear wave propagation in cemented-sand specimens. *Géotechnique Lett.*, Vol. 1, No. 3, pp. 79-84.
- [28] Amaral, M.F., Viana da Fonseca, A., Carvalho, J., Consoli, N.C. (2011). Dynamic Poisson ratio analysis. *Proc. 15th Eur. Conf. on Soil Mech. & Geotech. Engin.*, Vol. 0, pp. 115-120.
- [29] Richart, F.E., Hall, J.R., Woods, R.D. (1970). *Vibrations of soils and foundations*. Prentice-Hall, Inc., Englewood Cliffs, NJ.
- [30] Tallavó, F., Cascante, G., Pandey, M. D. (2010). New Methodology for Source Characterization in Pulse Velocity Testing. *Geotech. Test. J.*, Vol. 32, No. 6, pp. 1-16.
- [31] Khan, Z., Cascante, G., and El-Naggar, H. (2011). Dynamic properties of cemented sands using the ultrasonic waves. *Can. Geotech. J.*, Vol. 48, pp. 1-15.

- [32] Dolinar, B. (2004). Undrained shear strength of saturated cohesive soils depending on consolidation pressure and mineralogical properties. *Acta Geotechnica Slovenica*, Vol. 2, pp. 5-9.

RAZLAGA PROSTORSKE STRUKTURE PLITVEGA PLAZIŠČA Z UPORABO RAZLIČNIH GEOFIZIKALNIH METOD

ALEKSANDAR RISTIĆ, BILJANA ABOLMASOV, MIRO GOVEDARICA,
DUŠAN PETROVAČKI IŃ ALEKSANDRA RISTIĆ

o avtorjih

Aleksandar Ristić
University of Novi Sad,
Faculty of technical sciences
Trg Dositeja Obradovića 6, 21000 Novi Sad, Srbija
E-pošta: aristic@uns.ac.rs

Biljana Abolmasov
University of Belgrade,
Faculty of Mining and Geology
Đušina 7, 11000 Beograd, Srbija
E-pošta: biljana@rgf.bg.ac.rs

Miro Govedarica
University of Novi Sad,
Faculty of technical sciences
Trg Dositeja Obradovića 6, 21000 Novi Sad, Srbija
E-pošta: miro@uns.ac.rs

Dušan Petrovački
University of Novi Sad,
Faculty of technical sciences
Trg Dositeja Obradovića 6, 21000 Novi Sad, Srbija
E-pošta: petrovacki@uns.ac.rs

Aleksandra Ristić
University of Novi Sad,
Faculty of technical sciences
Trg Dositeja Obradovića 6, 21000 Novi Sad, Srbija
E-pošta: sanjica@uns.ac.rs

izvleček

Predstavljamo metodologijo za natančnejšo in manj negotovo prostorsko strukturalno razlago majhnih, plitkih plazišč. Razlaga prostorske strukture to vrstnih plazov temelji na podzemnem in površinskem modelu in zahteva veliko gostoto podatkov. Ta metodologija vključuje uporabo metod georadarja (GPR), električne upornostne tomografije (ERT) in lasersko skeniranje površja (TLS). GPR metoda, s katero določamo podzemeljski strukturalni model, je časovno učinkovita in daje podatke visoke resolucije, zato je primerna za analize plitvega podpovršja. ERT metodo uporabimo samo za potrditev dobljenih rezultatov z GPR preiskavami, ker je dolgotrajna in primernejša preiskava za večja in globlja plazišča. Površinski model je ustvarjen z uporabo TLS metodo, ki je časovno in stroškovno učinkovita, z njo dobimo veliko podatkov in je primernejša za manjše površine, kot so analizirani tipi plazišč.

Kakor nam je znano, se obstoječi postopki, ki temeljijo na običajnih ali neudarnih geofizikalnih metodah, uporabljajo izključno za opazovanje večjih in globljih plazišč. Njihovo sprotno opazovanje vključuje številne senzorje zato se težko uporablja na majhnih plaziščih zaradi njihovega števila, mesta in obsega. Ob upoštevanju prednosti vsake uporabljene metode in razlage rezultatov s terena, je jasno, da je največja prednost opravljene študije njena učinkovitost in uporabnost za majhna plitva plazišča, čigar število je veliko in vpliv na okolje prevladajoč. Zato je lahko dobra osnova za olajšano obdelavo plazišč.

Metodologijo smo preverili na majhnem, plitvem plazišču v vasi Vinča, blizu Beograda v Srbiji.

ključne besede

plitvi udori, GPR, ERT, TLS

SHALLOW-LANDSLIDE SPATIAL STRUCTURE INTERPRETATION USING A MULTI-GEOPHYSICAL APPROACH

ALEKSANDAR RISTIĆ, BILJANA ABOLMASOV, MIRO GOVEDARICA,
DUŠAN PETROVAČKI AND ALEKSANDRA RISTIĆ

about the authors

Aleksandar Ristić
University of Novi Sad,
Faculty of technical sciences
Trg Dositeja Obradovića 6, 21000 Novi Sad, Serbia
E-mail: aristic@uns.ac.rs

Biljana Abolmasov
University of Belgrade,
Faculty of Mining and Geology
Đušina 7, 11000 Beograd, Serbia
E-mail: biljana@rgf.bg.ac.rs

Miro Govedarica
University of Novi Sad,
Faculty of technical sciences
Trg Dositeja Obradovića 6, 21000 Novi Sad, Serbia
E-mail: miro@uns.ac.rs

Dušan Petrovački
University of Novi Sad,
Faculty of technical sciences
Trg Dositeja Obradovića 6, 21000 Novi Sad, Serbia
E-mail: petrovacki@uns.ac.rs

Aleksandra Ristić
University of Novi Sad,
Faculty of technical sciences
Trg Dositeja Obradovića 6, 21000 Novi Sad, Serbia
E-mail: sanjica@uns.ac.rs

abstract

We present an methodology for a more detailed and less ambiguous spatial structure interpretation of small, shallow landslides. The spatial structure interpretation of this type of landslides bases on both underground and surface models and requires high-density data. This methodology involves the use of ground-penetrating radar (GPR), electrical resistivity tomography (ERT) and terrestrial laser scanning (TLS) techniques. GPR technique, used for the definition of the underground structure model, provides a time-efficient survey that yields high-resolution data, making it suitable for a shallow subsurface analysis. ERT

technique was used only to confirm the results obtained by the GPR survey, since it is more time consuming and more convenient for larger and deeper landslides investigations. The surface model is created using TLS technique, which is time- and cost-effective, produces a large amount of data and is favourable for smaller areas, such as the analysed type of landslides.

To the best of the authors' knowledge, existing procedures based on either conventional or non-invasive geophysical methods, observe, almost exclusively, larger and deeper landslides. Their real-time monitoring involves a number of sensors and is hardly applicable to small landslides because of their number, location and dimensions.

Considering the benefits of each applied technique and the interpretation of the results obtained from field data, it is clear that the main advantages of the realized application are the efficiency and applicability for small shallow landslides whose number and impact on the environment are dominant. Therefore, it represents a solid basis for landslide mitigation.

The verification of the methodology was made on a small, shallow landslide in the village of Vinča, near Belgrade, Serbia.

keywords

shallow landslide, GPR, ERT, TLS

1 INTRODUCTION

Determining the characteristics of the underground and surface structures of landslides represents the principal result necessary for an adequate assessment of the status and monitoring of landslide activities [1]. The conventional methods for landslide-status assessment are based on geo-morphological analyses, in most cases combined with borehole drilling and standard penetration test (SPT) methods. Conventional methods are expensive and relatively slow, whereas the results of an analysis are based on processing a limited range

of subsurface data [2]. These disadvantages may be overcome by the combined or independent application of non-invasive, geophysical methods whose expansion follows the development of modern techniques and instruments [3]. Simultaneously with the development of these methods, the possibilities for their application in the detailed research of landslides were analysed [2,4]. These analyses were carried out almost exclusively for large landslides with a sliding depth greater than 20m, and showed that ERT technology is appropriate in these conditions [5,6,7,8,9,10].

ERT measurements are conducted by applying a constant current into the ground through two current electrodes and measuring the resulting voltage differences at two potential electrodes. From the current and voltage values, an apparent resistivity value is calculated. ERT uses 25 or more electrodes connected by a multi-core cable. To determine the subsurface resistivity in different zones or layers, an "inversion" of the measured apparent resistivity values (generally a total of some 100 single values) must be carried out. The result gives information about the spatial averages of the subsurface resistivity in a 2D-section. The main disadvantage of the ERT method is the wide range and the broad overlap of the possible subsurface resistivity of different geological units. Thus, resistivity changes due to varying moisture conditions may be orders of magnitude higher than the differences between geological units [1,9,15].

In terms of large, deep landslides, GPR technology has only been used to confirm the results of ERT technology, due to maximum penetration depth of electromagnetic (EM) waves and the site accessibility [2].

The GPR method is used for the very shallow subsurface, i.e., of the order of a few tens of metres. The technology is based on an EM pulse emitted from a transmitter antenna, reflected at inhomogeneities and layer boundaries and received by a second antenna after a measured travel time. The whole array is moved along a profile line, which creates a 2D-section of the subsurface called the B-scan. The possible antenna frequencies range from 20MHz to 2GHz. A higher antenna frequency enhances the resolution of the data, while lower frequencies increase the maximum penetration depth. In the frequency range used for geological investigations, GPR signals can reach depths of up to 20 m with 100-MHz antennas, but the signal penetration decreases dramatically with the increasing soil conductivity. Because of the high dielectric constant of water, this method is well suited for detecting changes in water content [2,3,9,17].

Considering that the main goal of the research is to determine the characteristics of small, shallow landslides

with a sliding depth in the range from 1 to 5m, then the application of GPR technology, which is characterized by the swift and completely non-invasive acquisition of high-resolution data, becomes very appropriate [11]. Taking into account the possibilities for non-invasive geophysical methods, they are rarely carried out independently. More often, they are used in combination with other methods and then a correlation of the obtained results is carried out. Such a multi-geophysical approach of using different methods combined with traditional methods of research is described in various articles [12,13]. The advantages and disadvantages of using geophysical methods in geomorphological studies are described on various examples in [14].

In addition to various field and laboratory research methods that define the structure and properties, it is appropriate to provide a topographic basis on a large scale. When research is more detailed, such a topographic basis is necessary in order to define the landslide geometry and the procedure of landslide mitigation. Conventional methods for a geodetic survey are used to provide a topographic basis in most practical cases. Occasionally, terrestrial photogrammetry [15] and terrestrial laser scanning of the terrain [16,17] were used.

A laser scanner is a system that scans real objects to produce three-dimensional, discretely sampled surfaces that represent those real objects. Scanning can be airborne (ALS) or terrestrial (TLS). Laser scanning allows the generation of high-resolution, digital surface models (DSM), which is a topographic model of the reflected surface of the earth, including vegetation and man-made structures, and digital terrain models (DTM), which is a topographic model of the bare earth. Elevation data collected by TLS have proven to be useful in the determination of some specific landform features, such as landslides and fault scarps [5,16,17].

On the basis of previously mentioned points, it can be concluded that the recent results of landslide analyses point to a multi-geophysical approach. Also, the structure analysis of small, shallow landslides was rarely tackled in the available literature, while GPR technology was not applied to any great extent.

The given analysis, along with the defined main goal of the research, leads to the conclusion that it is necessary to realize an application based on the usage of the main advantages of the GPR, ERT and TLS technologies. The application then has to be verified on a typical landslide example.

During the research the emphasis was put on non-invasive geophysical methods since a landslide has a specific

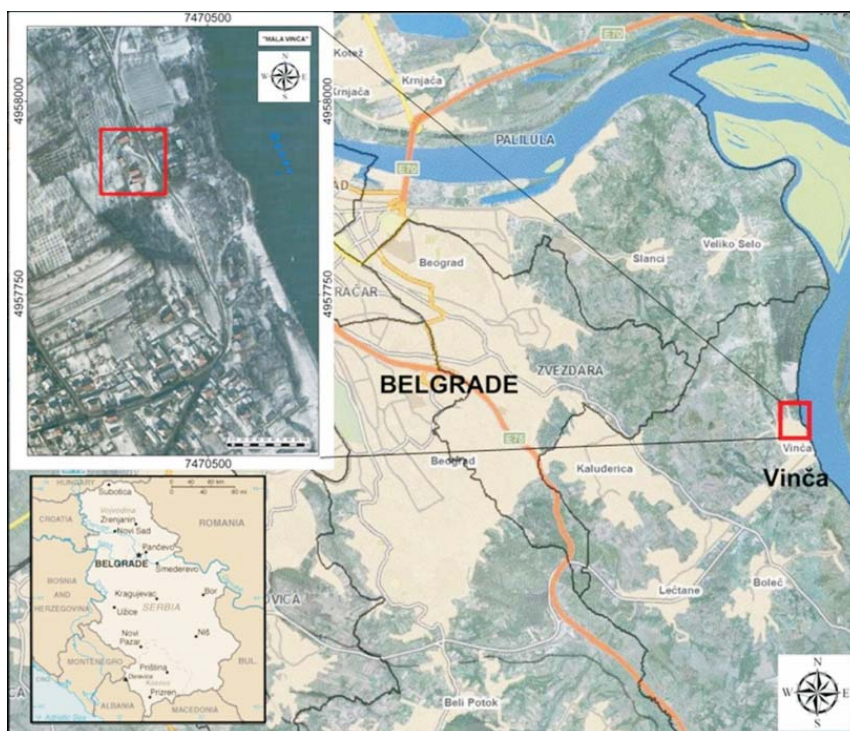


Figure 1. Location of the study area.

position and geometry. Due to the capabilities of non-invasive geophysical methods for landslide research [2], field work was conducted during the summertime (July 2009), in a dry period, after a period of heavy precipitation in the previous winter and spring, which reactivated the landslide. The results presented in this paper clearly show that in the case of small, shallow landslides, applied geophysical methods give reliable data about the structure of a landslide body and the spatial disposition of the rupture surface. The TLS scanning of the landslide surface provided a topographic basis for creating DTMs, locating the research work and monitoring the landslide activities.

2 STUDY AREA

The integrated geophysical research was carried out on a landslide located 14km southeast of Belgrade, in the village of Vinča, on the right bank of the Danube (Fig. 1). The right valley bank of the Danube is characterized by hills (altitude 80–130m) and numerous deep landslides whose feet reach the Danube [18]. The geological composition of the study area (Fig. 2) includes a continuous surface layer of diluvium (dl) with a thickness of 0.2–0.5m and beneath it there is loess (Q) with a

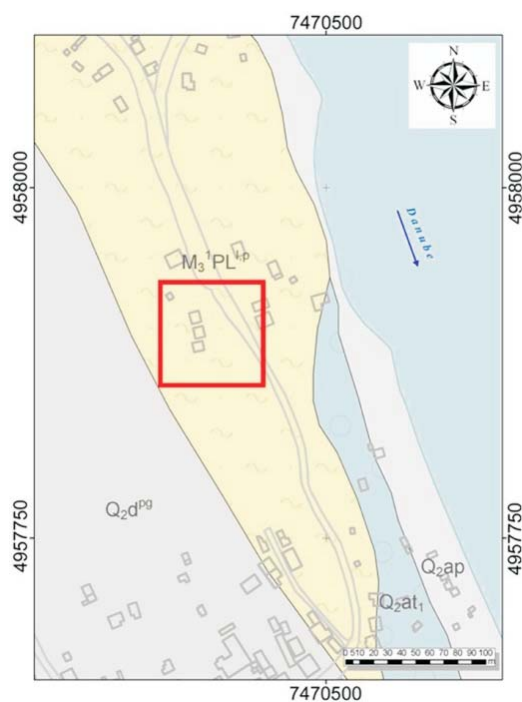


Figure 2. Complex geological map of Belgrade 1:10000 [19]. Legend: Q_{2at_1} - Fluvial terrace (first), Q_{2ap} - Alluvial sediments, Q_{2dps} - Deluvial dusty-sandy-clayish deposits, $M_3^1PL^1p$ - Sarmatian dusty-clayish formation.

thickness of 0.5–2.0m, with traces of secondary carbonate sediments. The bedrock consists of Sarmatian sand (M_3^1), brownish marlstone (M_3^1GL) and grey marlstone (M_3^1L).

The analysed landslide has the dimensions of 50x40m and it is situated in the middle of the Danube slope above the local road and three private residential objects that are directly endangered by the landslide (Fig. 1, Fig. 2). The landslide is on private property and, due to the specific terrain configuration and the problems with the owners of nearby properties, it is almost impossible to reach the body of the landslide equipped with drill tools and tools for SPT experiments.

The landslide activated in March 2008 was triggered by heavy rainfall and slope indentation. The indentation occurred while building the residential objects. The first reactivation occurred in March 2009 (Fig. 3), also triggered by heavy rainfall. The second reactivation occurred in late December 2009 and was triggered by instant snow melting. According to classification [20], this landslide can be classified as a shallow retrogressive and active landslide, very slow to slow, in the phase of active movement. The main scarp, with a height of 1.7m, is obvious with the visible zone of mass deficit. The lithological structure of the landslide comprises a thin diluvium with a thickness up to 0.3m, loess with a thickness of 1–1.5m and bedrock consisting of Sarmatian, laminated, well-compacted sand with weathered marlstone.

3 SURVEY PROCEDURE

The geological recognition of the landslide was conducted in March 2009, then again during the research in July 2009, and finally after the reactivation in December 2009. The pre-failure DTM was formed on the basis of the available cartographic material for the study area prior to the formation of the landslide.

3.1 TERRESTRIAL LASER SCANNING

The acquisition was made in July 2009 with a Leica Scan Station 2 terrestrial laser scanner (scanning resolution 10cm/10m). The raw data were processed and used as input data for the topographic map and the post-failure DTM time series 1. The point cloud was formed by scanning from four different positions of the scanner, and it covers an area of about 2200m², composed of the landslide itself and the nearby area. The data processing was done in order to eliminate the errors of the measurement and to classify the points belonging to the ground, buildings and trees. The resulting topographic map and DTM time series 1 were used to geo-reference the data collected by all the used technologies, and for the purpose of calculating the landslide volume [17,21]. Fig. 4a shows DTM time series 1 in the form of a triangle irregular network (TIN) with contour lines (continuous black and green lines) and with the positions of the laser scanner during the acquisition (bolded black circles marked B1 to B4). In Fig. 4b is the rendered TIN view of the landslide with its basic geometric characteristics.



Figure 3. Photo of landslide in Vinča – March 2009.

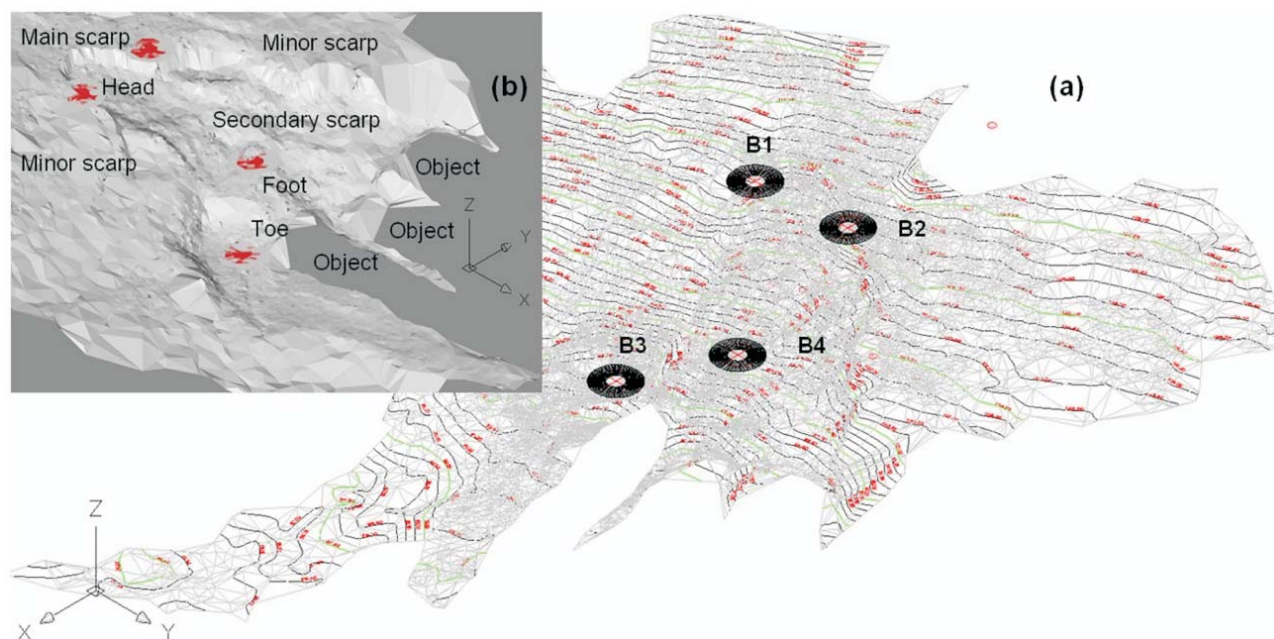


Figure 4. DTM time series 1 with characteristic elements of the landslide.

After a second reactivation of the landslide in December 2009, scanning with a terrestrial laser scanner (Leica Scan Station 2) was carried out in April 2010, and a post-failure DTM time series 2 was produced. The comparative analysis of the DTM time series 1 and 2 defines the landslide volume during the second reactivation.

3.2 GROUND-PENETRATION RADAR SCANNING

The data acquisition was carried out in July 2009 with the GSSI SIR3000 system. The formation of B scans was carried out using antennas with a central frequency of 200, 400 and 900 MHz and a high scan resolution of 1024 samples/scan, and 100 scan/m. The maximum scanning depth of 4 m was achieved by an antenna with a central frequency of 200 MHz, taking into consideration the soil structure in the landslide body and the capabilities of used antenna. The GPR calibration, in terms of determining the dielectric constant of soil, was made according to the known lithological structure of the main scarp area [11,22]. It was created with 30 B scans labelled from F029 to F059, on and around the landslide body. Fig. 5 shows the layout of the B scans selected for further discussion. The B scans are represented with the direction of the antenna motion (marked by arrow) and

the label. The points used to geo-reference the B scans were measured using two Trimble 5800 Global Positioning System (GPS) rovers in Real-Time Kinematic (RTK) mode (first covers the points 01–16, while the second covers the points p001–p011). The set of characteristic points for the B scan geo-referencing contains a start and end point. The B scan post-processing, conducted with the software package RADAN, included a determination of the time zero distance (the distance from the antenna centre to the soil surface), and the application of several digital signal-processing algorithms for reflected signals' processing. It was done in order to obtain a clear view of all the structural characteristics of landslides [11,22].

3.3 ELECTRICAL RESISTIVITY TOMOGRAPHY

In addition to the acquisition by GPR, another profile of detailed ERT scanning was done and its location is shown by the discontinuous line in Fig. 5. The equipment used for the data acquisition was an ABEM SAS 300B with a sensitivity of 0.01 mV. The length of the profile was 45 metres, and there was 113 points at 6 depth levels. The distance between two measuring points (step) was 2 m, while the total depth was approximately 4 m. The processing of the measured data was conducted

using the software packet RES2DINV. The complete profile was carried out by a combination of Wenner-Schlumberger array electrodes. The first depth level was made using the Wenner array configuration; the distances between A-M-N-B were equal (2m), whereas A and B are electrodes for introducing electric current J (mA) into the ground, and M and N are electrodes for measuring the difference in the electric potential ΔV (mV). From the level 2 to level 6 electrode configuration the Schlumberger was used, where the distance M-N remains the same (2m) while the distance between the current electrodes A-B successively increases (10, 14, 18, 22 and 26 m). The measurements on the points consisted of placing M and N at a distance of 2 metres, and a series of measuring $\Delta V/J$ ratio at the increasing distances A and B from 6m (Wenner, 2-2-2) to 26m (Schlumberger, 12-2-12, for last sixth level). In case of the Schlumberger configuration A-M-N-B, A-M and N-B, the distances between the electrodes increased successively (2, 4, 6, 8, 10 and 12m).

4 RESULTS AND DISCUSSION

4.1 GEOPHYSICAL RESULTS

Using the technologies of GPR and ERT, 31 profiles are generated: 30 GPR profiles and 1 ERT profile. Several GPR profiles that characterize the most important features have been selected for discussion. The interpretation and relation of the geophysical data to the lithological data are then presented in the following.

The disposition of the B scans F032, F033 and F034 and its starting and ending points (formed in nearby, undisturbed terrain) is shown in Fig. 5. Lithological elements that can be found in the landslide body are noticed in these B scans as well. The marks from 1 to 4 define the positions of the borders between the soil horizons in these B scans. The horizontal axis in the B scan represents the sequence of EM wave reflections recorded during the antenna movement. The number of these reflections depends on the travelled distance and the scanning resolution (the number of reflections per distance unit). For this research we used 100scans/1m resolution. The vertical axis in the B scan represents the depth of the recorded layers in meters. Initially, GPR records the two-way travel time in nanoseconds for each anomaly in one reflection. Then, from these values the depth in meters is calculated, considering the soil characteristics described with the dielectric constant ϵR . The borders between the soil horizons in the B scan correspond to the local maximum values of the reflections. If these values are determined for each reflection in the B scan then the border line between the soil horizons can be formed.

4.1.1 Right-side scarp

The B scan F032, 16m¹ long, is formed in undisturbed terrain, about 1m parallel to the edge of the right side scarp (Fig. 5). The coordinates of the beginning of the B scan F032 (0m¹) are not measured by GPS (surrounded by trees), and the end of the B scan corresponds to the point 07 (16m¹). The changes in terms of the phase inversion of the reflected signal and the disorder of the structure range from 7m¹ to 16m¹ (Fig. 6). The changes are especially visible from 7m¹ to 12m¹.

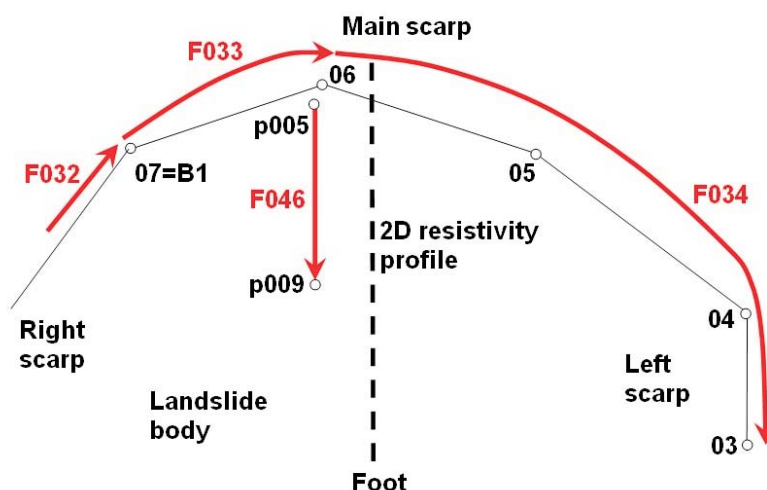


Figure 5. Disposition and parameters of the acquisition for the B scans (red line) and the ERT profile (dashed line). Thin black line represents the landslide edges.

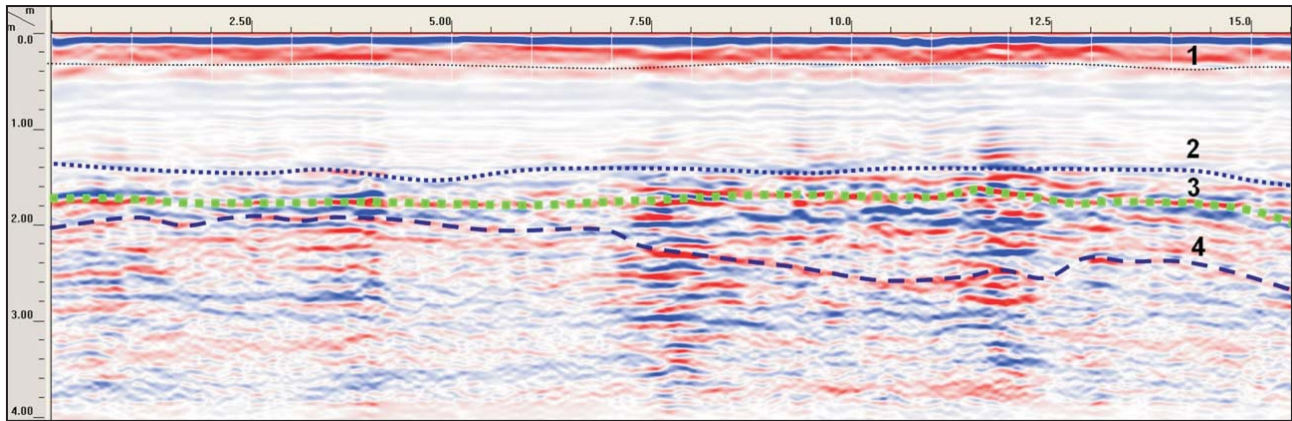


Figure 6. Interpretation of the B scan F032 on the right-side scarp.

4.1.2 head scarp apex

The B scan F033, 7m¹ long, is formed in undisturbed terrain left from the head scarp apex (Fig. 5). The beginning of the F033 B scan (0m¹) corresponds to the coordinates of the point 07 (the position of the scanner B1), and the end of the B scan corresponds to the point 06 (7m¹) – the head scarp apex (Fig. 7a). The scanning resolution in the B scan F033 was 100scan/1m. In Fig. 7a scan 390 (at 3.9m from starting point 07) is represented by an oscilloscope preview of the reflected signal with clearly visible borders between the soil horizons (local maximum values of the reflection 390).

Since it was possible to see a part of the soil horizons on the main scarp apex, they served as a solid basis for interpreting the geophysical data. Therefore, the B scan

F033 is formed directly above the scarp, so the geophysical parameters can be defined and correlation between the borders in the B scan and the visible soil horizons are established. Fig. 7b shows a visual representation of the borders 2 and 3, which served as a basis for the recalibration of a device and defining the dielectric constant $\epsilon_R=28$ [23].

4.1.3 head scarp apex – left-side scarp

The B scan F034, 33m¹ long, is formed in undisturbed terrain (at the time of acquisition) and involves the entire left-side scarp starting from the head scarp apex (Fig. 5). The beginning of the B scan F034 (0m¹) corresponds to the coordinates of the point 06, 8m¹ corresponds to the point 05, 24m¹ to the point 04, and the end corresponds to the point 03 (33m¹). The changes in

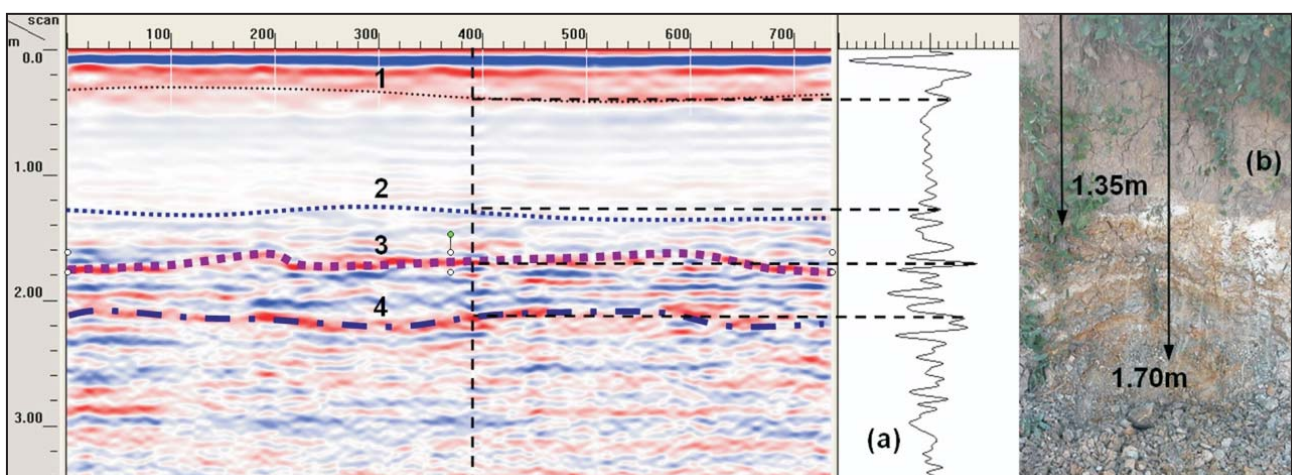


Figure 7. Interpretation of B scan F033 on the head scarp apex.

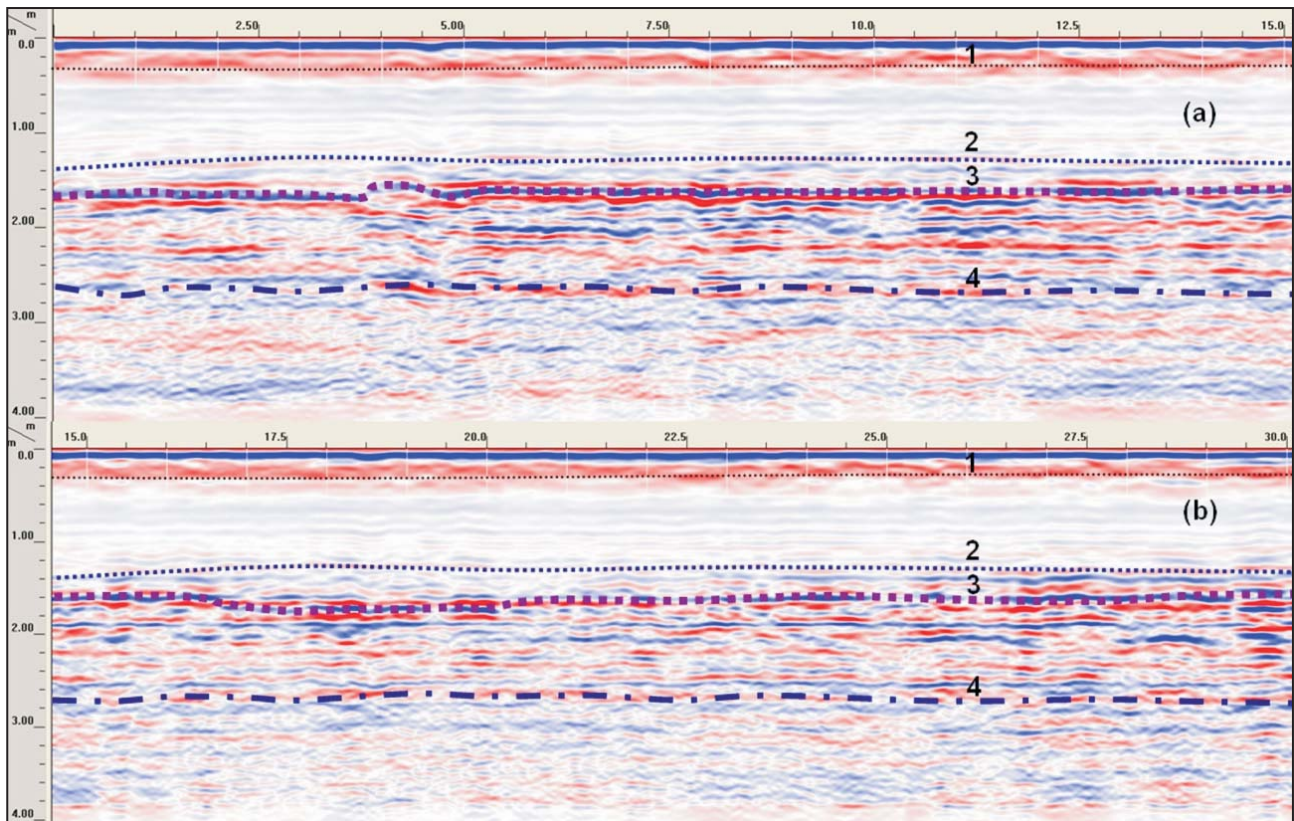


Figure 8. Interpretation of B scan F034 on the head scarp apex – left side scarp.

terms of the phase inversion of the reflected signal and the disorder of the structure can be seen in a complete B scan (Fig. 8a and 8b). The changes are especially noticeable from 2m¹ to 20m¹.

The interpretation of the B scans F032, F033 and F034 (Fig. 6, 7 and 8)

- Soil horizon from the surface to the border 1 – from 0 to 30cm – humificated loess diluvium, dark brown, dry
- Soil horizon between borders 1 and 2 – from 30 to 135cm – loess diluvium, pale brown, dry with variable amount of carbonates
- Soil horizon between borders 2 and 3 – from 135 to 170cm – incoherent sand, pale brown
- Soil horizon between borders 3 and 4 – from 170 to 210cm – on F032, that is, 260cm on F034 – altered marlstone; at 170 cm there is maximum reflected amplitude, probably clay sediments but also distorted structures and air-filled fractures, which was confirmed after the second reactivation of the landslide in December 2009 (Fig. 9)

- Soil horizon beneath border 4 – high reflection amplitude, probably weak consolidated sand, no phase inversion and a small amount of moisture.



Figure 9. Detail of distorted structure of marlstones in the left side scarp (photo December 2009).

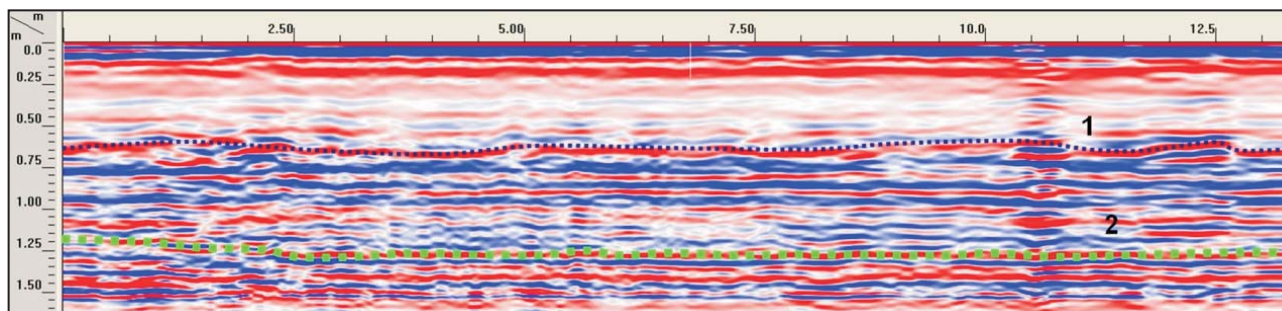


Figure 10. Interpretation of B scan F046 – central cross section, landslide body.

4.1.4 central cross section – in landslide body

The B scan F046, 13.6m¹ long, is formed in the landslide body starting from the head scarp apex to the centre of the landslide body (Fig. 5). The beginning of B scan F046 (0m¹) corresponds to the point p005, and the end of the B scan corresponds to the point p009 (13.6m¹) (Fig. 10). The trace of the B scan F046 overlaps part of the ERT profile (Fig. 11), where the starting point of the B scan p005 corresponds to 37m¹ of the ERT profile, and the ending point of the B scan p009 corresponds to 23m¹ of the ERT profile. Since the height of the starting point p005 is 113.9m above mean sea level and the end point p009 is at 109.4m, then the difference in height of the profile is 4.5m.

The comparative analysis of the geophysical data from the common parts of the B scan trace F046 and ERT profile showed an excellent correlation. It is explained in more detail when interpreting the results from the ERT profile.

The labels 1 and 2 define the position of the interpreted borders on the B scan F046:

- Soil horizon from the surface to the border 1 – from 0 to 65cm – homogenous lithological composition and structure
- Soil horizon between borders 1 and 2 – from 65 to 120cm – disorder in structure and phase inversion of reflected signal
- Soil horizon beneath border 2 – completely disordered structure with a high percentage of clay and significant attenuation of the signal. Possible surface of the rupture is expected in this soil horizon, but deeper than the maximum penetration depth of the EM wave.

4.1.5 ERT profile – central cross-section in landslide body

In the raw ERT profile (Fig. 11a) three resistivity zones can be identified [9, 13, 15]. First, there is a clearly visible zone with a low specific electrical resistivity with values between 10 and 20 Ωm (marked with shades of blue colour). This zone reaches a depth of 65cm and it can be related to moved diluvium and loess sediments and incoherent sands.

Second, the resistivity zone with values between 20 and 70 Ωm (in the ERT profile marked with shades of green), can be related to the landslide body consisting of moved diluvium, loess and sand, and at the bottom there is marlstone where, at a depth of maximum 170cm, the surface of rupture was formed.

The third, clearly identified, resistivity zone in ERT profile was coloured in yellow to the nuances of red with corresponding resistivity ranging from 70 to 250 Ωm. This zone most probably corresponds to weak consolidated sand that can be seen in immediate adjacency to the landslide on a smaller vertical cut. Also, there are traces of clay.

In ERT profile the debris can be distinguished, i.e., the material that is deposited from 0m¹ to 10m¹ of the profile length.

According to the identified resistivity values a re-interpretation was made and the resistivity zones became more visible (Fig. 11b).

Comparing the interpretation results of the B scan F046 and the ERT profile it can be seen that border 1 on the B scan corresponds to the resistivity zone 1 on the ERT profile. Also, border 2 on the B scan corresponds to the

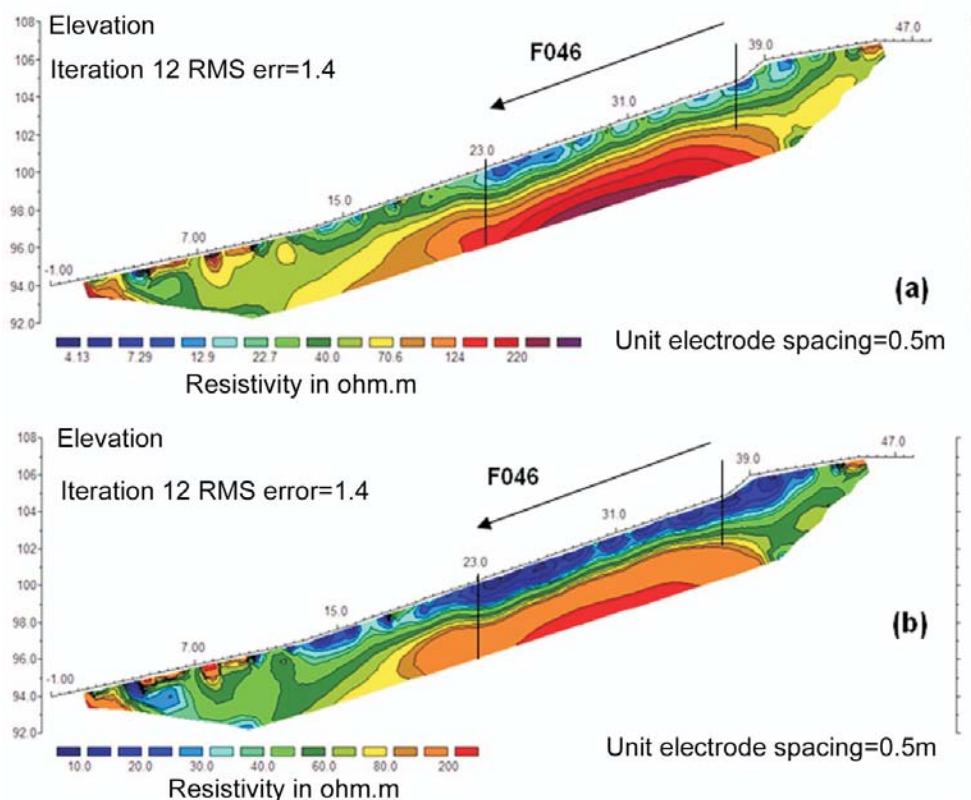


Figure 11. Interpretation of the ERT profile.

light-green colour from resistivity zone 2 on the ERT profile. It means, in this case, these two methods resulted in well-correlated data.

The ERT profile is perpendicular to head scarp and crosses the B scans F033 and F034. Since there is an overlapping zone above the head scarp apex it is possible to compare the interpretation results of the B scans and the profile. There are overt changes in the soil structure in a length of maximum 3m^1 (from 39m^1 to 42m^1 in ERT profile) and to a depth of maximum 170cm that can be noticed on the B scans as well. This leads to the conclusion that in this zone it is expected to have a further expansion of the landslide. After the landslide reactivation in December 2009 this assumption was confirmed. Reactivation occurred in zones of the left-side and head scarp. The surface of the rupture was revealed at the depth of 170–180cm (Fig. 12).

4.2 DTM ANALYSIS

In Fig. 13a DTM time series 1 is represented in cyan colour, and it includes the landslide body and the zone around the landslide. It was created by terrestrial laser

scanning in July 2009, a year and so after the landslide activation (March 2008), and a few months after the first reactivation (March 2009). The DTM time series 1 is used to geo-reference all the data obtained by the acquisition in the field, as well as for the calculation of



Figure 12. Revealed surface of rupture after the landslide reactivation in December 2009.

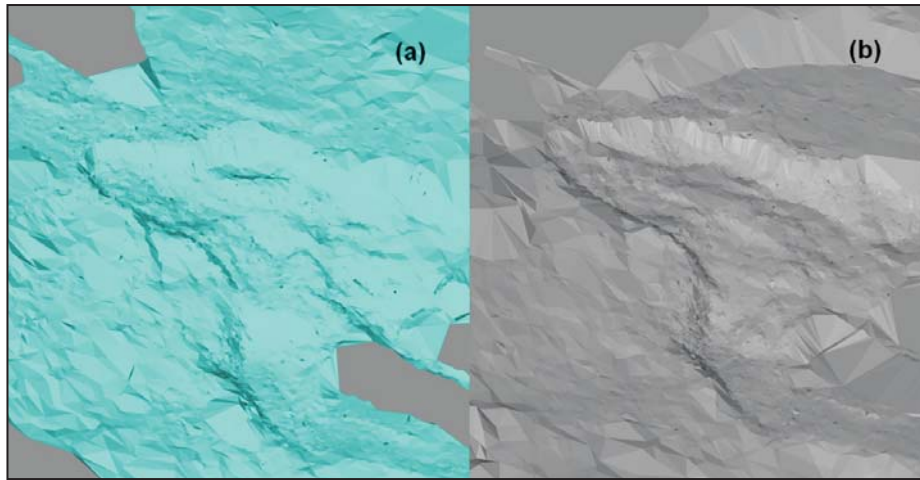


Figure 13. DTM time series 1 and 2.

the landslide volume from the moment of the landslide activation to the time of the first scanning in July 2009. The results of the comparative geometric analysis of time series 1 and the pre-failure DTM showed that the landslide volume was 1219m^3 [17].

Since in late December 2009 the second reactivation occurred in zones of the left-side and head scarp, a new data acquisition was made in April 2010 by terrestrial laser scanning with the same geo-referencing parameters. The aim of the second scanning was to monitor the movement of the material between the first and

second reactivation of the landslide and to determine the differences in the dimensions of the landslide. The DTM time series 2 formed as represented in the grey in Fig. 13b. The results of the comparative geometric analysis of the DTMs time series 1 and 2 [17] showed that a new 117m^3 was moved, and that the total landslide volume was 1336m^3 .

Fig. 14 shows a comparative representation of the DTM time series 1 and 2. It can be clearly seen that there is a movement of material in the top zone of left-side scarp and the main scarp. The DTM time series 1 is repre-

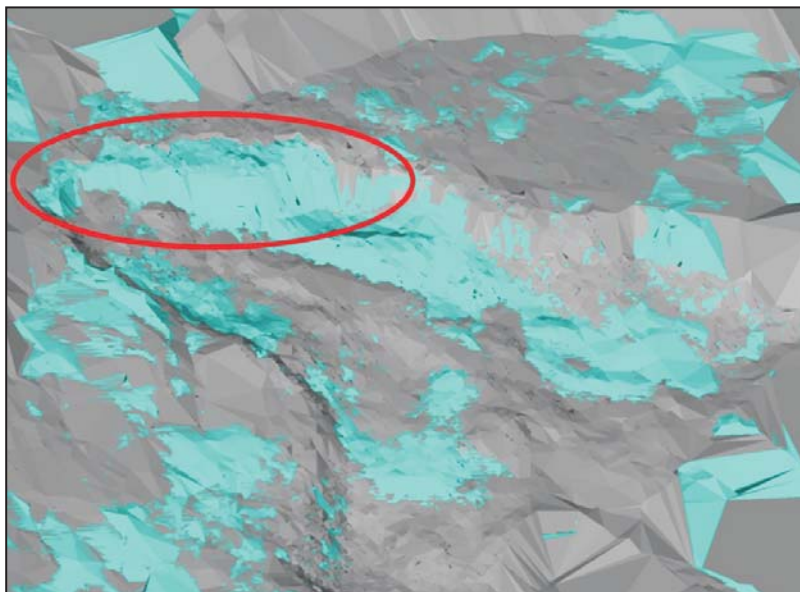


Figure 14. DTM time series 1 and 2 – comparative representation.

sented in cyan, whereas the DTM time series 2 is shown in grey. There are some variations of the DTM in the landslide body due to discarding the moved material by the owner of the building objects at the bottom.

If the final results of the geophysical research in the zone landslide are integrated with the results obtained by comparative analysis of the DTM time series 1 and 2, there is an evident tendency of movement of material at the top part of the left-side scarp.

5 CONCLUSIONS

The spatial structure interpretation of small, shallow landslides was analysed in this paper. The characteristics of these landslides require high-density data, while their number and size demands ground-based technologies able to collect a large amount of data in a short time. Considering the capabilities of existing technologies the landslide spatial structure has to be divided into surface and underground models. Therefore, an application for spatial structure interpretation should be based on a multi-geophysical approach.

Our application combines GPR, ERT and TLS technologies and it has been successfully verified on a typical example of the landslide in the village of Vinča, near Belgrade. GPR technology was chosen for a definition of the underground structure model, since it provides a time-efficient survey and high-resolution data. The ERT data were used as control data for the GPR results, because the ERT technology is slow and convenient for larger and deeper landslides. The most important results include estimation of the surface of the rupture at the depth of 1.70m, the composition of the landslide body and the prediction of the landslide enlargement directions.

The surface model is represented as a DTM created using TLS technology, which appeared to be most appropriate considering the small, shallow, landslide dimensions, accessibility and vegetation. The DTMs are obtained in pre- and post-failure time series. A comparative analysis of the DTMs provided the data on the total landslide volume of 1336m³. The geophysical data are interpreted on the basis of a lithological analysis as well as the analysis of DTMs used to monitor the activities of the landslide. The conclusions derived from an interpretation of the GPR data were confirmed by the DTM analysis by means of landslide enlargement directions.

The technology used for real-time monitoring of large and deeper landslides involves a number of sensors

and it is hardly applicable to small ones because of their number, location and dimensions. Therefore, the technology for periodic monitoring is more appropriate for small, shallow landslides. Our application provides fast acquisition and data processing and is applicable for periodic monitoring. Also, the obtained results can be used as a high-quality input for landslide mitigation. We use achieved results as the basis for designing a GIS application in the form of a shallow landslide cadastre.

REFERENCES

- [1] Bruno, F., Marillier, F. (2000). Test of high-resolution seismic reflection and other geophysical techniques on the Boup landslide in the Swiss Alps. *Surveys in Geophysics* 21, pp. 333-348.
- [2] Bichler, A., Bobrowsky, P., Best, M., Douma, M., Hunter, J., Calvert, T., Burns, R. (2004). Three-dimensional mapping of a landslide using multi-geophysical approach: The Quesnel Forks landslide. *Landslides* 1, pp. 29-40.
- [3] McGuffey, V.C., Modeer, V.A., Turner, K.A. (1996). Subsurface exploration. In: *Landslides investigation and Mitigation*. Special report 247, Transportation Research Board, National Research Council, National Academy Press, Washington D.C., pp. 231-277.
- [4] Hack, R. (2000). Geophysics for slope stability. *Surveys in Geophysics* 21, pp. 423-448.
- [5] Godio, A., Bottino, G. (2001). Electrical and Electromagnetic Investigation for landslide characterisation. *Physics and Chemistry of the Earth, Part C: Solar, Terrestrial & Planetary Science* 26, pp. 705-710.
- [6] Lapenna, V., Lorenzo, P., Perrone, A., Piscitelli, S., Sdao, F., Rizzo, E. (2003). High resolution geoelectrical tomographies in the study of Giarrossa landslide (southern Italy). *Bulletin of Engineering Geology and the Environment* 62, pp. 259-268.
- [7] Xiujun, G., Xiaoyu, H., Yonggang, J. (2005). Forward modeling of different types of landslides with Multi-electrode electric method. *Applied Geophysics* 2, pp. 14-20.
- [8] Friedel, S., Thielen, A., and Springman, S.M. (2006). Investigation of a slope endangered by rainfall-induced landslides using 3D resistivity tomography and geotechnical testing. *Journal of Applied Geophysics* 60, pp. 100-114.
- [9] Marescot, L., Monnet, R., Chapellier, D. (2008). Resistivity and induced polarization surveys for slope instability studies in the Swiss Alps. *Engineering Geology* 98, pp. 18-28.

- [10] Göktürkler, G., Balkaya, Ç., Erhan, Z. (2008). Geophysical investigation of a landslide: The Altındağ landslide site, Izmir (western Turkey). *Journal of Applied Geophysics* 65, pp. 84-96.
- [11] Ristić, A., Petrovački, D., Govedarica, M. (2009). A new method to simultaneously estimate the radius of a cylindrical object and the wave propagation velocity from GPR data. *Computers & Geosciences* 35, pp. 1620-1630.
- [12] Sass, O., Bell, R., Glade, T. (2008). Comparison of GPR, 2D-resistivity and traditional techniques for the subsurface exploration of the Öschingen landslide, Swabian Alb (Germany). *Geomorphology* 93, pp. 89-103.
- [13] Naudet, V., Lazzari, M., Perrone, A., Loperte, A., Piscitelli, S., Lapenna, V. (2008). Integrated geophysical and geomorphological approach to investigate the snowmelt-triggered landslide of Bosco Piccolo village (Basilicata, southern Italy). *Engineering Geology* 98, pp. 156-167.
- [14] Schrott, L., Sass, O. (2008). Application of field geophysics in geomorphology: Advances and limitations exemplified by case studies. *Geomorphology* 93, pp. 55-73.
- [15] Sturzenegger, M., Stead, D. (2009). Close range digital photogrammetry and terrestrial laser scanning for discontinuity characterization on rock cuts. *Engineering Geology* 106, pp. 163-182.
- [16] van Westen, C., Castellanos, E., Kuriakose, S.L. (2008). Spatial data for landslide susceptibility, hazard and vulnerability assessment: An overview. *Engineering Geology* 102, pp. 112-131.
- [17] Du, J.C., Teng, H.C. (2007). 3D laser scanning and GPS technology for landslide earthwork volume estimation. *Automation in Construction* 16, pp. 657-663.
- [18] Rokić, L. (1997). Origins of landslides on the right bank of Danube river near Novi Sad. *International Symposium on Engineering Geology and the Environment*, Athens, June 23-27, 1997, pp. 1003-1008.
- [19] Jevremović, M., Kuzmić, V. (2001). Complex geological map of Belgrade KGK 10 (1:10.000). Geozavod, Beograd.
- [20] Cruden, D.M., Varnes, D.J. (1996). Landslide types and processes, in: Turner, K.A., Schuster, R.L. (eds.), *Landslides investigation and Mitigation*. Special report 247, Transportation Research Board, National Research Council, National Academy Press, Washington D.C., pp. 36-75.
- [21] Abolmasov, B., Milenković, S., Ristić, A., Hadžiniković, G., Đurić U. (2010). 3D terrestrial laser scanning and GPS technology for slope stability investigations-case studies. *3rd Symposium of Macedonian Association for Geotechnics*, Struga, June 24-26, pp. 2010, 9-16.
- [22] Ristić, A., Petrovački, D., Govedarica, M., Popov, S. (2007). Detection of underground water flows by ground penetrating radar. *Vodoprivreda* 39, pp. 228-230, (in Serbian with English abstract).
- [23] Saarenketo, T. (1998). Electrical properties of water in clay and silty soils. *Journal of Applied Geophysics* 40, pp. 73-88.

NUMERIČNA ANALIZA OKROGLEGA TEMELJA NA NARAVNI GLINI, STABILIZIRANI Z ZRNATIM POLNILOM

MURAT ORNEK, AHMET DEMIR, MUSTAFA LAMAN İN ABDULAZIM YILDIZ

o avtorjih

Murat Ornek
Mustafa Kemal University,
Civil Engineering Department
Iskenderun/Hatay, Turčija
E-pošta: mornek@mku.edu.tr

Ahmet Demir
Korkut Ata University,
Civil Engineering Department
80000 Osmaniye, Turčija
E-pošta: ahmetdemir@osmaniye.edu.tr

Abdulazim Yildiz
Cukurova University,
Civil Engineering Department
01330 Balcali/Adana, Turčija
E-pošta: azim@cukurova.edu.tr

vodilni avtor

Mustafa Laman
Cukurova University,
Civil Engineering Department
01330 Balcali/Adana, Turčija
E-pošta: mlaman@cukurova.edu.tr

izvleček

V tej študiji so predstavljene numerične napovedi obsega učinka na okrogle temelje, podprtih z delno zamenjanimi in zgoščenimi plastmi na usedlinah naravne gline. Pojav obsega učinka je analiziran glede na velikost temelja. Numerične analize so bile izvedene z uporabo osno simetričnega, dvodimenzionalnega programa s končnimi elementi. Pred izvedbo analize je bila potrjena veljavnost osnovnega modela z uporabo terenskih testov s sedmimi različnimi premeri temeljev do 0,90 m in s tremi različnimi delno zamenjanimi debelinami. Izkazalo se je, da lahko obnašanje okroglih temeljev na tleh iz naravne gline in delno zamenjanim sistemom dovolj primerno prikažemo z Mohr-Coulombovim modelom. Parametri Mohr Coulombovega modela so izpeljani iz rezultatov z običajnimi laboratorijskimi in s terenskimi testi. Z doseženo dobro složnostjo med rezultati testa in numeričnimi analizami, so bile nadaljevane numerične analize s povečevanjem premera temeljev do 25m in upoštevanjem z delno zamenjavo debeline do dvakratnega premera temeljev. Rezultati te parametrične študije so pokazale, da ima stabilizacija precejšen učinek na nosilno kapaciteto okroglih temeljev in da se pri dani vrednosti H/D magnituda mejne nosilne kapacitete poveča s premerom temelja na nelinearni način. Določen je količnik nosilne kapacitete (BCR) za določitev izboljšane učinka ojačenega sistema. Na podlagi rezultatov numeričnih in terenskih testov je ugotovljeno, da se BCR delno zamenjanih odloženih naravnih glin poveča s povečanjem premera temeljev in da ni pomembnega obsega učinka okroglega temelja ležečega na usedlini z naravno glino.

ključne besede

obseg učinka, okrogli temelji, terenski test, analiza končnih elementov, naravna glina, zrnato polnilo

NUMERICAL ANALYSIS OF CIRCULAR FOOTINGS ON NATURAL CLAY STABILIZED WITH A GRANULAR FILL

MURAT ORNEK, AHMET DEMIR, MUSTAFA LAMAN and ABDULAZIM YILDIZ

about the authors

Murat Ornek
Mustafa Kemal University,
Civil Engineering Department
Iskenderun/Hatay, Turkey
E-mail: mornek@mku.edu.tr

Ahmet Demir
Korkut Ata University,
Civil Engineering Department
80000 Osmaniye, Turkey
E-mail: ahmetdemir@osmaniye.edu.tr

Abdulazim Yildiz
Cukurova University,
Civil Engineering Department
01330 Balcali/Adana, Turkey
E-mail: azim@cukurova.edu.tr

corresponding author

Mustafa Laman
Cukurova University,
Civil Engineering Department
01330 Balcali/Adana, Turkey
E-mail: mlaman@cukurova.edu.tr

abstract

In this study, numerical predictions of the scale effect for circular footings supported by partially replaced, compacted, layers on natural clay deposits are presented. The scale-effect phenomenon was analyzed according to the footing sizes. Numerical analyses were carried out using an axisymmetric, two-dimensional, finite-element program. Before conducting the analysis, the validity of the constitutive model was validated using field tests performed by authors with seven different footing diameters up to 0.90 m and with three different partial replacement thicknesses. It is shown that the behavior of the circular footings on natural clay soil and the partial replacement system can be reasonably well represented by the Mohr Coulomb model. The Mohr-Coulomb model parameters were derived from the results of conventional laboratory and field tests. After achieving a good consistency between the results of the test and the

numerical analysis, the numerical analyses were continued by increasing the footing diameter up to 25 m, considering the partial replacement thickness up to two times the footing diameter. The results of this parametric study showed that the stabilization had a considerable effect on the bearing capacity of the circular footings and for a given value of H/D the magnitude of the ultimate bearing capacity increases in a nonlinear manner with the footing diameter. The Bearing Capacity Ratio (BCR) was defined to evaluate the improved performance of the reinforced system. It was found, based on numerical and field-test results that the BCR of the partially replaced, natural clay deposits increased with an increase in the footing diameter and there was no significant scale effect of the circular footing resting on natural clay deposits.

keywords

scale effect, circular footing, field test, finite-element analysis, natural clay, granular fill

1 INTRODUCTION

The bearing capacity of shallow footings has been studied since Terzaghi's original observation during the 1940s. Although additional considerations to the governing criteria of bearing capacity have been proposed, the ultimate bearing-capacity calculation of a footing has changed very little since Terzaghi's [1] first general equation for the ultimate bearing capacity, q_{ult} . The classic bearing-capacity formulation cannot be used directly in large-scaled footing design without a correlation.

Small-scale, laboratory-model tests are easier to operate due to their small sizes and the cost is significantly less than large and full-scale in-situ tests. Because of these advantages, small-scale laboratory tests are preferable for studying the behavior of soil. However, it is difficult to simulate a soil's characteristics (water content, density, strength etc.), exactly, especially in cohesive soils. Despite their operational and financial disadvantages, large and full-scale in-situ tests give more reasonable

results in when simulating soil behavior. It is known from the literature that most of the experimental studies on soils have been conducted using small-scale laboratory tests and formulations have been derived from small-scale model footing tests. Small-scale model footing tests produce higher values for the bearing capacities than those of theoretical equations and therefore they should not be used for the design of full-scale footings without a reduction [2, 3].

The difference in performance between the actual large and/or full scaled soil footings and the model footing tests should be considered. The relationship between the tests with small- and large-scaled footing is known as the “scale effect” in geotechnical engineering. This relation validated by theoretical, analytical and numerical analyses gives advantages in geotechnical design. An effective, suitable scale-effect investigation or, in other words, a proper scale-effect ratio helps to decrease the design expenses, gain time for design procedures and get simpler operational processes. Siddiquee et al. [4] reported that the scale effect is the variation in the bearing capacity characteristics with the variation in the footing size.

The literature review is divided into the “scale-effect” and the “reinforcement of weak soils” in this study. There are limited studies focused directly on a “scale-effect” investigation in the literature [5-10]. Berry [5] was an early reporter of the scale-effect phenomenon and showed that the bearing capacity of circular footings decreases with the increasing footing size on dense sand at a constant relative density. This means that the bearing capacity factor, N_y , decreases with increasing footing size, when N_y was obtained from a back-calculation. Fukushima et al. [11] identified appropriate design constants to take into account scale effects. They investigated the scale-effect properties of the ultimate bearing capacity that accompanies the changes in the shape of the spread footing by conducting the plate-loading test on soft-rock ground, gravelly soil and rock-fill embankment, where the dimensional shape of the loading plates are changed. They concluded that plate loading tests in which the loading-plate scale is changed, are practical as an investigation method for design constants to take into consideration the scale effects in spread-footing design. Cerato and Lutenecker [2] concluded that the scale effect occurs because of the stress dependency of sand soils and they described it as “different sized footings have different mean stresses; the smaller the footing is the smaller the mean stresses”.

A shortage of the availability of proper construction sites in city centers has led to the increased use of problematic areas where the bearing capacity of the underlying deposits is very low. The partial replacement of these

problematic soils with a layer is one of the soil-improvement techniques that is widely used. Problematic soil behavior can be improved by totally or partially replacing inadequate soils with compacted in layers. Several experimental and numerical studies have been described about the reinforcement of a weak soft soil [12-19]. Adams and Collin [2] conducted 34 large model load tests to evaluate the potential benefits of geosynthetic-reinforced spread foundations. It was concluded that the soil-geosynthetic system formed a composite material that inhibited the development of the soil-failure wedge beneath the shallow spread foundations. Alawaji [13] discussed the effects of reinforcing the sand pad over collapsible soil and reported that a successive reduction in the collapse settlement up to 75% was obtained. Dash et al. [14] performed model tests in the laboratory to study the response of the reinforcing granular fill overlying soft clay beds and showed that substantial improvements in the load-carrying capacity and a reduction in surface heaving of the foundation bed were obtained.

This study is focused directly on the scale-effect investigation in circular footings rested on natural clay deposits stabilized with compacted granular-fill layers. Numerical analyses were carried out using two-dimensional, finite-element formulations. Before conducting the analysis, the validity of the constitutive model was proved using field tests performed by the authors, with seven different footing diameters up to 0.90 m and three different compacted granular-fill layer thicknesses. After achieving a good consistency, the numerical analyses were continued by increasing the footing diameter up to 25 m. In this parametric study, the granular-fill layer thicknesses were selected as 0.17D; 0.33D; 0.67D; 1.00D; 1.33D; 1.67D and 2.00D according to the footing diameter. The results of this study showed that the partial replacement with compacted granular-fill layer had a considerable effect on the bearing capacity of the circular footings. It was found based on the numerical and field test results that the Bearing Capacity Ratio (BCR) of the stabilized natural clay deposits increased with an increase in the footing diameter and there was no significant scale effect of circular footing resting on natural clay deposits.

2 FIELD TESTS

2.1 SITE CHARACTERIZATION

A total of 28 field tests were conducted at the Adana Metropolitan Municipality's (AMM) Water Treatment Facility Center (WTFC) located in west part of Adana, Turkey. The soil conditions at the experimental test

site (WTFC) were determined from a geotechnical site investigation comprised of both field and laboratory tests. Two test-pit excavations (TP1 and TP2) and four borehole drillings (BH1, BH2, BH3 and BH4) were performed in the WTFC test area. The test area has dimensions of 30m (length) by 11.6m (width). The test pits were excavated to a depth of 2.50 m and boreholes were drilled with diameters of 10cm and depths of 13m. The borehole drilled in the south side was 20 m deep. The ground-water level was observed to be 2.2m, from the borehole drillings. The field tests were conducted at a depth of about 2.0m from the ground surface. The degree of saturation ratio was measured to be around 80% at this level. Three subsoil layers were clearly identified by visual inspection and by a unified soil-classification system. The first layer, with a depth of 0.80 m, observed as topsoil, was removed before the tests. The intermediate layer between the depths of 0.80 m and 7.0 m exhibits a silty clay stratum with high plasticity (CH). A silty clay layer with the intrusion of sand (CL) was observed in the bottom layer up to 10.0 m depth. A Standard Penetration Test (SPT) was carried out during the drilling of each borehole and the soil tested was classified as medium stiff clay. The distribution of the SPT values with depth, including the soil profile, is shown in Figure 1. Conventional laboratory tests, such as a sieve analysis, moisture content, Atterberg limit, specific gravity, standard Proctor, unconfined compression, laboratory vane, triaxial and consolidation tests, were performed in the Geotechnical Laboratory of Civil Engineering Department at Cukurova University, Adana, Turkey. The clay content of the soil layers varies

in the range between 60 and 70%. The upper homogeneous layer where all the loading tests were carried out is classified as a high plasticity clay (CH) according to the Unified Soil Classification System (USCS). The water content of the stratified soil layers varies between 20 and 25% depending on the depth, and is almost the same as, or greater than, the plastic limit. The specific gravities (G_s) vary from 2.60 to 2.65 along the depths. The triaxial, consolidation and unconfined compression tests were conducted on undisturbed soil samples derived from the field. The values of the undrained shear strengths, c_u were determined by unconfined compression tests in the range 60 to 80 kN/m². The values of the undrained shear strengths c_u from the unconsolidated undrained, triaxial test were obtained as 70-80 kN/m². The clay soil layer can generally be classified as a lightly overconsolidated clay based on odometer test results. The typical soil characteristics of the natural clay soil are given in Figure 2.

2.2 DETAILS OF THE MODEL FOOTINGS AND GRANULAR-FILL MATERIAL USED

Seven different footings with diameters of 0.06, 0.09, 0.12, 0.30, 0.45, 0.60 and 0.90 m were used in this study. These rigid, steel-made footings have a thickness of 2cm for $D \leq 12$ cm and 3 cm for $D > 12$ cm, where D is the footing diameter. The granular-fill material used in the model tests was obtained from the Kabasakal region situated northwest of Adana, Turkey. Some conventional tests (sieve analysis, moisture content, unit weight, direct shear and proctor tests) were conducted on this material.

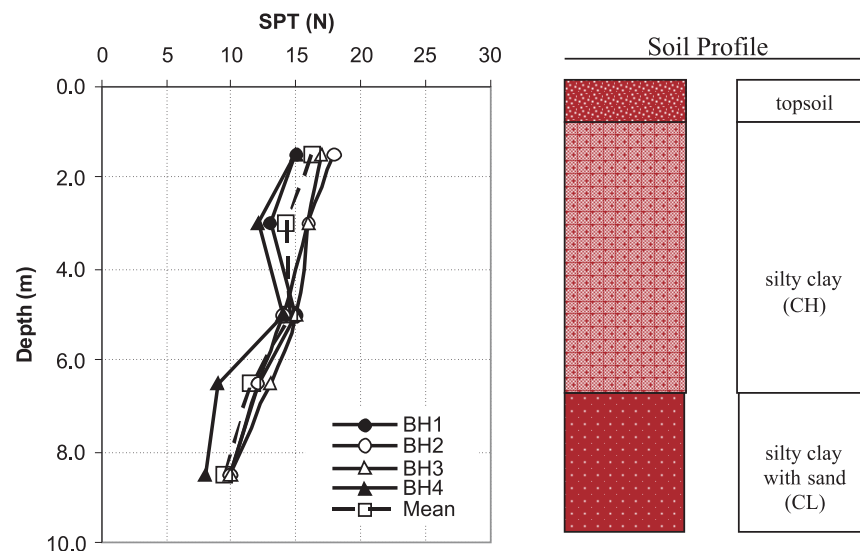


Figure 1. SPT(N) values measured from the boreholes.

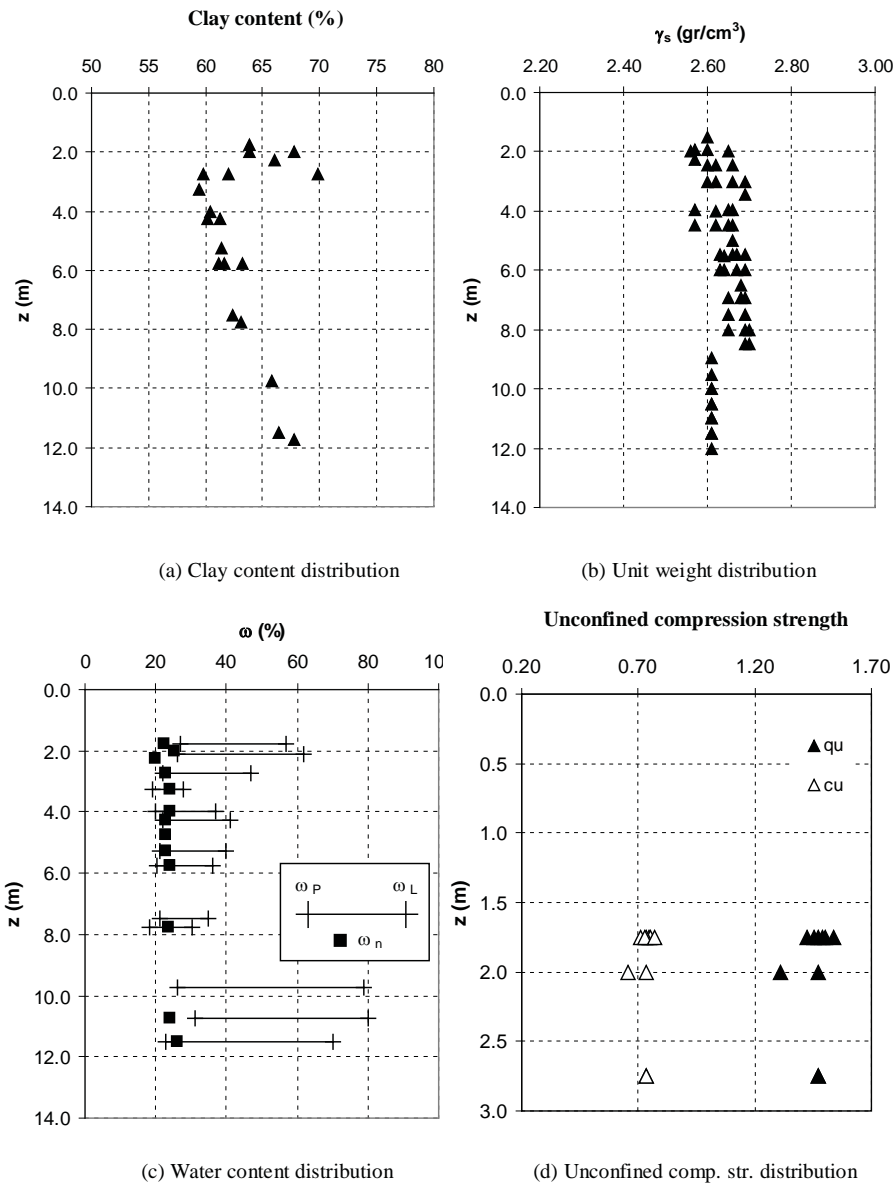


Figure 2. Typical soil characteristics of natural clay soil.

The granular soil was prepared at a value of the optimum moisture content of 7% and a maximum dry unit weight of 21.7kN/m³ obtained from the standard Proctor test. The values of the internal friction angle and the cohesion of the granular fill were obtained as 43° and 15kN/m², respectively from direct shear tests. The square-shaped direct shear box has a width of 60 mm. The specific gravity of the granular soil was obtained as 2.64. Typical soil characteristics of the granular-fill material are given in Figure 3. From the sieve analysis, the granular soil was classified as a well-graded, gravel-silty gravel, GW-GM according to the unified soil-classification system. Figure 3 (a) shows that the particle size distribution of the natu-

ral granular-fill material. However, the granular-fill material used in conventional laboratory and field tests was obtained from natural granular material passing through a 4.75-mm-opening sieve. The reason was to provide homogeneity in the laboratory and field-test conditions.

2.3 EXPERIMENTAL SETUP AND TEST PROGRAM

After obtaining the soil properties of the WTFC test area, a total of 24 piles were constructed. The topsoil was removed before the tests. Then, the reaction piles were connected with a steel beam. The top surface of

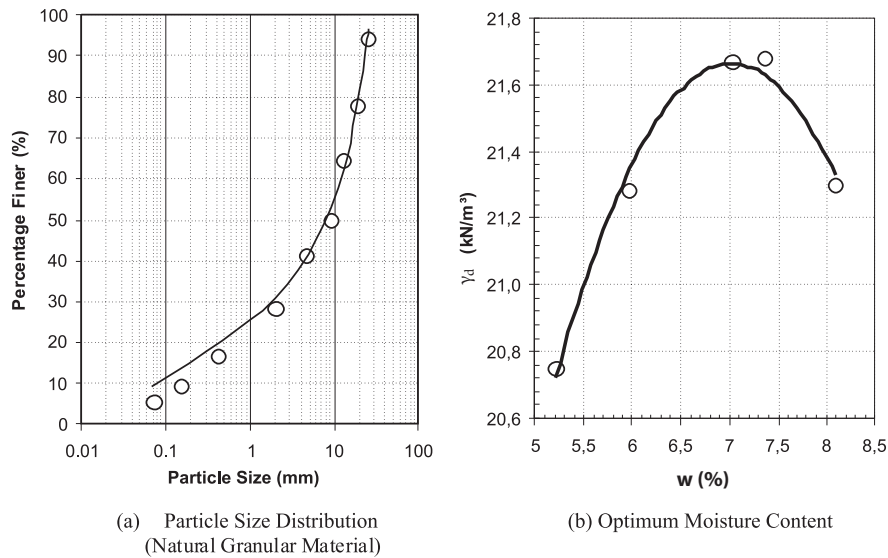


Figure 3. Typical soil characteristics of granular-fill material.

the test area was leveled and the footing was placed on a predefined alignment such that the loads from the hydraulic jack and the loading frame would be transferred concentrically to the footing. A hydraulic jack against the steel beam provided the downward load. The hydraulic jack and two linear variable displacement transducers (LVDTs) were connected to a data logger unit and the data logger unit was connected to a computer. The granular-fill material was placed and compacted in layers. The thickness of each layer was changed depending on the footing diameter. The amount of granular-fill material and water needed for each layer was first calculated. Then, the granular-fill material was compacted using a plate compactor to a predetermined height to achieve the desired densities. The compacted,

granular-fill layer has a moisture content of 7% and a unit weight of 20.2 kN/m³. Load was applied with a hydraulic jack and maintained manually with a hand pump. The load and the corresponding footing settlement were measured with a calibrated pressure gauge and two LVDTs, respectively. The testing procedure was performed according to the ASTM D 1196-93 [20], where the load increments applied and maintained until the rate of settlement were less than 0.03 mm/min over three consecutive minutes. To maintain the same density throughout the test area, a convenient compactive effort was applied to each layer of the granular fill. Some tests were repeated twice to verify the repeatability and the consistency of the test data. The same pattern of the load-settlement relationship with a difference of the

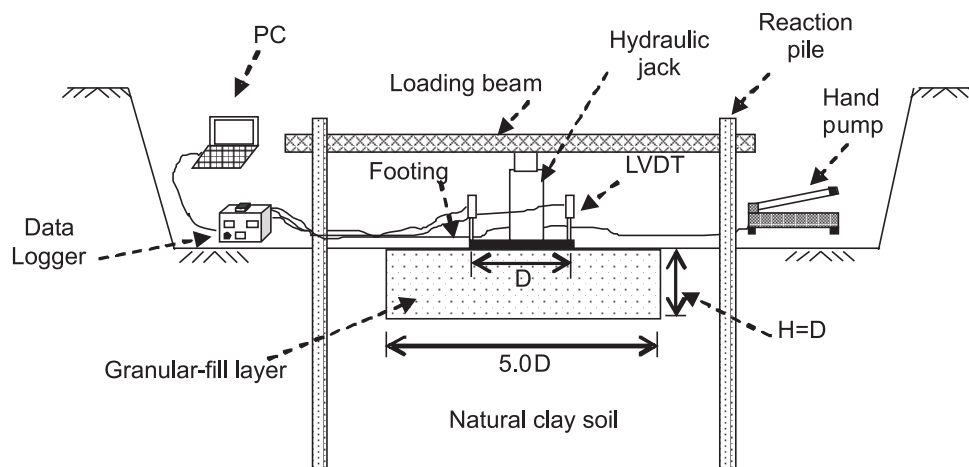


Figure 4. Schematic view of test setup, loading, reaction system and typical layout of the instrumentation.

ultimate load values less than 2.0% was obtained. This difference was considered to be small and neglected. The tests were continued until the applied vertical load was clearly reduced or a considerable settlement of the footing was obtained from a relatively small increase of the vertical load. Detailed information about the testing procedure can be found in Laman et al. [21] and Ornek [22]. The general layout of the test setup is given in Figure 4.

The research was conducted in two series. Series I consisted of the testing of seven different footing diameters (0.06, 0.09, 0.12, 0.30, 0.45, 0.60 and 0.90 m) on the surface of a natural clay deposit. Series II was the same as Series I, except that the footings were placed on a granular-fill layer settled on a natural clay deposit. The granular-fill layers were designed in three different thicknesses according to the footing diameters (0.33D; 0.67D and 1.00D).

3 FINITE-ELEMENT ANALYSIS

Numerical analysis is a powerful mathematical tool that makes it possible to solve complex engineering problems. The finite-element method is a well-established numerical analysis technique used widely in many civil engineering applications, both for research and the design of real engineering problems. The constitutive behavior of soils can be successfully modeled with numerical analyses. The finite-element method is one of the mathematical methods in which continuous media is divided into finite elements with different geometries. It provides the advantage of idealizing the material behavior of the soil, which is non-linear with plastic deformations and is stress-path dependent, in a more rational manner. The finite-element method can also be particularly useful for identifying the patterns of deformations and stress distribution during deformation and at the ultimate state. Because of these capabilities of the finite-element method, it is possible to model the construction method and investigate the behavior of shallow footings and the surrounding soil throughout the construction process, not just at the limit equilibrium conditions [23].

Numerical analyses were conducted using the program Plaxis 2D V8.6. It is a finite-element package that is specially developed for the analysis of deformation and stability in geotechnical engineering problems [24]. The stresses, strains and failure states of a given problem can be calculated.

Plaxis incorporates a fully automatic, mesh-generation procedure, in which the geometry is divided into

elements of the basic element type and compatible structural elements. Five different mesh densities are available in Plaxis, ranging from very coarse to very fine. In order to obtain the most suitable mesh for the present study, preliminary computations using the five available levels of global-mesh coarseness were conducted. In the work reported herein, the number of elements was about 600 with a fine mesh type. In the sensitivity analysis, the number of elements was changed from 149 (very coarse) to 1128 (very fine) for the axisymmetric condition. As seen in Figure 5, the mesh size has a minimum effect on the results after about 500 to 600 elements. This corresponds to the fine mesh. Consequently this mesh procedure was adopted in the numerical part of the study.

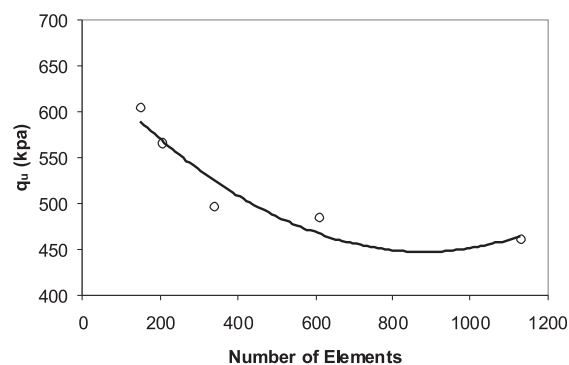


Figure 5. Influence of mesh size on the finite-element results.

Plaxis generates full fixity at the base of the geometry and smooth conditions at the vertical sides, including the symmetric boundary. The modeled boundary conditions were assumed such that the vertical boundaries are free vertically and constrained horizontally, while the bottom horizontal boundary is fixed in both the horizontal and vertical directions. In the analyses, the dimensions of the medium were created according to the footing size in the 2D area. To eliminate boundary effects due to loading, the horizontal and vertical dimensions were taken as 5D and 4D, respectively. The soil medium was modeled using 15-node triangular elements. Because of the symmetry, only one half of the soil-footing system is considered. A typical graded finite-element mesh composed of the soil and foundation, together with the boundary conditions and the geometry of the soil system used is shown in Figure 6.

An elastic-plastic Mohr Coulomb (MC) model was selected for the clay and granular-fill material behavior in this study. The MC model is a practical and user-friendly model that includes only a limited number of features that the soil behavior shows in reality. Although

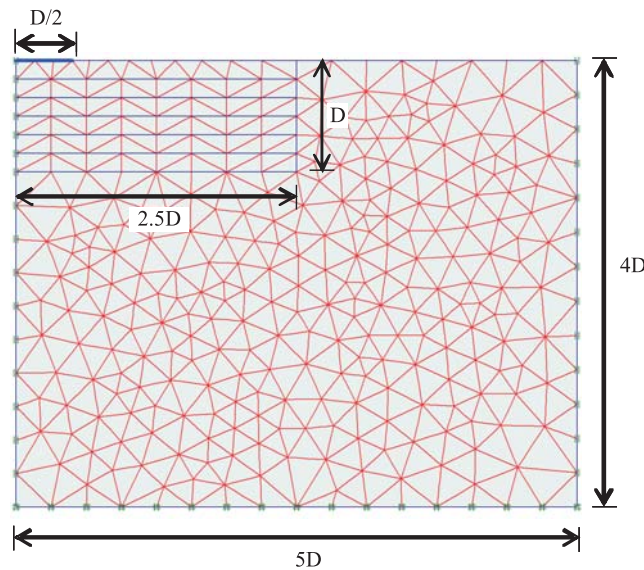


Figure 6. Typical mesh configurations in the numerical analyses.

Table 1. Mohr-Coulomb model parameters

Parameter	Clay Value	Granular-fill Material Value
Unit weight, γ_n (kN/m ³)	18	21
Loading stiffness, E_u (kN/m ²)	8500	42500
Cohesion, c (kN/m ²)	75	1
Poisson's ratio, ν	0.35	0.2
Friction angle, ϕ (degrees)	0	43
Dilatancy angle, Ψ (degrees) ($\phi-30^\circ$)	0	13

the increase of the stiffness with depth can be taken into account, the MC model does not include either the stress dependency or the stress-path dependency of the stiffness or the anisotropic stiffness. In general, the stress states at failure are quite well described using the MC failure criterion with effective strength parameters. The MC model involves five input parameters, i.e. E and ν for the soil elasticity; ϕ and c for the soil plasticity and Ψ as an angle of dilatancy. The MC model represents a "first-order" approximation of the soil behavior [24]. It is clear from the literature that homogeneous and saturated clay soils were analyzed in the undrained soil condition with the MC model. It is reported that the undrained bearing capacity of soil increases generally with depth. Some researchers indicate that selecting a proper value of undrained cohesion and using the MC model is sufficient for simulating the behavior of clay soil [25-28]. Table 1 presents the clay soil and granular-fill bed

material parameters used in the numerical analyses. The dilatancy angle Ψ is taken as 13° , ($\phi-30^\circ$) based on the equation proposed by Bolton [29] and the remaining model parameters were measured.

4 VALIDATION OF FIELD TEST RESULTS WITH THE FINITE-ELEMENT APPROACH

4.1 TEST SERIES I: TESTS ON THE NATURAL CLAY DEPOSIT

In test Series I, a total of seven in-situ tests were conducted using seven different circular foundations (diameters of 0.06, 0.09, 0.12, 0.30, 0.45, 0.60 and 0.90 m) rested on a natural clay deposit. The load-settlement curves for all sizes, including the numerical analysis, are presented in Figure 7. The horizontal and vertical axes show the bearing capacities and the settlement ratios, respectively. The settlement ratio (s/D) is defined as the ratio of the footing settlement (s) to the footing diameter (D), expressed as a percentage. It is clear from the figure that the vertical displacements predicted by the numerical analysis are in very good agreement with the experimental results. Since the load was applied directly through the natural clay soil in test Series I, the settlement pattern generally resembles a typical local shear failure and the maximum load bearing capacity was not clearly well defined in each case.

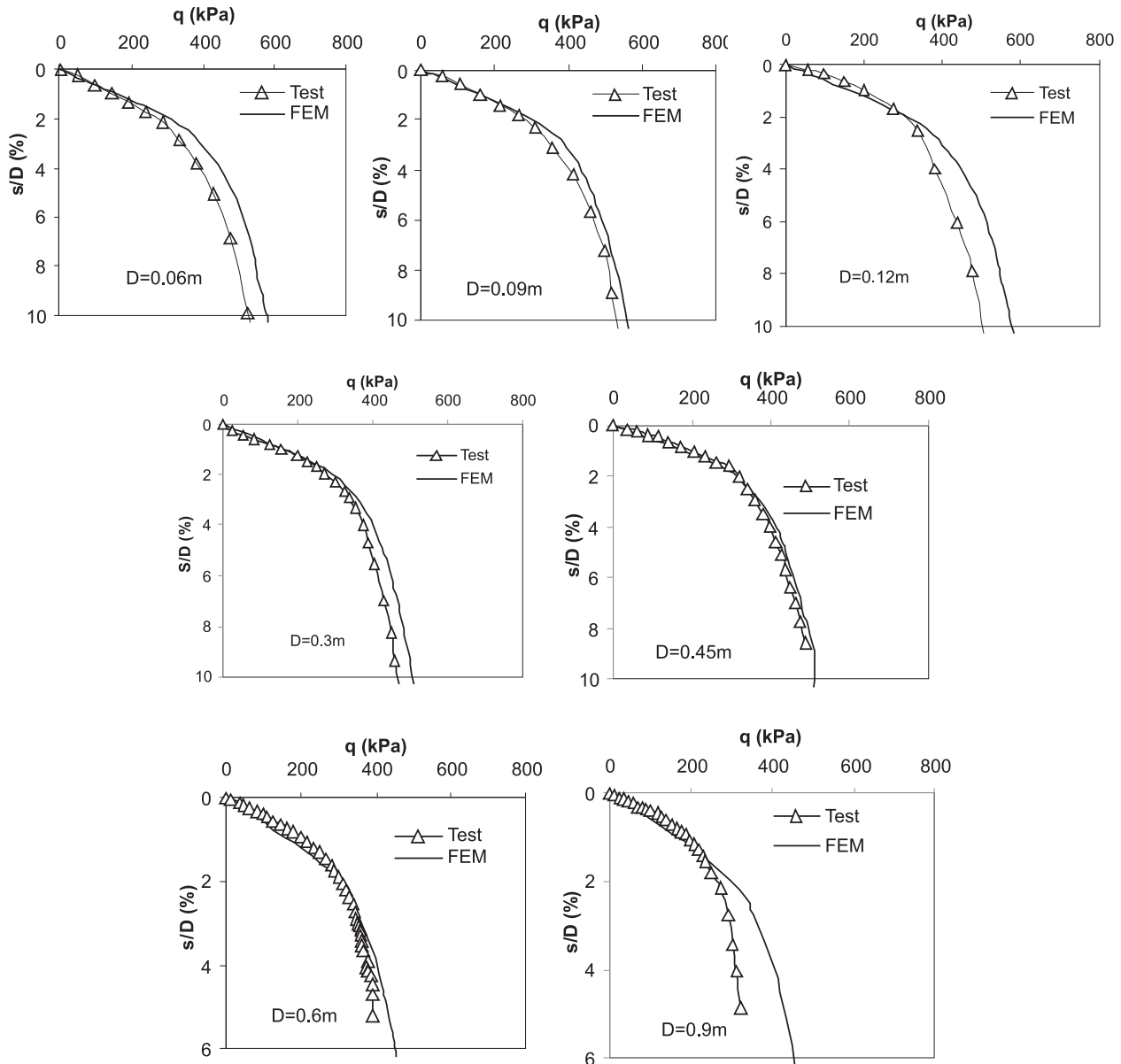


Figure 7. Curves of bearing capacity against settlement for test Series I.

4.2 TEST SERIES II: TESTS ON THE GRANULAR-FILL LAYER PLACED ON NATURAL CLAY DEPOSIT

The effect of the granular-fill layer thickness on the bearing capacity and the settlement behavior was investigated in tests Series II. In these tests, the granular-fill thickness was changed, depending on the footing diameter, to 0.33, 0.67 and 1.00D.

The contributions from the granular-fill layer on the bearing capacity are represented by the term of the Bearing Capacity Ratio (BCR).

The term BCR is commonly used to express and compare the test data of the stabilized and clay soils. The following well-established definition [30] is used for BCR:

$$\text{BCR} = q_R / q_0 \quad (1)$$

where q_R and q_0 are the bearing capacity for the stabilized (granular-fill layer placed on the natural clay deposit) and natural clay soils, respectively. The granular-fill layer thickness H and the settlement of footing plate s are normalized by the diameter of the footing plate, D [31]. The bearing capacity was defined as the tangent intersection between the initial, stiff, straighter

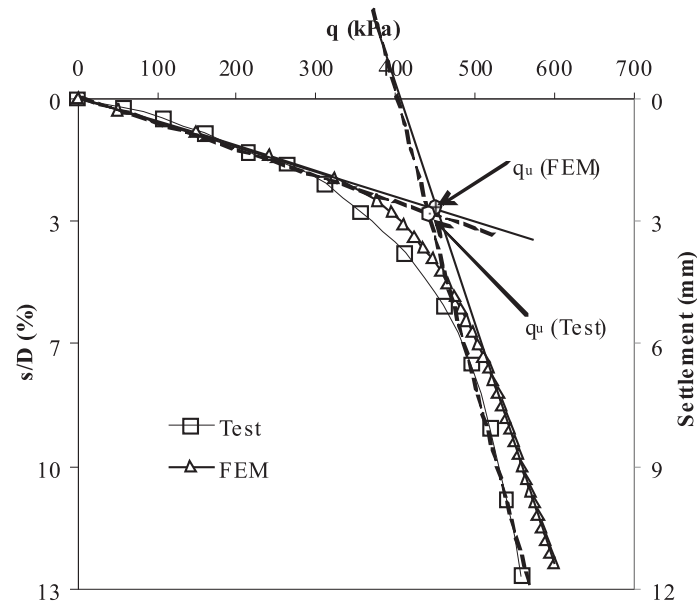


Figure 8. Determination of the ultimate bearing-capacity value.

portion of the loading-pressure-settlement curve and the following steeper, straight portion of the curve [12]. All the test and numerical results were interpreted using this approach (Figure 8). It is also clear that the ultimate bearing-capacity values obtained from the experimental and numerical studies are very close to each other. The settlement ratio (s/D) is defined as the ratio of the footing settlement (s) to the footing diameter (D). The q_u (ultimate bearing capacity) and s (settlement) values were obtained from load-settlement curves of the tests.

The field-test configurations of “ $D=0.12\text{m}-H/D=0.33$ ” and “ $D=0.30\text{m}-H/D=0.33$ ”, including the numerical

analysis, were selected to give typical examples in Figure 9. As seen from the figure, the vertical displacement predicted by the numerical analysis are in very good agreement with the experimental results. Figure 10 shows the relation of BCR to H/D ratio obtained from the numerical studies and the tests of Series II using the values of the ultimate bearing capacity evaluated using Equation 1. H/D is a ratio defined as the ratio of the granular-fill thickness (H) to the footing diameter (D). It is shown that the BCR increases with an increase in the granular-fill thickness for all footing diameters. The main reason for this phenomenon is that the thickness of the granular-fill material is increasing and

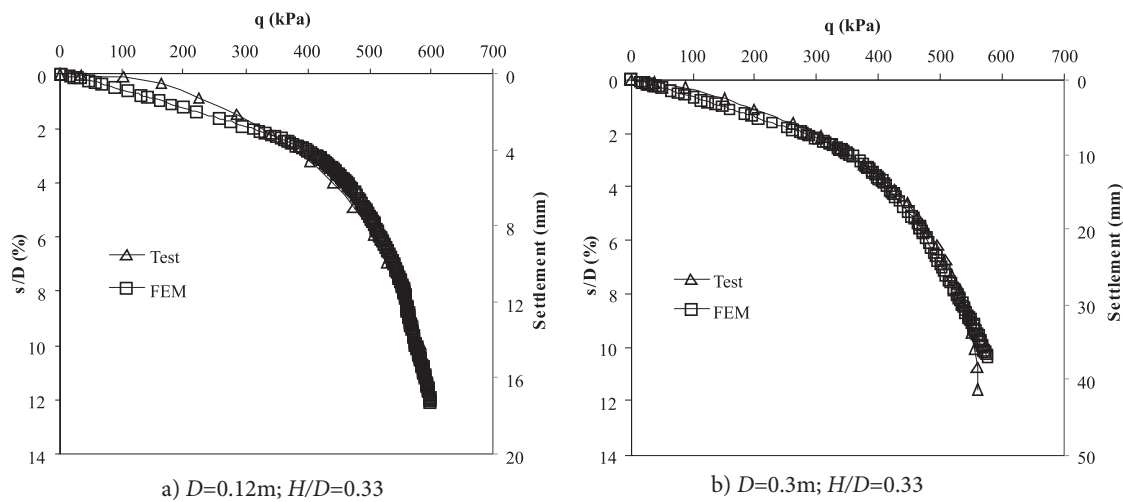


Figure 9. Curves of bearing capacity against settlement for test Series II.

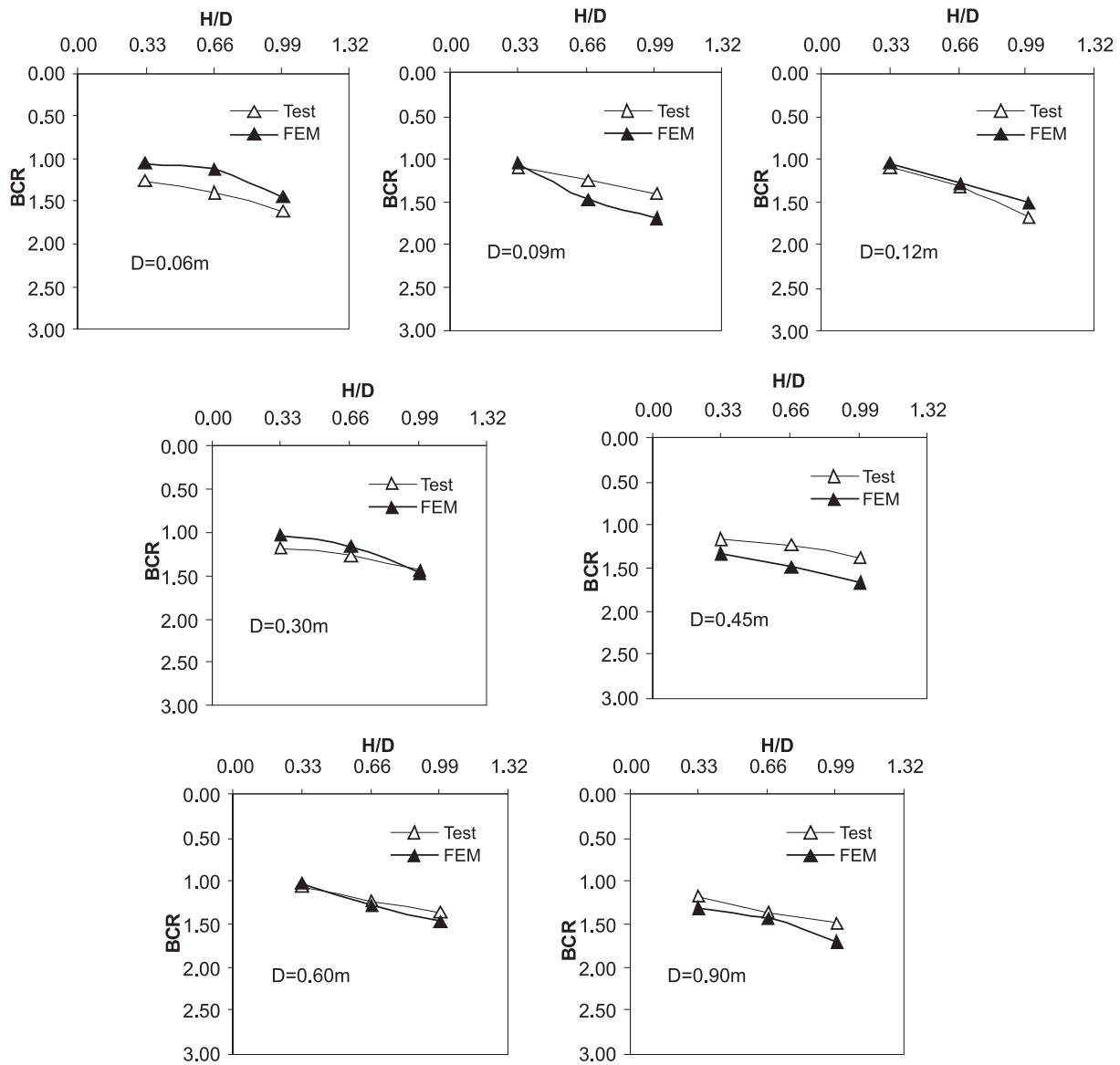


Figure 10. BCR relations in tests Series II.

the granular-fill material is being more effective. The numerical and experimental results are closer to each other in comparison to the BCRs at $H/D=0.33$, while the results are far away from each other at $H/D=0.67$ and $H/D=1.00$. In test Series II, the ultimate bearing capacity is obviously a function of H/D [32, 33], as the weaker clay is partially replaced by firmer granular soil. It is shown that the granular-fill layer helps to increase the load-bearing capacity of the footing and decreases the settlement allowable load since the granular-fill layer is stiffer and stronger than the natural clay. The

partial replacement of the soil with the granular-fill layer results in a redistribution of the applied load to a wider area and thus minimizing the stress concentration and achieving an improved distribution of induced stress. For this reason, the bearing capacity can be improved while the footing settlement is reduced. It is observed that the load-settlement curve is rounded and becomes steeper and takes on an almost a linear shape. A peak load is never observed and no definite failure point can be established. The mode of failure can be described as a local shear failure.

5 SCALE EFFECT INVESTIGATION

5.1 DETAILS OF THE PARAMETRIC STUDY

A parametric study was carried out after obtaining a good relationship between the test and numerical results. A footing-size-based scale-effect analysis was performed under the clay soil (Analysis Series I: Analysis on the Natural Clay Deposit) and partial replacement (Analysis Series II: Analysis on the Granular-fill Layer Placed on Natural Clay Deposit) soil conditions. Six additional footing diameters up to 25.0 m (1.2; 1.5; 3.0; 6.0; 12.0 and 25.0 m) were used in the analysis. In addition to the field tests, three different granular-fill thicknesses, $1.33D$, $1.67D$ and $2.00D$ were used. The non-dimensional relationships between the footing diameter and the ultimate bearing-capacity/bearing-capacity ratio were presented with using seven different footing diameters ($D=0.9\text{m}$ was also added) and six different granular-fill layer thicknesses (clay soil state, $H/D=0$ was also added). The footing size varies in the range between 0.06 m and 25.0 m.

5.2 ANALYSIS SERIES I: ANALYSIS ON THE NATURAL CLAY DEPOSIT

Terzaghi proposed the following relationship to define the ultimate bearing capacity q_u for circular footings [34]:

$$q_u = 1.3cN_c + qN_q + 0.3\gamma BN_\gamma \quad (2)$$

where, c is the soil cohesion, B is the footing width and N_c , N_q , N_γ are Terzaghi's bearing-capacity factors. In addition, q can also be identified as (γD_f) , where D_f is the footing depth.

In the tests and analysis made, the footings were placed at soil surface of the clay soil; therefore there are no contributions from the second and third parameters in Equation 2 to the footing-bearing capacity.

Then, the net bearing capacity ($q_{u(net)}$) equation can be written as follows:

$$q_{u(net)} = c_u N_c \quad (3)$$

From Equation 3, the bearing capacity factor N_c is defined as:

$$N_c = q_{u(net)} / c_u \quad (4)$$

For the local shear failure, the modified cohesion value (c_u^*) should be calculated as $c_u^* = 2c_u / 3$ [34]. Therefore, equation 4 is rearranged as follows;

$$N_c = q_{net} / (1.3c_u^*) \quad (5)$$

Figure 11 shows the relationship between the bearing-capacity factor N_c and the footing diameter D . The bearing-capacity factor N_c was back-calculated from Equation 5 where c_u^* equals 50kPa and plotted to observe the footing-size effect. The bearing-capacity values were obtained from load-settlement curves using the method as mentioned in Figure 8. The N_c values are almost the same for all the footing sizes. The existence of a scale effect in the footing sizes rested on natural clay soils cannot be directly observed from these figures. Consoli et al. [35], Fellenium and Altaee [36] and Ismael [37] reported similar findings. These studies indicate that the footing resting on silty clay has no footing-size effect, if the settlement is expressed in a non-dimensional relative settlement of s/D reported similar findings. The studies performed by Consoli et al. [35] show that the behavior of the pressure to settlement (q/q_u) to a diameter ratio (s/D) seems to be independent of the footing-plate size.

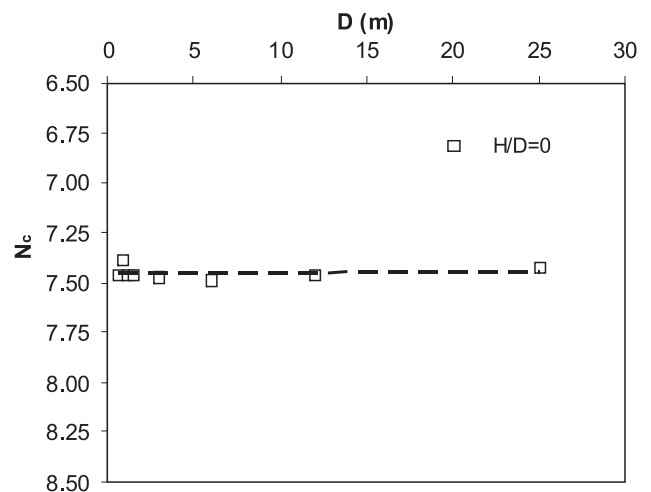


Figure 11. Variation of D with N_c for Series I.

5.3 ANALYSIS SERIES II: ANALYSIS ON THE GRANULAR-FILL LAYER PLACED ON NATURAL CLAY DEPOSIT

In the analysis Series II, the footing-size-effect investigation was carried out with the granular-fill soil replacement beneath the footings. Figure 12 shows the plots of the ultimate bearing capacity (q_u) versus footing diameter (D) for the analysis conducted on the soil replacement placed on a natural clay deposit. For a given value of H/D , the magnitude of the ultimate bearing capacity increases in a nonlinear manner with the footing diameter. The variation of the magnitudes of q_u with the soil-replacement thickness (H/D) obtained from the analysis are shown in Figure 13. For a given value of D , the magnitude of q_u increases with the increase in the soil-

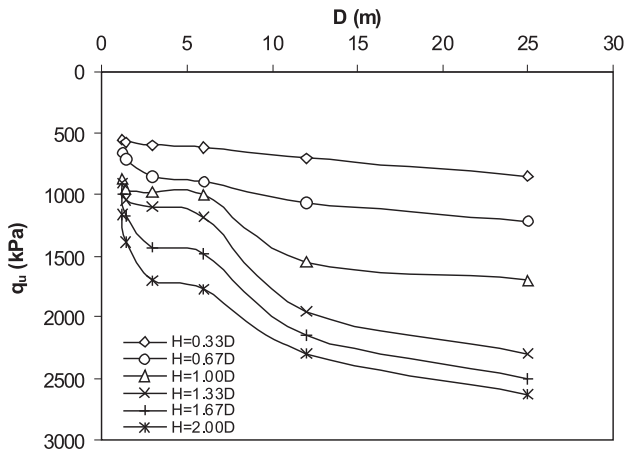


Figure 12. Variation of ultimate bearing capacity with footing diameter for Series II.

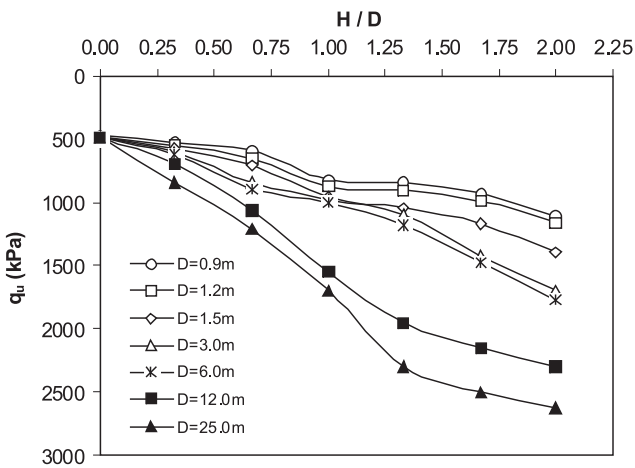


Figure 13. Variation of ultimate bearing capacity with granular-fill thickness for Series II.

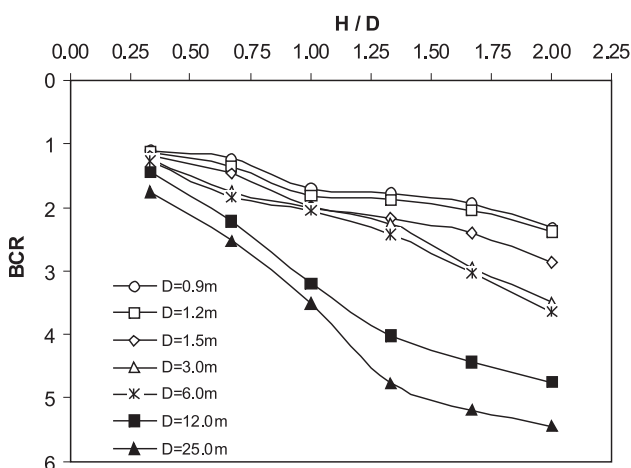


Figure 14. Variation of bearing capacity ratio with granular-fill thickness for Series II.

replacement thickness H . For the values of $H/D > 1.33$, the increasing trend in q_u becomes decremental for footing diameters greater than about 12 m. This observation is true for all the soil-replacement thicknesses. For a given value of D , the magnitude of BCR increases with the increase in the soil replacement, H/D . The effect of the soil-replacement thickness minimizes after $H > 1.33D$.

The variations of the magnitudes of BCR with the ratio of H/D obtained from the analysis are shown in Figure 14. Similar behavior was also obtained in Figure 13. The maximum value in BCR was obtained at $H = 2.0D$ for all the footing sizes.

The finite-element method generates an effective analysis and evaluation of displacements, stress and forces in and around the soil, stabilized bodies and footing. Figures 15 and 16 show some typical examples of the resultant vertical and horizontal displacement fields below the 1.5-m-diameter circular footing for clay soil ($H/D = 0$) and stabilized cases ($H/D = 0.67$) at a loading pressure $q = 450 \text{ kPa}$ (this value is very close to the ultimate bearing capacity of the natural clay deposit). It can be seen that there is a clear reduction of the vertical and horizontal displacements for the stabilized case (compacted granular-fill bed over natural clay deposit) compared with the clay soil case (over natural clay deposit). The compacted granular-fill bed structure behaves as a rigid slab below the footing and distributes the load into the underlying ground. This reduces the vertical and lateral displacements, resulting in a uniform settlement.

6 CONCLUSIONS

This study is focused directly on a scale-effect investigation in circular footings resting on natural clay deposits stabilized with compacted granular-fill layers. Based on the results from this investigation, the following main conclusions can be drawn:

- Vertical load increases with an increase in footing size. Vertical displacements predicted by the numerical analysis are in very good agreement with the experimental results.
- The field test results indicate that the use of partially replaced granular-fill layers over natural clay soil has considerable effects on the bearing capacity and the settlement characteristics.
- In the tests, granular-fill thickness (H) was changed depending on the footing diameter as 0.33 , 0.67 and $1.00D$. The bearing-capacity ratio (BCR) increases with an increase in the granular-fill thickness for all the footing diameter.

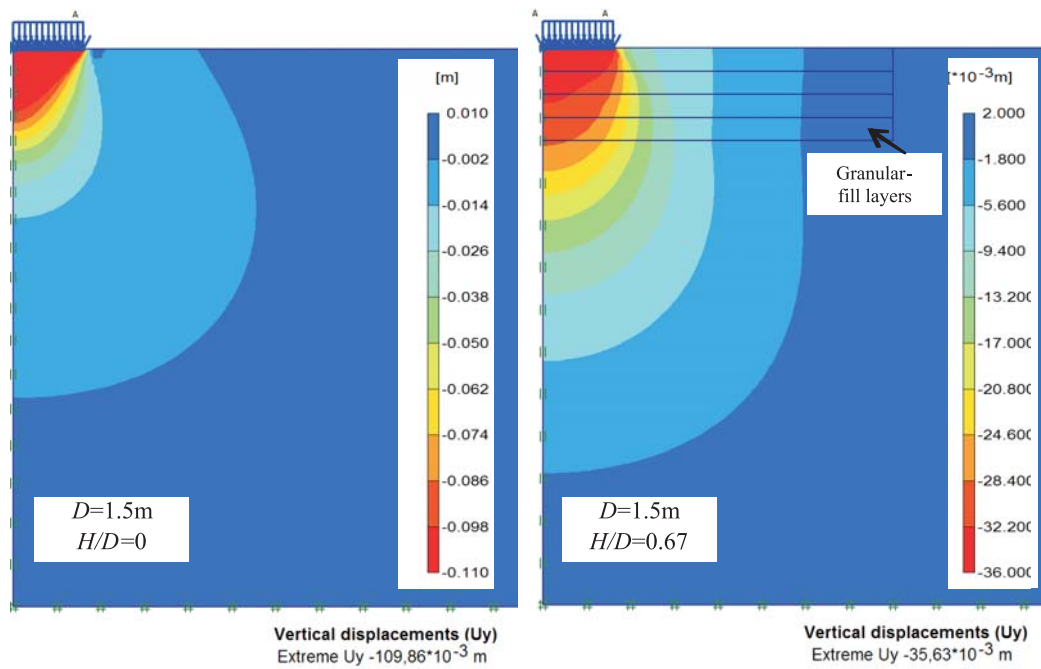


Figure 15. Vertical displacement fields below circular footings ($q=450\text{kPa}$).

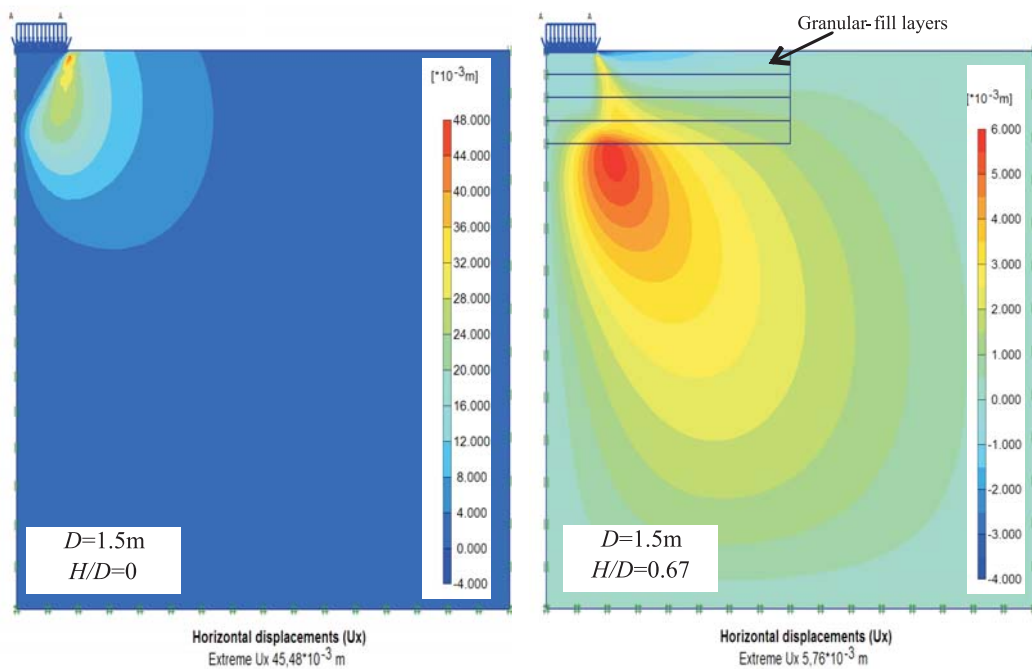


Figure 16. Horizontal displacement fields below circular footings ($q=450\text{kPa}$).

- The ultimate bearing capacity is a function of H/D . The partial replacement of soil with the granular-fill layer results in a redistribution of the applied load to a wider area and thus minimizing the stress concentration and achieving an improved distribution of induced stress.
- In the parametric part of the study, six different footing diameters up to 25.0 m (1.2; 1.5; 3.0; 6.0; 12.0 and 25.0 m) and five different compacted granular-fill thicknesses, $0.33D$; $0.67D$; $1.00D$; $1.33D$, $1.67D$ and $2.00D$ were used. It is concluded from Series I that the existence of scale effect in footing

sizes resting on natural clay soils cannot be directly implied.

- The footing size-effect investigation was carried out with the partially replaced compacted granular-fill layer beneath the footings in Series II. For a given value of H/D , the magnitude of the ultimate bearing capacity increases in a nonlinear manner with the footing diameter. On the other hand, for a given value of D , the magnitude of q_u increases with the increase in the compacted granular-fill layer thickness, H .
- The BCR values increase with an increase in H/D and these values remain relatively constant when $H/D > 1.33$. The maximum values in BCR were obtained at $H = 2.0D$ for all the footing sizes.

ACKNOWLEDGMENTS

The work presented in this paper was carried out with funding from TUBITAK (The Scientific and Technological Research Council of Turkey) grant number 106M496, and Cukurova University Scientific Research Project Directorate grant number MMF2006D28.

REFERENCES

- [1] Terzaghi, K. (1943). Theoretical soil mechanics. Wiley, New York.
- [2] Cerato, A. B. and Lutenecker, A. J. (2007). Scale effects of shallow foundation bearing capacity on granular material. *Journal of Geotechnical and Geoenvironmental Engineering*, ASCE, 133(10), 1192-1202.
- [3] Dewaiker, D. M. and Mohapatro, B. G. (2003). Computation of bearing capacity factor N_γ -Terzaghi's mechanism. *International Journal of Geomechanics*, 3(1), 123-128.
- [4] Siddiquee, M. S. A., Tanaka, T., Tatsuoka, F., Tani, K. and Morimoto, T. (1999). Numerical simulation of bearing capacity characteristics of strip footing on sand. *Soils and Foundations*, 39 (4), 93-109.
- [5] Berry, D. S. (1935). Stability of granular mixtures. *Proceedings of 38th Annual Meeting*, (35), ASTM, Philadelphia, 491-507.
- [6] Das, B. M. and Omar, M. T. (1994). The effects of foundation width on model tests for the bearing capacity of sand with geogrid reinforcement. *Geotechnical and Geological Engineering*, Technical Note (12), 133-141.
- [7] De Beer, E. E. (1965). The scale effect in the transposition of the results of deep-sounding tests on the ultimate bearing capacity of pile sand caisson foundations. *Geotechnique*, 13(1), 39-75.
- [8] Hettler, A. and Gudehus, G. (1988). Influence of the foundation width on the bearing capacity factor. *Soils Foundation*, 28(4), 81-92.
- [9] Ueno, K., Miura, K. and Maeda, Y. (1998). Prediction of ultimate bearing capacity of surface footing with regard to size effects. *Soils Foundation*, 38 (3), 165-178.
- [10] Zhu, F., Clark, J. I. and Phillips, R. (2001). Scale effect of strip and circular footings resting on dense sand. *Journal of Geotechnical and Geoenvironmental Engineering*, ASCE 127(7), 613-621.
- [11] Fukushima, H., Nishimoto, S. and Tomisawa, K. (2005). Scale effect of spread foundation loading tests using various size plates. *Independent Administrative Institution Civil Engineering Research Institute for Cold Region*, 1-8.
- [12] Adams, M. and Collin, J. (1997). Large model spread footing load tests on geosynthetic reinforced soil footings. *Journal of Geotechnical and Geoenvironmental Engineering*, 123 (1), 66-72.
- [13] Alawaji, H. A. (2001). Settlement and bearing capacity of geogrid-reinforced sand over collapsible soil. *Geotextiles and Geomembranes*, 19, 75-88.
- [14] Dash, S. K., Sireesh, S. and Sitharam, T. G. (2003) Model Studies on circular footing supported on geocell reinforced sand underlain by soft clay. *Geotextiles and Geomembranes*, 21, 197-219.
- [15] Deb, K., Sivakugan, N., Chandra, S. and Basudhar, P. K. (2007). Numerical analysis of multi-layer geosynthetic-reinforced granular bed over soft fill. *Geotechnical and Geological Engineering*, 25, 639-646.
- [16] Ochiai, H., Watari, Y. and Tsukamoto, Y. (1996). Soil reinforcement practice for fills over soft ground in Japan. *Geosynthetics International*, 3 (1), 31-48.
- [17] Otani, J., Hidetoshi, O. and Yamamoto, K. (1998). Bearing capacity analysis of reinforced foundations on cohesive soil. *Geotextiles and Geomembranes*, 16, 195-206.
- [18] Thome, A., Donato, M., Consoli, N. C. and Graham, J. (2005). Circular footings on a cemented layer above weak foundation soil. *Canadian Geotechnical Journal*, 42, 1569-1584.
- [19] Yin, J. H. (1997). Modeling geosynthetic-reinforced granular fills over soft soil. *Geosynthetics International*, 4 (2), 165-185.
- [20] ASTM. (1997). Standard test method for non repetitive static plate load tests of soils and flexible pavement components, for use in evaluation and design of airport and highway pavements, 112-113.

- [21] Laman, M., Yildiz, A., Ornek, M. and Demir, A. (2009) Geogrid reinforcement on soft clay deposit" TUBITAK Scientific Research Project (No:106M496), Ankara, Turkey, 528p.
- [22] Ornek, M. (2009). Geogrid reinforcement on soft clay deposits. PhD Thesis, University of Cukurova, Turkey, 318 p. (in Turkish).
- [23] Laman, M. and Yildiz, A. (2007). Numerical studies of ring foundations on geogrid-reinforced sand. *Geosynthetics International*, 14 (2), 1–13.
- [24] Brinkgreve, R. B. J., Broere, W. and Waterman, D. (2004). Plaxis finite element code for soil and rock analysis, 2D –Version 8.6.
- [25] Lehane, B. M. (2003). Vertical loaded shallow foundation on soft clayey silt. Proceedings of the Institution of Civil Engineers, *Geotechnical Engineering*, 17–26.
- [26] Long, M.M. and O'riordan, O. (2001). Field behaviour of very soft clays at the Athlone embankments. *Geotechnique*, 51 (4) 293-309.
- [27] Osman, A. S. and Bolton, M. D. (2005). Simple plasticity-based prediction of the undrained settlement of shallow circular foundations on clay. *Geotechnique*, 55 (6), 435–447.
- [28] Taiebat, H. A. and Carter, J. P. (2002). Bearing capacity of strip and circular foundations on undrained clay subjected to eccentric loads. *Geotechnique*, 52 (1), 61–64.
- [29] Bolton, M.D. (1986). The strength and dilatancy of sands. *Geotechnique*, 36 (1), 65-78.
- [30] Binquet, J. and Lee, K. L. (1975a). Bearing capacity tests on reinforced earth slabs. *Journal of Geotechnical Engineering Division*, ASCE 101 (GT12), 1241-1255.
- [31] Laman, M. and Yildiz, A. (2003). Model studies of ring footings on geogrid-reinforced sand. *Geosynthetics International*, 10 (5), 142-152.
- [32] Hamed, J. T., Das, B. M. and Echelberger, W. F. (1986). Bearing capacity of a strip foundation on granular trench in soft clay. *Civil Engineering for Practising and Design Engineers*, Paragon Press 5 (5), 359-376.
- [33] Madhav, M. R. and Vitkar P. P. 1978. Strip footing on weak clay stabilized with a granular trench or pile. *Canadian Geotechnical Journal*, 15 (4), 605-609.
- [34] Das, B. M. (1999). Shallow foundations: bearing capacity and settlement. CRC Press, LLC.
- [35] Consoli, N. C., Schnaid, F. and Milititsky, J. (1998). Interpretation of plate load tests on residual soil site. *Journal of Geotechnical and Geoenvironmental Engineering*, 124 (9), 857-867.
- [36] Fellenium, B. H. and Altaee, A. (1994). Stress and settlement of footings in sand. Proceedings of the American Society of Civil Engineers, ASCE, Conference on Vertical and Horizontal Deformations for Foundations and Embankments, *Geotechnical Special Publication*, GSP, 2(40), College Station 1760-1773.
- [37] Ismael, N. F. (1985). Allowable bearing pressure from loading tests on Kuwaiti soils. *Canadian Geotechnical Journal*, 22 (2), 151-157.

POENOSTAVLJEN PRISTOP ZA OCENO POSEDANJA TEMELJNE PLOŠČE NA PILOTIH

VOLKAN KALPAKCI İN M. YENER ÖZKAN

o avtorjih

vodilni avtor

Volkan Kalpakci
Middle East Technical University,
Department of Civil Engineering
K-1 Building, Room:115/B, Ankara, Turčija
E-pošta: kvolkan@metu.edu.tr

M. Yener Özkan
Middle East Technical University,
Department of Civil Engineering
K-1 Building, Room:115/B, Ankara, Turčija
E-pošta: myozkan@metu.edu.tr

izvleček

V študiji je prikazan poenostavljen pristop za oceno posedanja temeljnih plošč na pilotih, ki ležijo na sedimentiranih prekonsolidiranih glinah. Za ta namen je bil izveden niz ravninsko deformacijskih in tridimenzionalnih analiz, njihovi rezultati pa so bili primerjani z razpoložljivimi podatki iz literature. Ugotovljeno je bilo, da je bil delež znižanja celotnih posedkov s piloti glede na primer brez pilotov zelo natančno ocenjen z obema - ravninsko deformacijsko in poenostavljeno tridimenzionalno numerično analizo. Zaradi tega je predlagana enostavna metoda za oceno posedanja temeljnih plošč na pilotih. Za obravnavane primere (samo za določene pogoje temeljnih tal) pa so podani tudi projektni diagrami za oceno posedanja temeljnih plošč na pilotih.

ključne besede

temeljne plošče na pilotih, posedek, prekonsolidirana glina, projektiranje temeljev

A SIMPLIFIED APPROACH TO THE SETTLEMENT ESTIMATION OF PILED RAFTS

VOLKAN KALPAKCI and M. YENER ÖZKAN

about the authors

corresponding author

Volkan Kalpakci
Middle East Technical University,
Department of Civil Engineering
K-1 Building, Room:115/B, Ankara, Turkey
E-mail: kvolkan@metu.edu.tr

M. Yener Özkan
Middle East Technical University,
Department of Civil Engineering
K-1 Building, Room:115/B, Ankara, Turkey
E-mail: myozkan@metu.edu.tr

abstract

In this study, a simplified approach to the settlement estimation of piled rafts resting on over-consolidated clay deposits is presented. For this purpose, a series of plane-strain and three-dimensional analyses were performed and their results are compared with the available data in the literature. It was found that the percentage decrease in the total settlements with the addition of piles with respect to the unpiled case is very closely estimated by both the plane-strain and the three-dimensional, simplified, numerical analyses. Using this phenomenon, a simple method of analysis is suggested for the total settlement estimation of the piled raft foundations and design charts are provided for the cases studied (for the specific soil conditions only) throughout this study.

keywords

piled rafts, settlement, over-consolidated clay, foundation design

1 INTRODUCTION

In the traditional design of a piled foundation the contribution of the raft to the overall bearing capacity

is disregarded. However, for deep foundations on stiff soils where the piles are used as settlement reducers rather than to provide additional bearing capacity, the traditional design concepts may lead to highly over-conservative solutions (Reul and Randolph 2003 [1], Reul and Randolph 2004 [2]; Randolph 2003 [3]). For such cases, it is very convenient to use the concepts of a piled-raft foundation in the design process. Utilizing the piled-raft concept, the number of piles in a project can be significantly reduced, generally at the expense of a slight increase in the settlements with respect to the traditional design of a pile foundation.

There are various detailed or approximate methods and design concepts available in the literature developed for piled-raft design (some of these methods and concepts are described in Clancy and Randolph 1993 [4]; Katzenbach et al. 1998 [5]; Katzenbach and Moormann 2001 [6]; Katzenbach et al. 2004 [7]; Katzenbach et al. 2005 [8]; Poulos 1994 [9]; Poulos et al. 1997 [10]; Poulos 2002 [11]; Prakoso and Kulhawy 2001 [12]; Randolph 1994 [13]). However, in this study the aim to provide a simple approach that can be used as a first approximation. For this purpose, plane-strain and three-dimensional finite-element analyses were performed using the Plaxis 2D and Plaxis 3D Foundation software packages respectively. The results of the present study are compared with those of [2] obtained by ABAQUS analyses, which were calibrated according to the in-situ measurements recorded on the foundations resting on over-consolidated Frankfurt clay. In order to provide compatibility, the analyzed cases and the parameters used for modeling the elements included in these analyses are similar to the ones given in [2].

2 ANALYSES

2.1 ANALYZED CASES

In this study, eight different piled-raft foundations were analyzed for three different pile lengths (L_p) and two different load levels in plane-strain and three-dimen-

Table 1. List of the analyzed cases¹.

Pile Configuration	B (m.)	s/D	n	L_p (m)	$n*L_p$ (m)	tr (m)	q (kPa)
Unpiled Raft	38	-	-	-	-	3	12.5
Unpiled Raft	38	-	-	-	-	3	50
Configuration I	38	3	169	10	1690	3	12.5
Configuration I	38	3	169	10	1690	3	50
Configuration I	38	3	169	30	5070	3	12.5
Configuration I	38	3	169	30	5070	3	50
Configuration I	38	3	169	50	8450	3	12.5
Configuration I	38	3	169	50	8450	3	50
Configuration I	38	6	49	10	490	3	12.5
Configuration I	38	6	49	10	490	3	50
Configuration I	38	6	49	30	1470	3	12.5
Configuration I	38	6	49	30	1470	3	50
Configuration I	38	6	49	50	2450	3	12.5
Configuration I	38	6	49	50	2450	3	50
Configuration II	38	3	49	10	490	3	12.5
Configuration II	38	3	49	10	490	3	50
Configuration II	38	3	49	30	1470	3	12.5
Configuration II	38	3	49	30	1470	3	50
Configuration II	38	3	49	50	2450	3	12.5
Configuration II	38	3	49	50	2450	3	50
Configuration II	38	6	16	10	160	3	12.5
Configuration II	38	6	16	10	160	3	50
Configuration II	38	6	16	30	480	3	12.5
Configuration II	38	6	16	30	480	3	50
Configuration II	38	6	16	50	800	3	12.5
Configuration II	38	6	16	50	800	3	50
Configuration II	38	6	9	10	90	3	12.5
Configuration II	38	6	9	10	90	3	50
Configuration II	38	6	9	30	270	3	12.5
Configuration II	38	6	9	30	270	3	50
Configuration II	38	6	9	50	450	3	12.5
Configuration II	38	6	9	50	450	3	50
Configuration III	38	3	73	10	730	3	12.5
Configuration III	38	3	73	10	730	3	50
Configuration III	38	3	73	30	2190	3	12.5
Configuration III	38	3	73	30	2190	3	50
Configuration III	38	3	73	50	3650	3	12.5
Configuration III	38	3	73	50	3650	3	50
Configuration III	38	6	40	10	400	3	12.5
Configuration III	38	6	40	10	400	3	50
Configuration III	38	6	40	30	1200	3	12.5
Configuration III	38	6	40	30	1200	3	50
Configuration III	38	6	40	50	2000	3	12.5
Configuration III	38	6	40	50	2000	3	50
Configuration III	38	6	33	10	330	3	12.5
Configuration III	38	6	33	10	330	3	50
Configuration III	38	6	33	30	990	3	12.5
Configuration III	38	6	33	30	990	3	50
Configuration III	38	6	33	50	1650	3	12.5
Configuration III	38	6	33	50	1650	3	50

¹ Each case is analyzed both in plane-strain and three-dimensions.

sions, which makes a total of 100 cases, when considered together with the unpiled raft analyses. The thickness (t) and the width (B) of the square raft are taken as 3 m and 38 m, respectively, for all the considered cases, while the number of piles (n) varies between 9 and 169, where the pile spacings (s) are equal to either $3 \times D$ (D : pile diameter) or $6 \times D$ (from centre to centre) and the pile lengths are either 10 m, 30 m or 50 m. The analyzed cases are listed in Table 1.

Three different configurations are considered in the study, as shown in Fig. 1. Configuration I corresponds to uniformly distributed piles, Configuration II represents the cases where the piles are concentrated near the centre, and Configuration III indicates the piles placed at the edges as well as near the centre. A uniform load of 12.5 kPa and 50 kPa, which corresponds to 5% and 20% of the net ultimate bearing capacity of an equivalent unpiled raft resting on Frankfurt clay, are applied for all the cases and named as “Load I” and “Load II”, respectively.

2.2 GENERAL CONDITIONS CONSIDERED IN THE MODELS

As indicated, the piled rafts are assumed to be resting on stiff Frankfurt clay. So, the finite-element model is created in such a way that it is representative of the average soil and groundwater conditions together with the average foundation depth for tall buildings in that region.

The clay layer is assumed to be 69 m thick and the Frankfurt limestone, which underlies the clay layer, is not included in the model, since it is relatively incompressible with respect to the overlying clay. The groundwater table is assumed to be at a depth of 7 m from the ground surface and the foundation depth is taken to be 14 m in the calculations.

The systems are modeled in 2-fold and 4-fold symmetry in plane-strain and 3D analyses, respectively. The model width is taken to be equal to ten times the half raft width (190 m) in order to minimize the boundary effects (see Fig. 2 and Fig. 3).

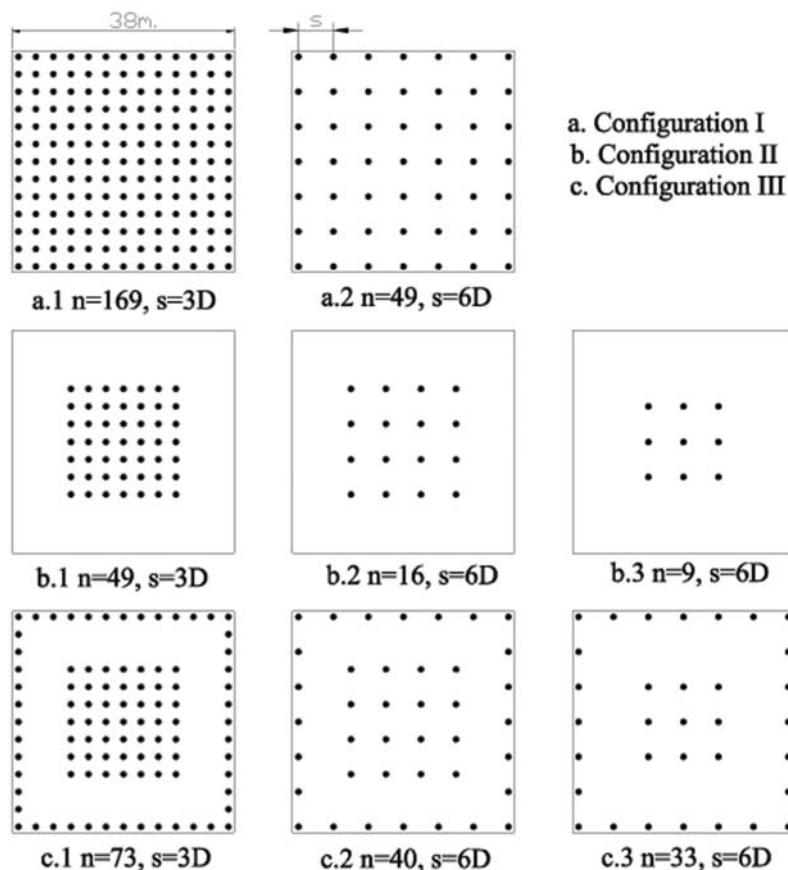


Figure 1. Analyzed cases.

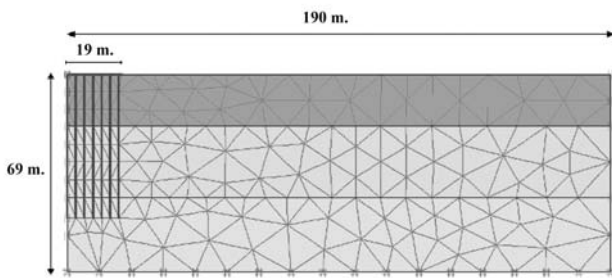


Figure 2. Sample 2D model used in the analyses.

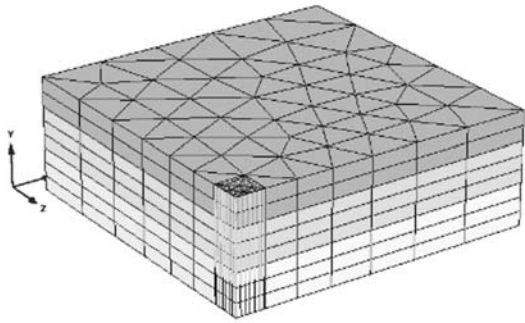


Figure 3. Sample 3D model used in the analyses.

2.3 MODELING OF THE SOIL

In the finite-element models the soil below the foundation level (assuming a groundwater level at the ground surface) is included and the soil above the foundation level (including the groundwater and its uplift pressure) is regarded as a dead load. Fifteen-node triangular elements are used in the plane-strain analyses whereas 15-node wedge (triangular prism) elements are utilized in the three-dimensional analyses.

The Mohr-Coulomb failure criterion is used in modeling the soil strength. The c' , Φ' and K_0 values are selected as given in [2], which are based upon the results of the laboratory and field tests.

The change of the Young's modulus (E) with depth (z) for the soil is considered based on the empirical formulation (1) suggested in Reul (2000) [14]. The assigned parameters for the soil profile are given in Table 2. (E in MPa; z in m.).

$$E = 45 + \left(\tanh\left(\frac{z-30}{15}\right) + 1 \right) \times 0.7z \quad (1)$$

2.4 MODELING OF THE STRUCTURAL ELEMENTS

In the plane-strain analyses, the rafts and the piles are modeled as plates with linear elastic material properties and represented in the model by 5-node line elements.

Table 2. The properties of the soil profile used in the analyses.

	Layer1	Layer 2	Layer3
Thickness (m.)	18	25	26
Initial E (MPa)	45	57	110
ΔE (MPa/m)	0.66	2.138	1.584
K_0	0.72	0.57	0.57
ν	0.15	0.15	0.15
C (kPa)	20	20	20
Φ^0	20	20	20
γ (kN/m ³)	19	19	19

Since the analyses are performed in two-dimensional space, the elastic parameters are converted in such a way that a row of pile provides the rigidity per meter of the system equal to that of the structure.

For the three-dimensional analyses the raft is modeled as a linear elastic plate by utilizing 6-node triangular plate elements. The piles, which are also assumed to behave linearly elastic, are modeled by 3-node line elements. The shaft and base resistances of the piles are obtained from [2].

3 RESULTS

Based on the approximation given in Davis and Taylor (1962) [15] the average total settlements of the analyzed piled raft foundations under given loads are calculated using equation (2) in which the s_{centre} and s_{corner} are the centre and the corner settlements of the raft respectively.

$$s_{avg} = \frac{1}{3}(2s_{centre} + s_{corner}) \quad (2)$$

In order to visualize the amount of percentage decrease in the average total settlement of the foundations with the addition of the piles with respect to the unpiled case (in other words, the efficiency of the piles), a parameter named as the coefficient for average settlement " ξ_s " [2] is used, which is defined as the ratio of the average total settlement of the investigated case " s_{avg} " to that of the unpiled case " $s_{avg,r}$ " under the same load (3).

$$\xi_s = \frac{s_{avg}}{s_{avg,r}} \quad (3)$$

The calculated ξ_s parameters based on the results of the parametric study revealed that the amount of percentage decrease in the average total settlement of the foundations with the addition of the piles can be closely approximated by the simplified numerical analyses performed in this study. Interestingly, it was found that

although the settlements estimated by three-dimensional analyses are closer to the reference values than those of plane-strain analyses, on average the ξ_s values are calculated with a smaller deviation by plane-strain analyses as compared to the three-dimensional analyses. This result does not mean that plane-strain solutions are closer to the reference values, but that the plane-strain analysis tools used in this study yield the efficiency of the piled rafts slightly better than the three-dimensional analysis.

For “Configuration I” in which the piles are uniformly distributed, the plane-strain analyses estimated the ξ_s values given in [2] with an average deviation of 3.15% for “Load I”, while it was 7.50% for “Load II”. On the other hand, for the same pile configuration, the average deviation in ξ_s values obtained from the results of the three-dimensional analyses was 3.32% for “Load I”, where it was 6.56% for “Load II”. The change of ξ_s with a total pile length ($n \cdot L_p$) is given in Fig. 4 for “Configuration I”.

In the case of “Configuration II” where piles are concentrated near the centre, the deviation in the estimated ξ_s values was 3.31% and 6.63% for “Load I” and “Load II”, respectively, for the plane-strain analyses, whereas it was equal to 6.41% and 8.62% for “Load I” and “Load II”, respectively, in the case of the three-dimensional analyses. The ξ_s vs. ($n \cdot L_p$) plot for “Configuration II” is given in Fig. 5. In addition, as can be observed in Fig.5, for the three-dimensional analysis and “Load II”, the deviation in ξ_s is found to be more noticeable than the other cases ($\xi_s > 1$ for some cases). This is attributed to hogging of the mat, since for the cases where hogging occurs the corner settlements are more remarkably overestimated by the utilized three-dimensional analysis method. As a result, the ξ_s values deviate from the reference values more than the average trend, due to the definition (2) of the average settlement “ s_{avg} ” value.

For “Configuration III”, where the piles are placed both at the edges and near the centre, in the case of plane-strain

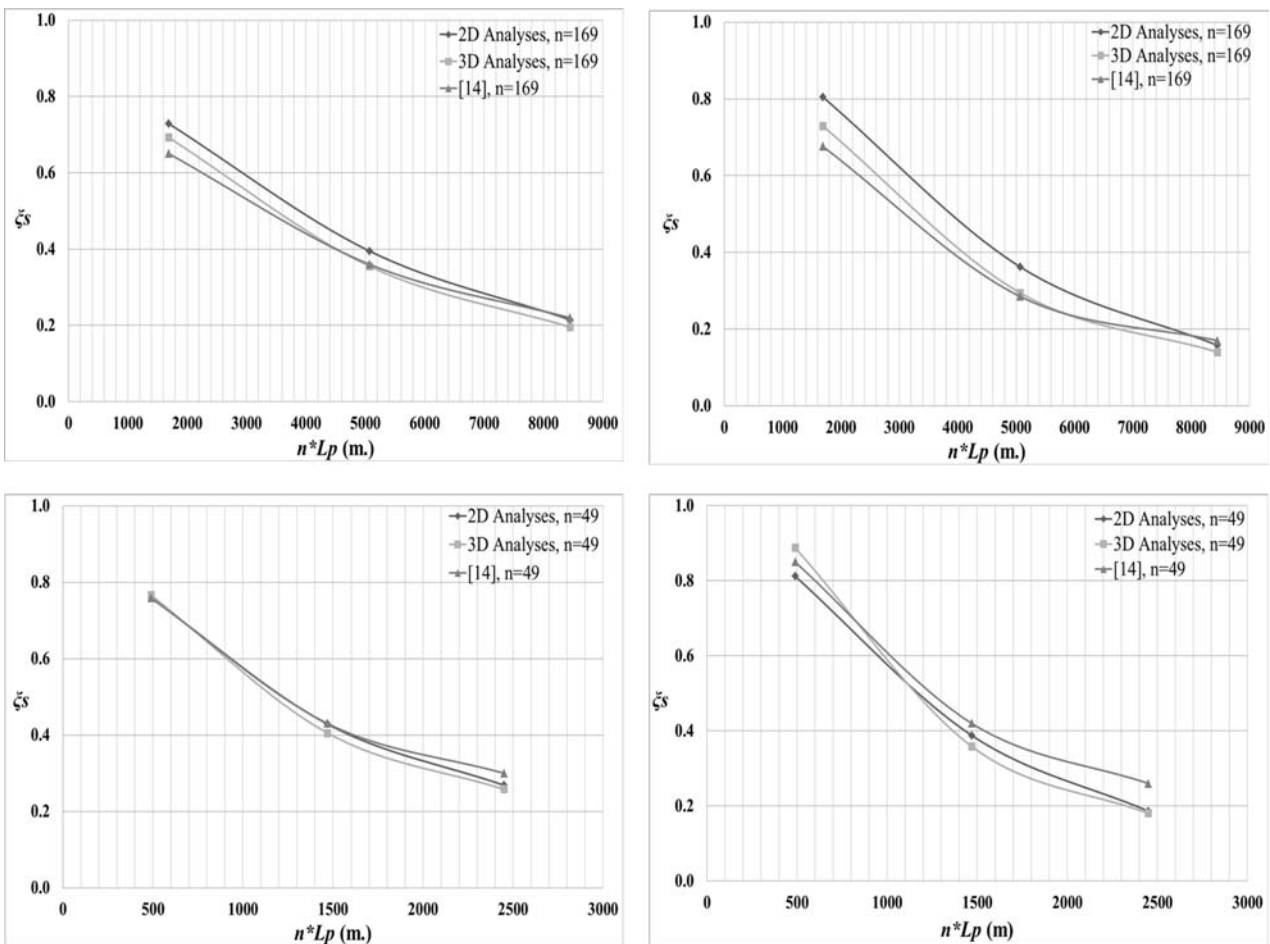


Figure 4. ξ_s vs. ($n \cdot L_p$) for Configuration I.

analyses, the ξ_s values were estimated with a deviation of 2.56% and 5.75% for “Load I” and “Load II”, respectively. On the other hand, the deviation was 2.60% for “Load I”, while it was 6.43% for “Load II” in the case of the three-dimensional analyses. The deviations in the estimated values for all the analyses are given in Table 3. The ξ_s vs. ($n \cdot L_p$) plot for “Configuration III” is given in Fig. 6.

Table 3. The average percentage deviation in ξ_s values.

Pile Configuration		I	II	III
2D	Load I	3.15%	3.31%	2.56%
	Load II	7.50%	6.63%	5.75%
3D	Load I	3.32%	6.41%	2.60%
	Load II	6.56%	8.62%	6.43%

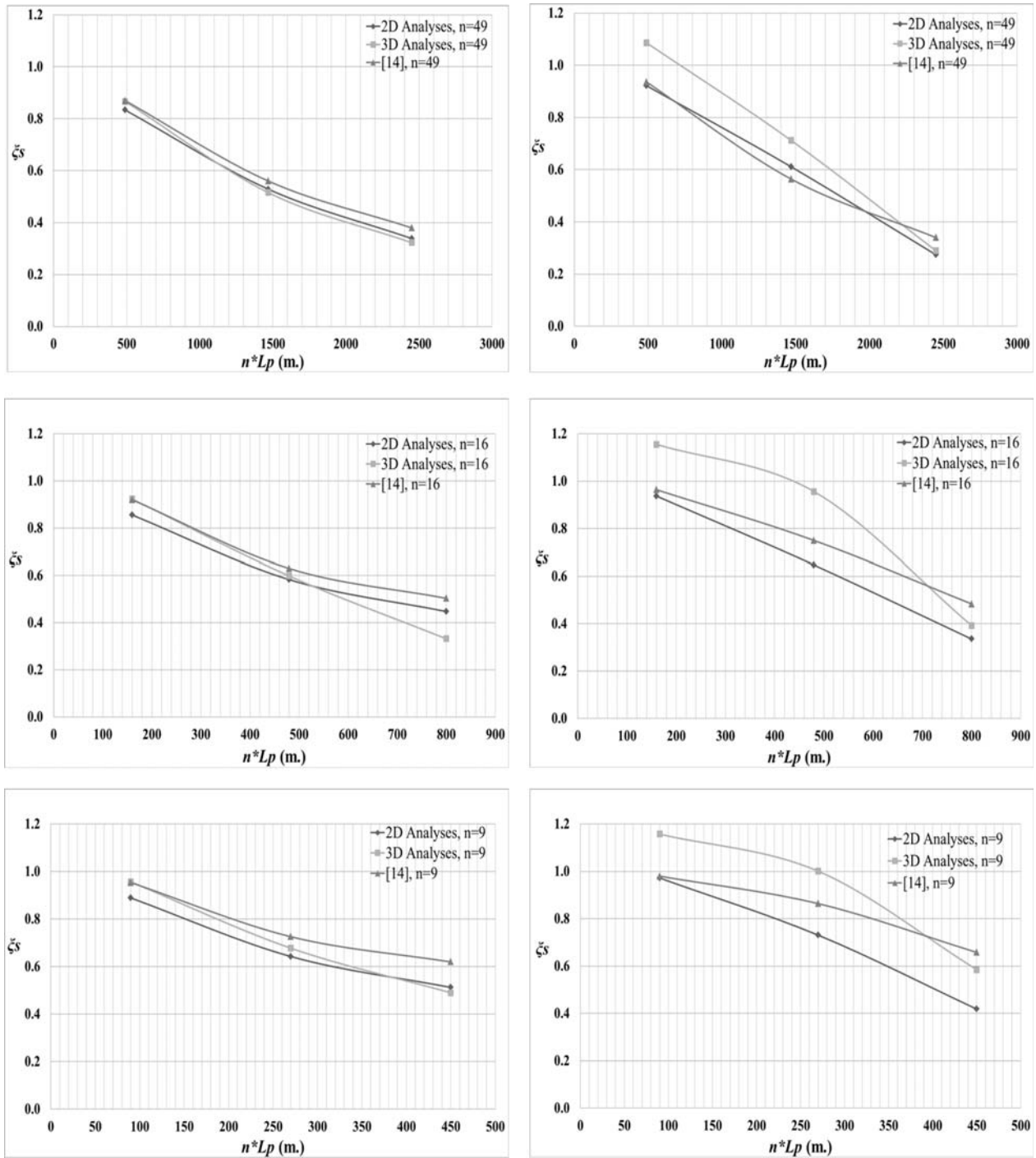


Figure 5. ξ_s vs. ($n \cdot L_p$) for Configuration II.

4 DISCUSSION

The results of the parametric study revealed that the simplified numerical analyses closely approximate the variation of the decrease in the total average settlements of the piled rafts with the addition of piles for the cases studied. The ultimate deviation in the estimated ξ_s

values is 7.50% for plane-strain analyses in the case of “Configuration I” and “Load II”, while it is 8.62% for “Configuration II” and “Load II” in the three-dimensional analyses. The deviation in the ξ_s values tends to increase with the increasing load level, where it almost varies in a narrow band for different pile configurations, provided that the load level is the same.

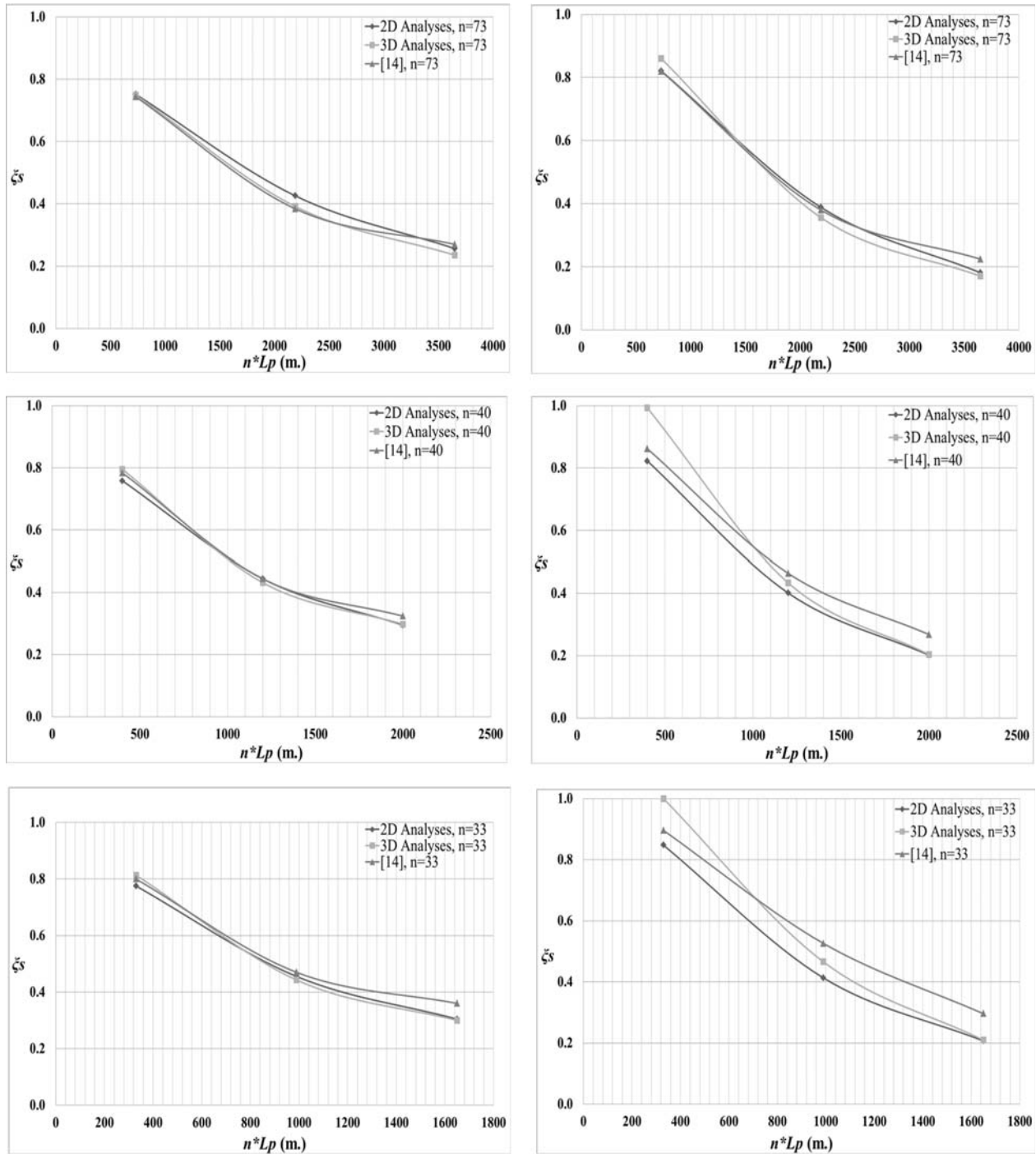


Figure 6. ξ_s vs. $(n \cdot L_p)$ for Configuration III.

The slight deviations in the results encourage the use of this type of approach in total settlement estimation of the piled raft foundations, in order to make an initial approximation about the performance of the piled raft prior to the more detailed analyses. Provided that the investigated case is compatible with the cases presented here, using the charts given in Fig.4, Fig.5 and Fig.6, the average total settlement of a piled raft foundation can be estimated by calculating the settlement of the raft without piles under a given load and multiplying this result with the corresponding ξ_s value. Alternatively, utilizing the described simple analysis tools, case-specific charts may be produced for cases with similar material, loading and geometrical conditions for a pile configuration with different pile lengths and load levels by analyzing these cases together with that of an unpiled raft analysis and obtaining the ξ_s values for the considered case. In this way, one can easily observe the efficiency of increasing the pile length (L_p) in reducing the total settlements for the case studied. Care should be taken where hogging is expected, since the ξ_s values may be noticeably overestimated (even $\xi_s > 1$) in such cases, especially by the described three-dimensional analysis method.

5 CONCLUSIONS

In order to facilitate the estimation of total settlements for piled raft foundations, a total of 100 numerical analyses were performed throughout the study. The results show that the average total settlement of a piled raft may be estimated by utilizing the simplified approach presented above.

The design charts presented in this study may be utilized as a first approximation to assess the performance of a piled raft for the cases compatible with those shown in the paper. Also, an approach is recommended to produce case-specific charts for other cases with similar material, loading and geometrical conditions.

ACKNOWLEDGMENTS

TÜBİTAK (The Scientific and Technological Research Council of Turkey) is sincerely thanked for the scholarship provided to V. Kalpakçı during this study.

REFERENCES

[1] Reul, O. and Randolph, M.F. (2003). Piled Rafts in Overconsolidated Clay: Comparison of In-situ

- Measurements and Numerical Analyses. *Geotechnique* 53, No.3, 301 – 315.
- [2] Reul, O. and Randolph, M.F. (2004). Design Strategies for Piled Rafts Subjected to Nonuniform Vertical Loading. *Journal of Geotechnical and Geoenvironmental Engineering* 130, No.1, 1 – 13.
- [3] Randolph, M.F. (2003). Science and empiricism in pile foundation design. *Geotechnique* 53, No.10, 847 – 875.
- [4] Clancy, P. and Randolph, M.F. (1993). An Approximate Analysis Procedure for Piled Raft Foundations. *International Journal for Numerical and Analytical Methods in Geomechanics* 17, No.12, 849 – 869.
- [5] Katzenbach, R., Arslan, U., Moormann, C. (1998). Design and Safety Concepts for Piled Raft Foundations. *Proc. of the Conf. on Deep Foundations on Bored Auger Piles*, Rotterdam, Germany, 439 – 449.
- [6] Katzenbach, R., Moormann, C. (2001). Recommendations for the Design and Construction of Piled Rafts. *Proc. of the fifteenth Int. Conf. on Soil Mechanics and Geotechnical Engineering*, Istanbul, Turkey, Vol. 2.
- [7] Katzenbach, R., Arslan, U., Moormann, C. (2004). Piled Raft Foundation Projects in Germany. *Design Applications of Raft Foundations*, Thomas Telford, 323 – 392.
- [8] Katzenbach, R., Schmitt, A., Turek, J., (2005). Assessing Settlement of High-Rise Structures by 3D Simulations. *Computer-Aided Civil and Infrastructure Engineering* 20, No.3, 221 - 229.
- [9] Poulos, H.G. (1994). An approximate numerical analysis of pile-raft interaction. *International Journal for Numerical and Analytical Methods in Geomechanics* 18, 73 – 92.
- [10] Poulos, H.G., Small, J.C., Ta, L.D., Sinha, J. and Chen, L. (1997). Comparison of some methods for analysis of piled rafts. *In Proceedings of the fourteenth International Conference on Soil Mechanics and Foundation Engineering*, Hamburg, 1119 – 1124.
- [11] Poulos, H.G. (2002). Simplified Design Procedure for Piled Raft Foundations. *In Deep Foundations. ASCE Geotechnical Special Publication No. 116*. ASCE, New York, 441 – 458.
- [12] Prakoso, A. W., and Kulhawy, H. F. (2001). Contribution to Piled Raft Foundation Design. *J. Geotech. Geoenviron. Eng.*, 127, No. 1, 17 – 24.
- [13] Randolph, M.F. (1994). Design Methods for Pile Groups and Piled Rafts. State-of-the-art Report. *In Proceedings of the thirteenth International Conference on Soil Mechanics and Foundation Engineering*, New Delhi, 61 – 82.

- [14] Reul, O. (2000). In-situ measurements and numerical studies on the bearing behaviour of piled rafts. *Ph.D. thesis*, Department of Civil Engineering, Darmstadt University of Technology, Darmstadt, Germany.
- [15] Davis, E.H. and Taylor, H. (1962). The movement of bridge approaches and abutments on soft foundation soils. *In Proceedings of the First Biennial Conference of Australian Road Research Board*, Australia, 740.

NAVODILA AVTORJEM

VSEBINA ČLANKA

Članek naj bo napisan v naslednji obliki:

- Naslov, ki primerno opisuje vsebino članka in ne presega 80 znakov.
- Izvleček, ki naj bo skrajšana oblika članka in naj ne presega 250 besed. Izvleček mora vsebovati osnove, jedro in cilje raziskave, uporabljeno metodologijo dela, povzetek izidov in osnovne sklepe.
- Največ 6 ključnih besed, ki bi morale biti napisane takoj po izvlečku.
- Uvod, v katerem naj bo pregled novejšega stanja in zadostne informacije za razumevanje ter pregled izidov dela, predstavljenih v članku.
- Teorija.
- Eksperimentalni del, ki naj vsebuje podatke o postavitvi preiskusa in metode, uporabljene pri pridobitvi izidov.
- Izidi, ki naj bodo jasno prikazani, po potrebi v obliki slik in preglednic.
- Razprava, v kateri naj bodo prikazane povezave in posplošitve, uporabljene za pridobitev izidov. Prikazana naj bo tudi pomembnost izidov in primerjava s poprej objavljenimi deli.
- Sklepi, v katerih naj bo prikazan en ali več sklepov, ki izhajajo iz izidov in razprave.
- Vse navedbe v besedilu morajo biti na koncu zbrane v seznamu literature, in obratno.

Dodatne zahteve

- Vrstice morajo biti zaporedno oštevilčene.
- Predložen članek ne sme imeti več kot 18 strani (brez tabel, legend in literature); velikost črk 12, dvojni razmik med vrsticami. V članek je lahko vključenih največ 10 slik. Isti rezultati so lahko prikazani v tabelah ali na slikah, ne pa na oba načina.
- Potrebno je priložiti imena, naslove in elektronske naslove štirih potencialnih recenzentov članka. Urednik ima izključno pravico do odločitve, ali bo te predloge upošteval.

ENOTE IN OKRAJŠAVE

V besedilu, preglednicah in slikah uporabljajte le standardne označbe in okrajšave SI. Simbole fizikalnih veličin v besedilu pišite poševno (npr. v , T itn.). Simbole enot, ki so sestavljene iz črk, pa pokončno (npr. Pa, m itn.). Vse okrajšave naj bodo, ko se prvič pojavijo, izpisane v celoti.

SLIKE

Slike morajo biti zaporedno oštevilčene in označene, v besedilu in podnaslovu, kot sl. 1, sl. 2 itn. Posnete naj

bodo v katerem koli od razširjenih formatov, npr. BMP, JPG, GIF. Za pripravo diagramov in risb priporočamo CDR format (CorelDraw), saj so slike v njem vektorske in jih lahko pri končni obdelavi preprosto povečujemo ali pomanjšujemo.

Pri označevanju osi v diagramih, kadar je le mogoče, uporabite označbe veličin (npr. v , T itn.). V diagramih z več krivuljami mora biti vsaka krivulja označena. Pomen oznake mora biti razložen v podnaslovu slike.

Za vse slike po fotografskih posnetkih je treba priložiti izvirne fotografije ali kakovostno narejen posnetek.

PREGLEDNICE

Preglednice morajo biti zaporedno oštevilčene in označene, v besedilu in podnaslovu, kot preglednica 1, preglednica 2 itn. V preglednicah ne uporabljajte izpisanih imen veličin, ampak samo ustrezne simbole. K fizikalnim količinam, npr. t (pisano poševno), pripišite enote (pisano pokončno) v novo vrsto brez oklepajev. Vse opombe naj bodo označene z uporabo dvignjene številke¹.

SEZNAM LITERATURE

navedba v besedilu

Vsaka navedba, na katero se sklicujete v besedilu, mora biti v seznamu literature (in obratno). Neobjavljeni rezultati in osebne komunikacije se ne priporočajo v seznamu literature, navedejo pa se lahko v besedilu, če je nujno potrebno.

oblika navajanja literature

V besedilu: Navedite reference zaporedno po številkah v oglatih oklepajih v skladu z besedilom. Dejanski avtorji so lahko navedeni, vendar mora obvezno biti podana referenčna številka.

Primer: »..... kot je razvidno [1,2]. Brandl and Blovsky [4], sta pridobila drugačen rezultat...«

V seznamu: Literaturni viri so oštevilčeni po vrstnem redu, kakor se pojavijo v članku. Označimo jih s številkami v oglatih oklepajih.

Sklicevanje na objave v revijah:

- [1] Desai, C.S. (2007). Unified DSC constitutive model for pavement materials with numerical implementation. *Int. J. of Geomech.*, Vol. 7, No. 2, pp. 83-101.

Sklicevanje na knjigo:

- [2] Šuklje, L. (1969). Rheological aspects of soil mechanics. Wiley-Interscience, London

Sklicevanje na poglavje v monografiji:

- [3] Mettam, G.R., Adams, L.B., 1999. How to prepare an electronic version of your article, in: Jones, B.S., Smith, R.Z. (Eds.), *Introduction to the Electronic Age*. E-Publishing Inc., New York, pp. 281–304.

Sklicevanje na objave v zbornikih konferenc:

- [4] Brandl, H. and Blovsky, S. (2005). Slope stabilization with socket walls using the observational method. *Proc. Int. conf. on Soil Mechanics and Geotechnical Engineering, Bratislava*, pp. 2485-2488.

Sklicevanje na spletne objave:

- [5] Kot najmanj, je potrebno podati celoten URL. Če so poznani drugi podatki (DOI, imena avtorjev, datumi, sklicevanje na izvirno literaturo), se naj prav tako dodajo.

PODATKI O AVTORJIH

Članku priložite tudi podatke o avtorjih: imena, nazive, popolne poštno naslove, številke telefona in faksa,

naslove elektronske pošte. Navedite kontaktno osebo.

SPREJEM ČLANKOV IN AVTORSKE PRAVICE

Uredništvo si pridržuje pravico do odločanja o sprejemu članka za objavo, strokovno oceno mednarodnih recenzentov in morebitnem predlogu za krajšanje ali izpopolnitev ter terminološke in jezikovne korekture. Z objavo preidejo avtorske pravice na revijo ACTA GEOTECHNICA SLOVENICA. Pri morebitnih kasnejših objavah mora biti AGS navedena kot vir.

Vsa nadaljnja pojasnila daje:

Uredništvo
ACTA GEOTECHNICA SLOVENICA
Univerza v Mariboru,
Fakulteta za gradbeništvo
Smetanova ulica 17, 2000 Maribor, Slovenija
E-pošta: ags@uni-mb.si

INSTRUCTIONS FOR AUTHORS

FORMAT OF THE PAPER

The paper should have the following structure:

- A Title, which adequately describes the content of the paper and should not exceed 80 characters;
- An Abstract, which should be viewed as a mini version of the paper and should not exceed 250 words. The Abstract should state the principal objectives and the scope of the investigation and the methodology employed; it should also summarise the results and state the principal conclusions;
- Immediately after the abstract, provide a maximum of 6 keywords;
- An Introduction, which should provide a review of recent literature and sufficient background information to allow the results of the paper to be understood and evaluated;
- A Theoretical section;
- An Experimental section, which should provide details of the experimental set-up and the methods used to obtain the results;
- A Results section, which should clearly and concisely present the data, using figures and tables where appropriate;
- A Discussion section, which should describe the relationships shown and the generalisations made possible by the results and discuss the significance of the results, making comparisons with previously published work;

- Conclusions, which should present one or more conclusions that have been drawn from the results and subsequent discussion;
- A list of References, which comprises all the references cited in the text, and vice versa.

Additional requirements for manuscripts

- Use double line-spacing.
- Insert continuous line numbering.
- The submitted text of Research Papers should cover no more than 18 pages (without Tables, Legends, and References, style: font size 12, double line spacing). The number of illustrations should not exceed 10. Results may be shown in tables or figures, but not in both of them.
- Please submit, with the manuscript, the names, addresses and e-mail addresses of four potential referees. Note that the editor retains the sole right to decide whether or not the suggested reviewers are used.

UNITS AND ABBREVIATIONS

Only standard SI symbols and abbreviations should be used in the text, tables and figures. Symbols for physical quantities in the text should be written in *Italics* (e.g. *v*, *T*, etc.). Symbols for units that consist of letters should be in plain text (e.g. Pa, m, etc.). All abbreviations should be spelt out in full on first appearance.

FIGURES

Figures must be cited in consecutive numerical order in the text and referred to in both the text and the caption as Fig. 1, Fig. 2, etc. Figures may be saved in any common format, e.g. BMP, JPG, GIF. However, the use of CDR format (CorelDraw) is recommended for graphs and line drawings, since vector images can be easily reduced or enlarged during final processing of the paper.

When labelling axes, physical quantities (e.g. v , T , etc.) should be used whenever possible. Multi-curve graphs should have individual curves marked with a symbol; the meaning of the symbol should be explained in the figure caption. Good quality black-and-white photographs or scanned images should be supplied for the illustrations.

TABLES

Tables must be cited in consecutive numerical order in the text and referred to in both the text and the caption as Table 1, Table 2, etc. The use of names for quantities in tables should be avoided if possible: corresponding symbols are preferred. In addition to the physical quantity, e.g. t (in Italics), units (normal text), should be added on a new line without brackets.

Any footnotes should be indicated by the use of the superscript¹.

LIST OF REFERENCES

citation in text

Please ensure that every reference cited in the text is also present in the reference list (and vice versa). Any references cited in the abstract must be given in full. Unpublished results and personal communications are not recommended in the reference list, but may be mentioned in the text, if necessary.

reference style

Text: Indicate references by number(s) in square brackets consecutively in line with the text. The actual authors can be referred to, but the reference number(s) must always be given:

Example: "... as demonstrated [1,2]. Brandl and Blovsky [4] obtained a different result ..."

List: Number the references (numbers in square brackets) in the list in the order in which they appear in the text.

Reference to a journal publication:

- [1] Desai, C.S. (2007). Unified DSC constitutive model for pavement materials with numerical implementation. *Int. J. of Geomech.*, Vol. 7, No. 2, pp. 83-101.

Reference to a book:

- [2] Šuklje, L. (1969). Rheological aspects of soil mechanics. Wiley-Interscience, London

Reference to a chapter in an edited book:

- [3] Mettam, G.R., Adams, L.B. (1999). How to prepare an electronic version of your article, in: Jones, B.S., Smith, R.Z. (Eds.), *Introduction to the Electronic Age*. E-Publishing Inc., New York, pp. 281–304.

Conference proceedings

- [4] Brandl, H. and Blovsky, S. (2005). Slope stabilization with socket walls using the observational method. *Proc. Int. conf. on Soil Mechanics and Geotechnical Engineering, Bratislava*, pp. 2485-2488.

Web references:

- [5] As a minimum, the full URL should be given and the date when the reference was last accessed. Any further information, if known (DOI, author names, dates, reference to a source publication, etc.), should also be given.

AUTHOR INFORMATION

The following information about the authors should be enclosed with the paper: names, complete postal addresses, telephone and fax numbers and E-mail addresses. Indicate the name of the corresponding author.

ACCEPTANCE OF PAPERS AND COPYRIGHT

The Editorial Committee of the Slovenian Geotechnical Review reserves the right to decide whether a paper is acceptable for publication, to obtain peer reviews for the submitted papers, and if necessary, to require changes in the content, length or language.

On publication, copyright for the paper shall pass to the ACTA GEOTECHNICA SLOVENICA. The AGS must be stated as a source in all later publication.

For further information contact:

Editorial Board
ACTA GEOTECHNICA SLOVENICA
University of Maribor,
Faculty of Civil Engineering
Smetanova ulica 17, 2000 Maribor, Slovenia
E-mail: ags@uni-mb.si

NAMEN REVIJE

Namen revije ACTA GEOTECHNICA SLOVENICA je objavljati kakovostnih teoretičnih člankov z novih pomembnih področij geomehanike in geotehnike, ki bodo dolgoročno vplivali na temeljne in praktične vidike teh področij.

ACTA GEOTECHNICA SLOVENICA objavlja članke s področij: mehanika zemljin in kamnin, inženirska geologija, okoljska geotehnika, geosintetika, geotehnične konstrukcije, numerične in analitične metode, računalniško modeliranje, optimizacija geotehničnih konstrukcij, terenske in laboratorijske preiskave.

Revija redno izhaja dvakrat letno.

AVTORSKE PRAVICE

Ko uredništvo prejme članek v objavo, prosi avtorja(je), da prenese(jo) avtorske pravice za članek na izdajatelja, da bi zagotovili kar se da obsežno razširjanje informacij. Naša revija in posamezni prispevki so zaščiteni z avtorskimi pravicami izdajatelja in zanje veljajo naslednji pogoji:

fotokopiranje

V skladu z našimi zakoni o zaščiti avtorskih pravic je dovoljeno narediti eno kopijo posameznega članka za osebno uporabo. Za naslednje fotokopije, vključno z večkratnim fotokopiranjem, sistematičnim fotokopiranjem, kopiranjem za reklamne ali predstavitvene namene, nadaljnjo prodajo in vsemi oblikami nedobičkonosne uporabe je treba pridobiti dovoljenje izdajatelja in plačati določen znesek.

Naročniki revije smejo kopirati kazalo z vsebino revije ali pripraviti seznam člankov z izvlečki za rabo v svojih ustanovah.

elektronsko shranjevanje

Za elektronsko shranjevanje vsakršnega gradiva iz revije, vključno z vsemi članki ali deli članka, je potrebno dovoljenje izdajatelja.

ODGOVORNOST

Revija ne prevzame nobene odgovornosti za poškodbe in/ali škodo na osebah in na lastnini na podlagi odgovornosti za izdelke, zaradi malomarnosti ali drugače, ali zaradi uporabe kakršnekoli metode, izdelka, navodil ali zamisli, ki so opisani v njej.

AIMS AND SCOPE

ACTA GEOTECHNICA SLOVENICA aims to play an important role in publishing high-quality, theoretical papers from important and emerging areas that will have a lasting impact on fundamental and practical aspects of geomechanics and geotechnical engineering.

ACTA GEOTECHNICA SLOVENICA publishes papers from the following areas: soil and rock mechanics, engineering geology, environmental geotechnics, geosynthetic, geotechnical structures, numerical and analytical methods, computer modelling, optimization of geotechnical structures, field and laboratory testing.

The journal is published twice a year.

COPYRIGHT

Upon acceptance of an article by the Editorial Board, the author(s) will be asked to transfer copyright for the article to the publisher. This transfer will ensure the widest possible dissemination of information. This review and the individual contributions contained in it are protected by publisher's copyright, and the following terms and conditions apply to their use:

photocopying

Single photocopies of single articles may be made for personal use, as allowed by national copyright laws. Permission of the publisher and payment of a fee are required for all other photocopying, including multiple or systematic copying, copying for advertising or promotional purposes, resale, and all forms of document delivery.

Subscribers may reproduce tables of contents or prepare lists of papers, including abstracts for internal circulation, within their institutions.

electronic storage

Permission of the publisher is required to store electronically any material contained in this review, including any paper or part of the paper.

RESPONSIBILITY

No responsibility is assumed by the publisher for any injury and/or damage to persons or property as a matter of product liability, negligence or otherwise, or from any use or operation of any methods, products, instructions or ideas contained in the material herein.